



Using Wearable Soft Sensors for Gesture Recognition

Gasak Chassib Abdul-Hussain

Thesis submitted to the School of Science, Engineering and Environment in partial fulfilment of the requirements for the degree of

Doctor of Philosophy

School of Science, Engineering and Environment
University of Salford, Salford, UK, 2024

Contents

Publications.....	iv
List of Figure.....	v
List of Tables.....	viii
Acknowledgements.....	ix
Declaration	x
Notation List.....	x
Abbreviations	xi
Abstract	xii
Chapter One: Introduction	1
1.1 Introduction	1
1.2 Research Motivation	2
1.3 Aims and Objectives	4
1.4 Methodology	5
1.5 List of Contributions	7
1.6 Organisation of the Research	8
Chapter Two: Literature Review	10
2.1 Introduction	10
2.2 Tactile Sensors.....	10
2.3 Upper Limb Anatomy.....	14
2.4 Sensors.....	18
2.5 Hysteresis Background and Neural Network Applications.....	20
2.6 Conclusion	23
Chapter Three:	24
Design and Implementation of a Soft Tactile Sensor	24
3.1 Introduction	24
3.2 Designing a Soft Tactile Sensor	25
3.3 Conclusion	34
Chapter Four:	36
Modified Nonlinear Hysteresis Approach of a Tactile Sensor	36
4.1 Introduction	36
4.2 Types of Hysteresis in Tactile Sensors.....	37

4.3 Key Concepts.....	40
4.4 Neural Networks and Their Relevance to Addressing Hysteresis in Sensor Data	46
4.5 Modelling the Hysteresis Nonlinearity	48
4.6 Design a Soft Tactile Sensor	50
4.6.1 Experimental Setup.....	50
4.6.2 Single-Layer and Multi-Layer Sensors.....	51
4.6.3 Calibration and Reoeatability Analysis.....	53
4.6.4 Loading-Unloading Cycle and Hysteresis.....	54
4.7 Results and Discussion.....	58
4.8 Analysis and Discussions.....	63
4.9 Conclusions	71
Chapter Five: Validation and Evaluation of a Low-Cost Fabric-Based Tactile Sensor in Comparison with an sEMG Sensor.....	73
5.1 Introduction	73
5.2 Materials and Methods.....	75
5.2.1 Experimental Setup and Exercise Protocol	75
5.2.2 Equipment and Sensor Systems' Description	78
5.2.3 Analysis Method.....	82
5.3 Validation Indicators	86
5.4 Participant Demographics, Informed Consent, and Validation Analysis	91
5.4.1 Participant Demographics and Informed Consent.....	91
5.4.2 Validation Analysis	91
5.5 Experimental Findings and Sensor Performance Analysis.....	91
5.5.1 Signal Filtering	91
5.5.2 Physical Exercises	96
5.5.3 Indicator Assessment.....	97
5.6 Discussion and Implications.....	102
5.7 Muscle Activity Analysis and Rehabilitation Potential: Insights from Parkinson's Disease and Stroke Individuals.....	106
5.7.1 Experimental Setup and Exercise Protocol	107
5.7.2 Experimental Results	110
5.7.3 Analysis of Muscle Activity Patterns and Clinical Implications.....	121
5.7.4 Clinical Implications and Future Research Directions	128
5.8 Conclusion	130
Chapter Six: Conclusion and Future Work	132

6.1 Conclusions	132
6.2 Contribution to Existing Research.....	133
6.3 Addressing Research Objectives in the Context of Existing Literature.....	133
6.4 Conclusion and Future Directions in Relation to Prior Work.....	134
6.5 Significance of the Findings.....	135
References.....	136
Appendix A.....	157

Publications

1. Gasak Abdul- Hussain, W. Holderbaum , T. Theodoridis , G. Wei , H. El-Hussieny and J. Ferriz-Papi. Using an EeonTex Conductive Stretchable Elastic Fibre for Hand Action Recognition Advances in Science and Technology Submitted: 2022-07-25 ISSN: 1662-0356, Vol. 133, pp.3-10 Revised: 2023-01-08 © 2023 Trans Tech Publications Ltd, Switzerland.
2. Gasak Abdul-Hussain, William Holderbaum, Theodoros Theodoridis and Guowu Wei. Modified Nonlinear Hysteresis Approach of a Tactile Sensor. Sensors 2023, 23, 7293. <https://doi.org/10.3390/s23167293>

List of Figures

Figure 2.1: Structure of the Human Upper Limb[1].....	14
Figure 2.2: Movement of the Shoulder Joint [3].....	15
Figure 2.3: Movement of the Elbow Joint[5]	16
Figure 2.4: The Human Fingers and Joint [3]	17
Figure 3.1: Materials used for sensor development: (a) conductive stretchable fabric; (b) a silverplated conductive thread; (c) Fully designed tactile sensor	27
Figure 3.2: Block diagram depicting the thread arrangement in the sensor and full circuit connections.....	29
Figure 3.3: Tactile Sensor Output.....	32
Figure 3.4: (a) The sensor output during slow opening/closing of hand; (b) The sensor output during fast opening/closing of hand	33
Figure 4.1: Rate-Dependent Hysteresis	38
Figure 4.2: Displacement-Dependent Hysteresis	39
Figure 4.3: Material-Dependent Hysteresis	40
Figure 4.4: Neural Network Architecture.....	42
Figure 4.5: A generic flow chart showing the integration of the hysteresis model, curve-fitting model, and NN.....	45
Figure 4.6: Neural Network Architecture for Resistance Prediction.....	47
Figure 4.7: Flow Diagram of the Experiment Setup and Hysteresis Error Reduction	49
Figure 4.8: The soft tactile sensor	50
Figure 4.9: Tactile sensors with different layers.....	52
Figure 4.10: (a) The Experimental Setup; (b) Force being applied to the sensor; (c) Functional diagram.....	52
Figure 4.11: Calibration of Tactile Sensor Force vs Resistance	54
Figure 4.12: The Hysteresis Phenomenon in the One-Layer Sensor.....	56
Figure 4.13: (a) The hysteresis phenomenon in the Three-Layer Sensor; (b) The hysteresis phenomenon in the Six-Layer Sensor; (c) The hysteresis phenomenon in the Twelve-Layer Sensor.....	57
Figure 4.14: The Approximated Curve Plotted for the One-Layer Sensor	59
Figure 4.15: Approximated Curves of all different Layer Sensors	61

Figure 4.16: Graphs showing the validation of the system of different Layers of Sensor.....	64
Figure 4.17: Validation of the system with new experimental results.....	66
Figure 4.18: One Layer Sensor (a) Neural network performance; (b)Neural network regression; (c) Neural network training.....	67
Figure 5.1: Diagram of the experiment.....	77
Figure 5.2: Equipment of the testbed used in the experiments. 1. & 3. Arduino Uno board. 2 Myoware EMG Muscle Sensor (SEN-13723 ROHS). 4. Soft Tactile sensor	78
Figure 5.3: Diagram followed to normalise the sEMG & low-cost soft Tactile sensor signal from the dynamic exercises	85
Figure 5.4: Comparison of Raw and Filtered Signals for Biceps, Forearm and Wrist Muscles	93
Figure 5.5: A visualisation of the filtered signals to illustrate the effectiveness of the noise reduction process (a)..... The tactile and EMG sensor output for the Bicep’s muscle; (b) The tactile and EMG sensor output for the Forearm muscle; (c) The tactile and EMG sensor output for the Wrist muscle.....	95
Figure 5.6: Figure 5.6: Illustration of the distribution of maximum voluntary contraction (MVC) values based on the exercise performed and the equipment used: (a) By using sEMG Sensor; (b) By using Tactile Sensor	96
Figure 5.7: The Comparison of Mean Values for Different Exercise Scenarios.....	101
Figure 5.8: Wrist Muscle Activity Measurement Setup for Key Use in Parkinson’s Patients	108
Figure 5.9: Forearm Muscle Activity During Grasping an Apple for Parkinson’s Patient.....	108
Figure 5.10: Wrist Muscle Activity During Key Use for Stroke Patient.....	109
Figure 5.11: Forearm Muscle Activity During Grasping an Apple for Parkinson’s Patient.....	109
Figure 5.12: Wrist Muscle Activity During Key Use for Healthy Subject	110
Figure 5.13: Forearm Muscle Activity During Grapping an Apple for Healthy Subject	110
Figure 5.14: Wrist Muscle Activity During Key Use for Parkinson’s Patient.....	111

Figure 5.15: Forearm Muscle Activity During Grapping an Apple for Parkinson's Patient	111
Figure 5.16: Wrist Muscle Activity During Key Use for Stroke Patient	112
Figure 5.17: Forearm Muscle Activity During Grapping an Apple for Stroke Patient	112
Figure 5.18: (a) Wrist Muscle Activity Across Subjects During Key Use (b) Forearm Muscle Activity Across Subjects During Grasp of an Apple.....	113
Figure 5.19: Filtered Signals with Wrist Muscle Activity During Key Use for Healthy Subject	115
Figure 5.20: Filtered Signals with Wrist Muscle Activity During Grapping an Apple with Healthy Subject.....	116
Figure 5.21: Filtered Signals with Wrist Muscle Activity During Key Use for Parkinson's Patient.....	116
Figure 5.22: Filtered Signals with Wrist Muscle Activity During Grapping an Apple Parkinson's Patient.....	117
Figure 5.23: Filtered Signals with Wrist Muscle Activity During Key Use for Stroke Patient.....	117
Figure 5.24: Filtered Signals with Forearm Muscle Activity During Grapping an Apple for Stroke Patient	118
Figure 5.25: Bode Plot of the 40-100 Hz bandpass filter used in the analysis.....	118
Figure 5.26: Wrist Muscle Activity Across Subjects During Key Use	120
Figure 5.27: Forearm Muscle Activity Across Subjects while Grapping an Apple ..	120
Figure 5.28: Wrist Muscle Activity.....	123
Figure 5.29: Forearm Muscle Activity	124
Figure 5.30: T-test Results: Key Use and Apple Grasping Tasks	127

List of Tables

Table 3.1: Statistic Calculations	34
Table 4.1: Regression Results and Accuracy Statistics of Datasets	68
Table 4.2: Comparison of Neural Network Performance with Different Numbers of Sensor Layers	69
Table 5.1: Description of Full Arm Movement	77
Table 5.2: Specifications of Soft Tactile Sensor	81
Table 5.3: Summary of Validation Indicators for Tactile Sensor and EMG Sensor Comparison	89
Table 5.4: Current validity. (KC), Kendall Correlation; (SP), Spearman's correlation; (TE), Energy Tactile sensor system; sEMGE, the energy of sEMG sensor system; (CC), Cross-correlation coefficient; (PC), Pearson Correlation	98
Table 5.5: Statistic Measurement with Different Muscle Groups	122
Table 5.6: T-test Results: Key Use and Apple Grasping Tasks	126

Acknowledgements

In dedicating this work as a tribute to my beloved son, Aymen, whose pure spirit serves as my daily inspiration, and to my father, Professor Chassib Abdul-Hussain, my unwavering guiding light, and to my cherished mother, I extend my deepest gratitude. To my extraordinary family, from my husband, Dr. Safaa, and our sons, Ali and Ahmed, and to my beautiful princess daughter, Fatima. Also to my steadfast siblings, your unwavering support has been my rock.

I wish to convey my heartfelt appreciation to the remarkable team of supervisors: Professor William Holderbaum, Dr Theodoros Theodoridis, and Dr Guowu Wei. Their unparalleled support, guidance, and understanding have been the cornerstone of my journey. Amidst challenges, their unwavering assistance and empathetic approach have been pivotal in reaching this significant milestone.

To my esteemed colleagues and all the dedicated members of staff at the Robotics Lab, I extend my sincere thanks for your invaluable help and support. Your contributions have greatly enriched the development of this work. To my fellow researchers, your assistance and insightful discussions have been instrumental in shaping the trajectory of this study.

Finally, to my beloved family, your boundless love, encouragement, and unwavering support have sustained me throughout this endeavour. I am deeply grateful for your presence in my life.

Declaration

This thesis is my original work and contains no material that has been previously submitted for a degree at any other institution. The research presented herein was conducted solely by me without contributions from joint research efforts. All research conducted in this thesis was approved under the Ethics Application ID: 8194.

Notation List

a_0, a_1, a_n	Coefficients in the space of real numbers
a_i^{l-1}	The output of node i in layer $l - 1$
b_j^l	Bias of node j in layer l
σ	Activation function
δ_j^l	The partial derivative of the total error E for the input z_j^l of node j in layer l
Δ	The learning rate for weight updates
Δb_j^l	Update for biases
η	The learning rate for bias updates
Δw_{ji}^l	Weight updates
w_{ji}^l	Weight connecting node i in layer $l - 1$ to node j in layer l
d	Difference between the ranks of corresponding values in two datasets
$\text{cov}(x, y)$	The covariance between variables x and y
F	Raw input
R	Corrected output
R_t	Static resistance value based on the current and historical resistance values
R_{t-1}	Historical resistance value
R_{est}	Corrected resistance as a target, the output layer
R_{static}	Static resistance
N	Population size

Abbreviations

AI	Artificial intelligence
ANN	Artificial Neural Network
BPNN	Backpropagation Neural Network
CC	Cross-correlation
CM	Carpometacarpal joint
CNNs	Convolutional Neural Networks
DIP	Distal interphalangeal joint
EEG	Electroencephalogram Sensors
EMG	Electromyography sensors
FEM	Finite Element Method
GPIM	Generalised Prandtl–Ishlinskii Model
IMU	Inertial Measurement Unit Sensors
IP	Interphalangeal joint
KC	Kendall Correlation
LSTMs	Long Short-Term Memory networks
Max	Maximum Value
MEMS	Micro-Electro-Mechanical System
Min	Minimum Value
MP	Metacarpophalangeal joint
MSE	Mean Squared Error
MVC	Maximum Voluntary Contraction
NN	Neural networks
PAMs	Pneumatic Artificial Muscles
PC	Pearson Correlation
PI	Prandtl–Ishlinskii
PIP	Proximal interphalangeal joint
RNNs	Recurrent Neural Networks
sEMG	Surface ElectroMyoGraphy
SP	Spearman Correlation
σ	Standard Deviation
sEMGE	The energy of sEMG sensor system
TE	Energy of Tactile sensor system
TENGs	Triboelectric Nanogenerators
μ	Mean Value
x(t)	Signal of amplitude

Abstract

The increasing prevalence of hand impairments due to conditions such as arthritis, Cerebral Palsy, Parkinson's Disease, and stroke presents significant challenges in everyday activities, such as tying shoes or getting dressed. In the UK, long-term musculoskeletal conditions are on the rise, highlighting the urgent need for effective rehabilitation methods. Despite physical therapy's potential to help regain motor skills, there is no consensus on optimal methods for promoting neuroplasticity. Robotic and wearable technologies have emerged as viable solutions, with soft robotics offering distinct advantages due to their flexibility, adaptability, and portability. However, limited evidence supports the superiority of conventional robotic devices over traditional therapies.

This PhD research investigates the development of a soft tactile sensor aimed at improving rehabilitation outcomes for individuals with upper limb impairments, focusing on muscle activity during hand movements in healthy, Parkinson's, and stroke patients. The motivation for this study lies in the growing demand for accessible rehabilitation solutions that address the UK's healthcare challenges, particularly for stroke survivors, where upper limb rehabilitation is under-resourced.

The primary aim of this research is to design and validate a novel fabric-based tactile sensor using Eeon-Tex conductive stretchable elastic fibre, capable of accurately detecting muscle activity. The methodology includes the fabrication of the sensor, an investigation into the nonlinear hysteresis phenomenon, and validation against a commercial surface electromyography (sEMG) sensor. A key focus is on developing reliable alternatives to traditional sEMG systems, making rehabilitation more accessible.

Key findings demonstrate that the soft tactile sensor is effective in capturing distinct muscle activity patterns across various patients, particularly during tasks involving gripping and manipulating objects. Statistical analysis showed high signal similarity between the tactile sensor and sEMG, confirming the sensor's reliability and potential for clinical application. Additionally, strategies were developed to mitigate the effects of nonlinear hysteresis on the sensor's performance.

In conclusion, this research contributes to the field of rehabilitation technology by providing a cost-effective, reliable alternative to conventional muscle monitoring systems. The significance of this work lies in its potential to improve the quality of life for individuals with mobility impairments, particularly in an ageing population, while addressing the resource challenges faced by healthcare systems such as the National Health Service(NHS).

Chapter One: Introduction

1.1 Introduction

When you imagine struggling to complete simple tasks in life, such as tying your shoes or getting dressed every day because of limited hand mobility, it is possible to focus on the issues encountered by many people who face hand impairments due to conditions including arthritis, Cerebral Palsy, Parkinson's Disease, or stroke, as these challenges are a daily reality. In the United Kingdom (UK) alone, the number of adults reporting long-term musculoskeletal conditions has been increasing, underlining the importance of effective rehabilitation methods [1,2]. Despite the potential of physical therapy to help regain motor skills, though, there is still no consensus on the best approaches to promote neuroplasticity. Additionally, access to therapy sessions can be limited by factors like frequency, duration, and cost. To make rehabilitation exercises more accessible, researchers have developed robotic devices as supplementary therapies.

However, while conventional robotics offer benefits, a review of numerous upper limb rehabilitation devices found insufficient evidence to support their effectiveness compared to traditional therapies [3-5]. This could be due to the rigid materials used in conventional robotics, which may limit their therapeutic potential. Conversely, soft robotics, made from flexible materials, such as fluids, gels, and soft polymers, offer promising advantages. These soft robotic devices can better adapt to the body's shape and movements, potentially enhancing rehabilitation outcomes. Moreover, their lightweight and portable nature makes at-home rehabilitation feasible. Accordingly, while soft robotic devices for hand rehabilitation are in development, a thorough examination of existing designs is essential to guide future development efforts.

1.2 Research Motivation

The current research investigates the application of tactile sensors, which are devices that mimic the human sense of touch by detecting and responding to mechanical stimuli such as pressure, force, or vibration. These sensors are critical across several domains, including wearable technology, healthcare, assistive technologies, and industrial operations. Tactile sensors hold significant potential for enhancing functionality and user experience in these areas by providing real-time feedback, improving precision, and enabling more intuitive interactions. In the domain of wearable technology, integrating tactile sensors can significantly impact user-device interactions. Wearable devices with tactile feedback can create a more immersive and responsive user experience, facilitating more intuitive interactions. The wearable technology market in the UK is growing rapidly, driven by consumer demand for innovative devices. In 2020, the UK wearable tech market was valued at approximately £2.9 billion, with projections indicating continued growth as consumer demand increases for more sophisticated and interactive devices [6]. The incorporation of advanced tactile sensors in these products could drive further innovation and user satisfaction. In healthcare, the application of tactile sensors is particularly compelling, especially in the context of the UK's healthcare challenges. The National Health Service (NHS) faces increasing pressure to deliver effective rehabilitation services for stroke survivors, among other conditions. Stroke is a leading cause of disability in the UK, with over 100,000 strokes occurring each year [7]. Approximately 75% of stroke survivors experience upper limb impairments, which can severely limit their ability to perform daily activities. However, rehabilitation services often focus more on lower limbs, potentially leaving upper limb recovery under-resourced. This can result in long-term disabilities, such as spasticity and reduced mobility, leading to ongoing care needs. For example, upper limb spasticity can develop if left untreated, affecting the ability to carry out daily tasks. Integrating tactile sensors into rehabilitation devices could provide real-time feedback, enhancing the precision and effectiveness of therapies, particularly in improving hand and arm movement. The motivation behind this research is grounded in the growing demand for advanced sensor technologies that can contribute to improving quality of life, optimising healthcare outcomes, and enhancing industrial processes, particularly within the UK.

The motivation behind this research is grounded in the growing demand for advanced sensor technologies that can contribute to improving quality of life, optimising healthcare outcomes, and enhancing industrial processes, particularly within the UK.

Functional Electrical Stimulation (FES) has shown promise in improving motor function in upper limbs, and similar benefits could be achieved by using tactile sensors to provide more accurate feedback on muscle activity and movement. This would potentially reduce long-term care costs for the NHS by aiding recovery and limiting the need for extended rehabilitation.

Additionally, tactile sensors play a crucial role in advancing assistive technologies, such as prosthetics and robotics, which are increasingly important in the UK's ageing population. The UK's prosthetics market is growing, driven by a rising demand for more responsive and sensitive prosthetic devices. The prevalence of amputations in the UK is significant, with over 5,000 major limb amputations carried out annually [7]. Tactile sensors can significantly improve the functionality of these devices by enabling them to better detect and respond to external stimuli, thus enhancing the user's ability to interact with their environment. For example, a prosthetic hand equipped with tactile sensors could adjust its grip based on the texture and hardness of an object, offering a more natural and effective user experience, which is essential for improving the quality of life for amputees in the UK.

In industrial settings, the integration of tactile sensors can enhance operational efficiency, product quality, and cost management, which are critical for maintaining the competitiveness of UK manufacturing. The UK's manufacturing sector contributes significantly to the economy, with a total output valued at £191 billion in 2022 [8]. However, the sector faces challenges related to precision, quality control, and automation. Tactile sensors can be employed in robotic systems to improve the accuracy of tasks such as assembly, material handling, and inspection. For instance, the use of tactile sensors in robotic grippers allows for more precise manipulation of objects, reducing the risk of damage and improving overall production quality. This is particularly important as the UK aims to enhance productivity and competitiveness in its manufacturing sector.

The motivation for this research lies in the substantial benefits that advanced tactile sensors can provide across various fields, with a specific focus on addressing challenges within the UK. By improving upper limb rehabilitation outcomes, enhancing the functionality of prosthetic devices, and optimising industrial processes, this research aims to contribute to the development of innovative solutions that have a meaningful impact on UK society.

1.3 Aims and Objectives

The current study aims to comprehensively analyse the field of soft robotics, focusing on evaluating the advantages and drawbacks of soft sensors in healthcare applications. Specifically, it explores the potential of soft sensors in aiding individuals with injuries, the elderly, and those with disabilities, particularly in the contexts of post-traumatic recovery, rehabilitation, and anomaly detection. By examining the capabilities and limitations of soft sensors, this research seeks to contribute valuable insights that enhance the well-being and quality of life of individuals facing mobility challenges.

To achieve this aim, the following objectives have been devised:

1. Develop a soft robotic sensor using Eeon-TeX Conductive stretchable elastic fibre, a specialised fabric, specifically designed to enhance therapy precision by providing accurate feedback on muscle movement during upper limb rehabilitation.
2. Investigate and understand the nonlinear hysteresis phenomenon in soft tactile sensors, where hysteresis describes the tendency of the sensor to retain a memory of past forces applied, leading to lag or deviation in its response. This will be studied through experiments with varying numbers of sensor layers, and strategies to mitigate this phenomenon will be developed. This is crucial in ensuring the sensor can provide real-time, reliable data that informs therapy adjustments.

3. Conduct a validation study comparing the proposed soft tactile sensor with a precise sEMG sensor, highlighting its effectiveness in detecting and interpreting muscle activity, thus demonstrating its capability to contribute to therapeutic interventions.
4. Validate the tactile sensor by comparing it with a commercial sEMG sensor, demonstrating its accuracy and reliability for diverse applications, including rehabilitation and assistive technologies.

1.4 Methodology

1. Soft Robotic Sensor Development

- Material Selection and Preparation;
- Identify and acquire Eeon-Tex Conductive stretchable elastic fibre;
- Conduct material testing to understand its mechanical and electrical properties.

2. Sensor Design and Fabrication

- Design the soft robotic sensor considering specific application requirements;
- Fabricate the sensor prototype using the identified material;
- Experiment with different layer configurations (one, three, six, and twelve) to observe the impact on sensor performance.

3. Nonlinear Hysteresis Investigation

- Develop experiments to investigate the nonlinear hysteresis phenomenon in soft tactile sensors;
- Conduct tests with varying numbers of sensor layers;
- Analyse the data to identify trends and characteristics of the hysteresis phenomenon.

4. Computer Control Hardware Development

- Selection of Components;
- Identify and procure necessary components, including Arduino Uno and other required hardware;
- Code Development;
- Utilise Excel, Arduino Uno, and MATLAB to develop code for recognising different muscle movements through the tactile sensor;
- Implement strategies for real-time data processing and classification.

5. Validation Study

- Comparison with sEMG Sensor;
- Conduct a validation study comparing the soft tactile sensor with a precise sEMG sensor;
- Record EMG signals during dynamic exercises from the Biceps muscle and the Flexor Carpi Ulnaris muscle;
- Ensure consistent experimental conditions for both sensors.

6. Performance Evaluation

- Evaluate the performance through statistical indicators;
- Spearman's correlation;
- Energy ratio;
- Pearson correlation coefficient.

7. Validation against Commercial sEMG Sensor

- Compare the tactile sensor with a commercial sEMG sensor;
- Assess accuracy and reliability across diverse applications;

- Use standardised tests to ensure a fair and comprehensive evaluation.

8. Data Analysis

- Analyse the collected data using appropriate statistical methods.
- Compare the signals from both sensors under different conditions.

1.5 List of Contributions

The contributions from the current research are multifaceted and encompass advancements in muscle behaviour analysis, rehabilitation, and assistive technology. This presents a comprehensive exploration of the development and application of a fabric-based tactile sensor for muscle behaviour analysis and rehabilitation, with the contributions summarised as follows:

1. Development and Evaluation of the Fabric-Based Tactile Sensor:

The primary contribution of the current research lies in the development and thorough evaluation of a novel fabric-based tactile sensor. Designed to monitor muscle behaviour during various activities, this sensor addresses accessibility challenges associated with expensive commercial Electromyography (EMG) systems, thereby making muscle behaviour analysis more affordable and widely accessible.

- **Introduction of a Fabric-Based Tactile Sensor:** The study introduces a novel fabric-based tactile sensor designed to monitor muscle behaviour during various activities. This sensor addresses accessibility challenges associated with expensive commercial EMG systems, making muscle behaviour analysis more affordable and widely accessible.
- **Development and Evaluation of the Sensor:** The study comprehensively develops and evaluates the fabric-based tactile sensor. Through dynamic exercises performed by volunteers, the sensor's performance is compared with standard surface EMG sensors, demonstrating its efficacy and reliability.
- **Demonstration of Signal Similarity:** The study demonstrates consistently high signal similarity between the fabric-based tactile sensor and conventional surface EMG sensors. Through rigorous evaluation, three performance

indicators confirm the reliability and cost-effectiveness of the new sensor technology.

2. Understanding and Mitigating Nonlinear Hysteresis:

In addition to sensor development, the current research investigates and proposes mitigation strategies for nonlinear hysteresis in soft tactile sensors, which is crucial for improving reliability and accuracy in muscle behaviour monitoring.

3. The initial trials and applications of the proposed sensing technology in the healthcare field;

Focusing on muscle activity patterns during hand movements in individuals with Parkinson's disease and stroke. Utilising a newly designed soft tactile sensor and advanced signal processing techniques, assessed its efficacy in capturing muscle activity and characterised motor control differences between patients and healthy controls during tasks involving gripping an apple and manipulating a key.

1.6 Organisation of the Research

The current research is organised into six chapters to present the different aspects of the research that have been undertaken to complete the goals described above.

Chapter One: Introduction: This chapter presents a general overview of the soft sensors, before illustrating the research motivation, aims and objectives. It also explains the research methodology and lists the research contributions.

Chapter Two: Literature Review: This chapter presents a review of previous research in the soft sensor area.

Chapter Three: Design and Implementation of a Soft Tactile Sensor: This Chapter focuses on soft tactile sensors, starting with materials, such as conductive fabrics and threads that utilise piezoresistivity to convert touch into electrical signals. The careful assembly process is detailed, including stitching techniques and optimising contact points to ensure sensor reliability. Experiments were subsequently devised using microcontrollers, including Arduino to analyse the sensor's response in real-life

scenarios by collecting data to improve performance. Lastly, the readout circuitry is explained using voltage dividers and multiplexing to enhance data acquisition, with detailed circuit diagrams and code for replication and further development.

Chapter Four: Modified Nonlinear Hysteresis Approach of a Tactile Sensor: In this chapter, a new technique is introduced using a backpropagation (BP) neural network to deal with hysteresis nonlinearity in tactile sensors made of conductive fibres. Hysteresis refers to the inconsistency in sensor response when the same force is applied, depending on whether the force is increasing or decreasing. This inconsistency can significantly affect the accuracy and reliability of tactile sensor readings. To test this method, four sensor units were created and applied force sequences were used to gather their corresponding output resistance data. The key aspect of my approach was training a BP network with these sequences to adjust the resistance values. During the training process, the network showed excellent convergence, adjusting its parameters to minimise the difference between predicted and actual resistance values.

Chapter Five: Validation and Evaluation of a Fabric-Based Tactile Sensor in Comparison with an sEMG Sensor: In this chapter, the aim is to assess the effectiveness and limitations of tactile sensors in measuring muscle activity. The study involves gathering Electromyography (EMG) signals from the Biceps and Flexor Carpi Ulnaris muscles during dynamic exercises. In this process, two types of sensors are compared: a commercial superficial electromyography (sEMG) sensor (Myoware EMG) and a fabric-based tactile sensor discussed in Chapter Three. The main goals are: 1) to determine whether the tactile sensor system is able to produce EMG output signals that differentiate between various exercises; and 2) to evaluate the consistency of the signal generated by the soft tactile sensor, especially during simple exercises. Through this experiment, the aim is to gain insights into the capabilities and limitations of tactile sensor systems for assessing muscle activity.

Chapter Six: Conclusion and Future Work: This chapter concludes the entire research and presents a plan for future work.

Chapter Two: Literature Review

2.1 Introduction

In today's world, technology is deeply woven into our everyday lives, driving the quest for innovations that boost human well-being. The UK's ageing population, coupled with a shortage of physiotherapists and occupational therapists, underscores the urgent need for fresh approaches to rehabilitation and independent living. In response, wearable devices and tools are joining forces to offer promising solutions, empowering individuals to regain control and mobility [9-13]. This chapter also creates the foundation by spotlighting the growing significance of tactile sensor technology in addressing the changing landscape of healthcare and robotics, particularly in upper limb rehabilitation.

With an increasing number of elderly individuals and a lack of healthcare professionals, there is a critical demand for inventive solutions to aid in rehabilitation and promote patients' autonomy. This section underscores the crucial role of wearable devices and assistive technologies in bridging this gap, with a specific focus on the development of stretchable tactile sensors tailored for upper limb applications. By offering a brief overview of the current challenges and opportunities in this domain, this introduction sets the stage for the ensuing sections, which explore deeper into the advancements and implications of tactile sensor technology.

2.2 Tactile Sensors

As the population in the UK ages, ensuring people's independence and daily activities has become a crucial focus. Accordingly, recent research [9-16] highlights a shortage of physiotherapists and occupational therapists to meet the needs of the growing elderly population. This has led to a growing interest in developing robots to aid in rehabilitation, taking on the role of providing controlled and repetitive motion assistance traditionally handled by physiotherapists. Simultaneously, wearable devices have risen as a promising form of technology, capable of recognising patients' motion intentions, ensuring control, and supplying the necessary force for intended limb movements [15,17-18]. Recent advancements in wearable devices and assistive

technologies have also led to the development of novel sensing modalities for detecting users' motion intentions. Specifically, surface electromyography (sEMG) and electroencephalography (EEG) readings, in conjunction with pressure and bend sensors placed on wrists and fingers, have emerged as promising tools in this domain [5,11]. These devices offer a spectrum of both positive and negative aspects concerning their ability to detect motion intentions. For instance, EEG signals can effectively detect signals at the initiation of motion, presenting potential benefits for patients with total paralysis. This approach, however, often necessitates a substantial number of electrodes and demands sophisticated signal-processing algorithms for accurate interpretation [9, 18-23].

In contrast, sEMG readings have gained popularity due to their reliability in signal acquisition and simplicity in implementation [14]. Nearly half of the devices designed for motion intention detection rely on sEMG readings, owing to their effectiveness in capturing user intent [15]. Moreover, the integration of sEMG with voice recognition techniques has shown promise in enhancing the detection of intent through a multi-modal approach [24]. Despite the potential of these methods to enhance the rehabilitation process, approaches focusing on feedback modalities for detecting motion intent have sometimes been overshadowed by the prevailing emphasis on robotics [17-19]. Tactile sensors directly measure physical contact properties by interacting with object surfaces [20]. In recent years, tactile sensors have become remarkably better at helping robots manipulate objects [21-25]. Indeed, researchers continue finding new applications across medical devices, surgeries, rehabilitation, and advanced robotics [26-27]. Tactile sensors have even reached a point where they can match or even excel human hands in performing delicate tasks, such as grasping and twisting [26]. This tactile sensing technology enables precise measurements during task execution that surpass human capabilities [27].

The key strengths are the sensor's direct surface contact and the resulting fine-grained force and pressure data. These attributes have driven rapid improvements in robotic manipulation. Additionally, tactile sensors' precision and objectivity offer benefits for medical interventions over qualitative human touch [28, 29]. Their progress opens up new possibilities, extending applications from precise surgeries to controlling prosthetic limbs [30]. Tactile sensors, with their detailed touch feedback and consistent

performance, have the potential to outperform human hands in specific tasks [28]. Meanwhile, capacitive sensors operate on the principle of detecting changes in capacitance upon physical touch. Accordingly, multiple studies have validated the effectiveness of this technology, which is now widely used in touchscreen interfaces on smartphones and other devices [32-34]. Research efforts have also explored the development of flexible and textile-based capacitive sensors [35-37]. However, capacitive sensors do present certain challenges, including issues, such as stray capacitance and crosstalk effects. These complications are able to interpret readout circuitry for capacitive sensors as more intricate compared to resistive sensors. Consequently, the detection capabilities of capacitive sensors are heavily dependent on the sensor's specific design properties [38, 39].

In contrast, textile-based sensors are exclusively constructed from textile materials, offering diverse manufacturing methods for producing conductive fabrics for sensor applications [40]. The key advantage is the ability to manufacture these fabrics in various forms, including yarns, fibres, and coatings [41,42]. Numerous approaches and materials have been explored for creating textile sensors; with these methods ranging from sewing or embroidering with conductive fabrics, painting or printing with conductive inks [34, 43], to the utilisation of conductive polymers [44]. Other studies have integrated conductive yarns through weaving [45, 46], although this process is often intricate. Such sensors are able to involve the combination of multiple conductive and non-conductive textile layers; and some research studies have explored the use of microfiber sensors for capacitive strain measurement [47]. Additionally, piezoelectric materials have been employed to create sensors capable of detecting bending and rotational movements [48]. Materials coated with PEDOT, a conductive polymer, have been harnessed to produce stretchable polymers capable of measuring resistance variations [49]. Research has also introduced a variety of materials with potential applications in wearable devices. Notable examples include elastic conductive webbing [50] and highly flexible fabrics [51], which have been chosen for their elasticity and recovery properties. One study, in particular, demonstrated that a sensor's stretchable nature is closely tied to its manufacturing method and the resulting structure, which is why knitted structures were deemed the most suitable selection [52].

Comparatively, the use of soft tactile sensors instead of sEMG sensors for measuring muscle activities offers specific advantages and targets certain applications [14]. While sEMG sensors capture electrical signals generated by muscle contractions, tactile sensors provide measurements based on direct contact between the sensor and the object, allowing for a more comprehensive understanding of the interaction between muscles and external stimuli [15]. Tactile sensors are particularly beneficial in scenarios where information regarding the contact force, pressure distribution, or object properties during muscle activities is crucial [53-55]. By utilising tactile sensors, researchers and practitioners are able to gain insights into tactile perception, grasping forces, or object manipulation strategies employed during tasks. This knowledge can be beneficial in many areas such as robotics, prosthetics, rehabilitation, computer interaction, and creating touch-based systems, which helps to develop more accurate and responsive technologies that imitate human touch abilities [56].

Tactile sensors are systems or devices that enable the measurement of object properties and contact events through direct contact between the sensor and the object [54]. Over the past three decades [58-60], tactile sensors have made significant advancements, particularly in assisting robots with object manipulation, and their potential benefits have been explored across various applications in different fields [61]. In the medical domain, tactile sensing has been utilised in clinical diagnoses, invasive surgeries, and rehabilitation. Similarly, in robotics, tactile sensors have demonstrated effectiveness in accomplishing complex tasks, such as grasping and twisting, often outperforming human hands in various tasks [62, 63]. Textile-based sensors, meanwhile, are characterised by their textile structure and are manufactured using different techniques and materials to achieve electrical conductivity [61]. Conductive fabrics used in textile sensors can be produced at various levels, including yarn, fibre, or coatings [65-70]; although the integration of conductive yarns is a complex process [71].

The properties of stretch sensors closely depend on their fabrication and structure [72-75], with knitted structures exhibiting optimal performance in this regard. Therefore, the focus primarily lies on knitted sensors that exhibit changes in electrical resistance under strain. These fabrics can, thus, serve as strain sensors, converting physical deformations into electrical signals. The fabrication of strain sensors, however,

necessitates the consideration of key factors, such as sensitivity, flexibility, and stretchability [76-79]. Overall, in this chapter, we aim to integrate this sensor with textiles, considering the complexities of upper limb anatomy and movement. Throughout this chapter, the essential design considerations are explored, as well as experimental methodologies that are crucial for developing effective stretchable tactile sensors tailored for upper limb applications.

2.3 Upper Limb Anatomy

Understanding how the upper limb works is imperative in making a stretchy sensor that fits well with fabrics. This helps design a sensor that moves smoothly with the limb, considering its complicated structure and making it work better. Structurally, the human upper limb is divided into three distinct segments: the arm, forearm, and hand. The hand encompasses two main joints – the wrist and fingers, the latter having three joints each. Additionally, the upper limb includes the shoulder and elbow (see Figure 2.1). This complex structure involves three bones: the humerus, extending from the shoulder to the elbow; the scapula; and the clavicle, consisting of two slender bones connected to the scapula and sternum. The elbow joint is positioned between the forearm and upper arm, while the wrist is situated in the lower section of the forearm [27].

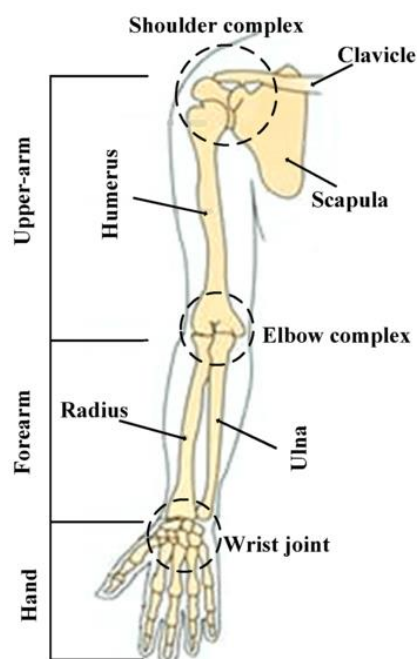


Figure 2.1: Structure of the Human Upper Limb[1]

a. Joint Movement of the Human Shoulder

Figure 2.2 below demonstrates how the shoulder is able to move in three main ways:

Adduction-Abduction: The shoulder lets the arm move towards the body's middle (adduction) or away from it (abduction), allowing for a wide range of motion.

Rotation of External-Internal: The shoulder is versatile, allowing the arm to rotate both externally and internally, enabling detailed movements and precise positioning.

Flexion-Extension: The shoulder is flexible, allowing forward (flexion) and backward (extension) movements. This flexibility helps the hand reach different positions.

These various movements highlight the importance of the shoulder, providing the upper limb with a wide range of actions crucial for everyday tasks [27].

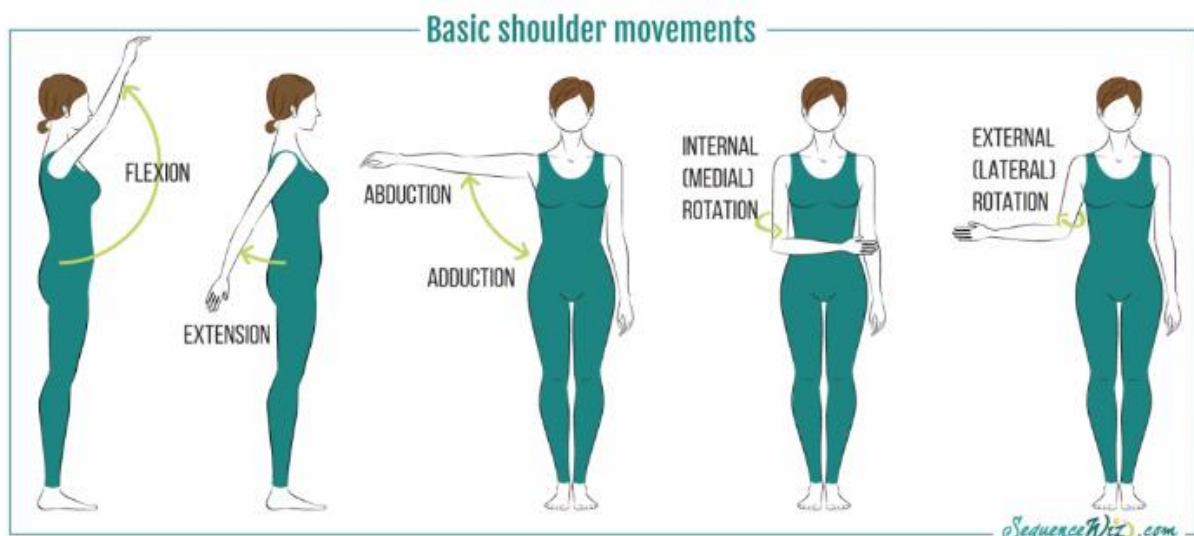


Figure 2.2: Movement of the Shoulder Joint [3]

b. Human Elbow and Motion of the Wrist Joint

Figure 2.3 below provides a clear understanding of the elbow's significance in the upper limb. Positioned between the shoulder and wrist, the elbow is a crucial joint that helps with essential movements, which has a significant two-degree freedom range,

making it essential for various motions. The first freedom dimension involves the forearm and hand rotating inward (pronation) or outward (supination). This rotation flexibility is handy, allowing the hand to take on different positions and be adaptable. Simultaneously, the second dimension includes the bending and straightening motions of the forearm (extension-flexion). This movement range not only helps with basic actions, such as reaching and grasping, but also plays a key role in more complicated tasks [28].

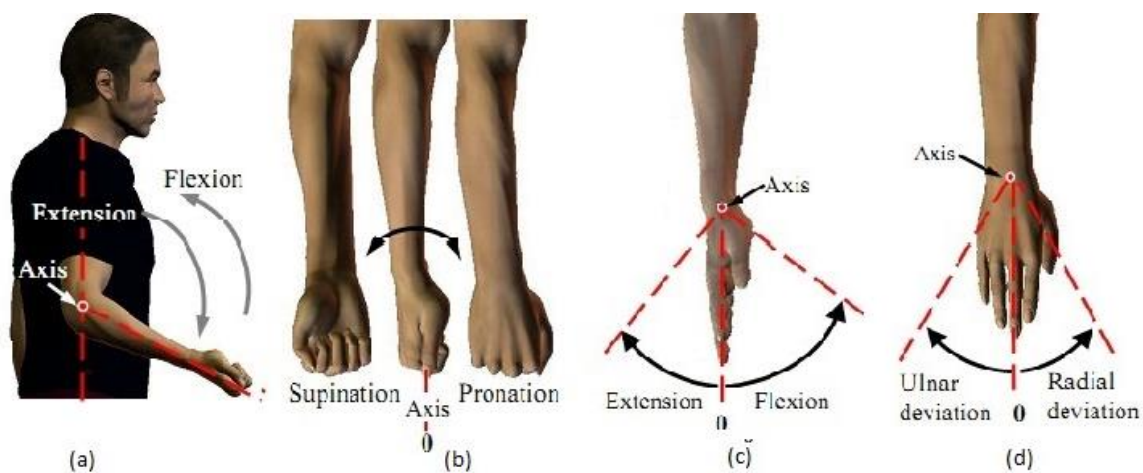


Figure 2.3: Movement of the Elbow Joint[5]

c. Motion of the Human Finger Joint

In the complex structure of the human hand, each finger has three important joints that work together to make it highly flexible. Starting at the base of each finger, there is the metacarpophalangeal joint (MP), connecting the finger to the hand's metacarpal bone. This joint allows for essential movements, including bending and straightening the finger. Moving toward the middle part of the finger, there is the proximal interphalangeal joint (PIP), positioned between the proximal and intermediate phalanges. This is a crucial hinge that enables controlled bending and straightening motions. At the tip of each finger is located the distal interphalangeal joint (DIP), situated between the intermediate and distal phalanges. This joint is crucial for precise movements, such as grasping and manipulating objects. The thumb also has its

unique setup. At the base, there is the carpometacarpal joint (CM) connecting the thumb to the carpal bones of the wrist. Moving to the middle segment, the metacarpophalangeal joint (MP) allows the thumb's pivotal movements, while the interphalangeal joint (IP) at the tip ensures fine control and manipulation.

The visual representation in Figure 2.4 below [26] illustrates this intricate arrangement, emphasising how these joints play a vital role in enabling various motions for intricate hand functions.

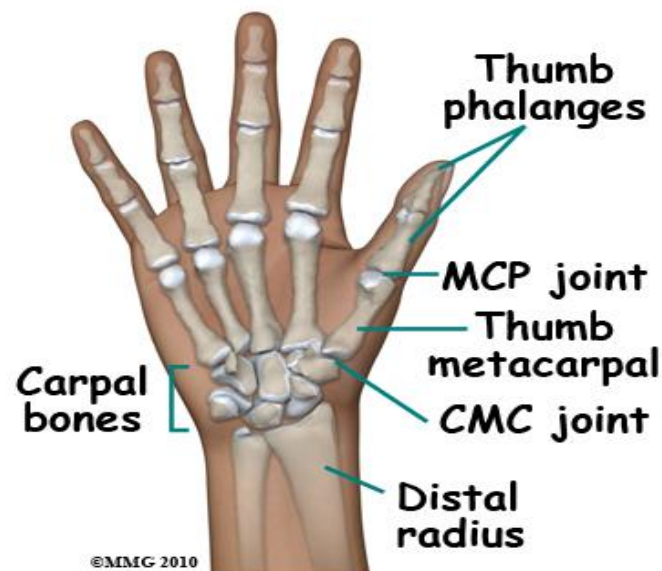


Figure 2.4: The Human Fingers and Joint [3]

2.4 Sensors

Various sensors have been specifically designed for wearable applications, collecting detailed information from the movements and activities of the human body. These sensors are crucial in both medical and consumer technologies, often using advanced machine learning algorithms to enhance recognition strategies. These methods complement traditional signal analysis and help to discern specific behavioural patterns [29]. In wearable technology, devices generally fall into two categories: primary and secondary.

- **Primary wearables**, such as wrist-worn smartphones and fitness trackers, operate independently, providing functionalities like communication, health monitoring, and activity tracking.
- **Secondary wearables** are more specialised, often measuring specific physiological parameters or movements, such as heart rate monitors used in fitness and medical applications [25,29].

Among these, smart clothing is a notable innovation, seamlessly integrating into daily life by offering physiological and contextual measurements. For instance, Neofect's RAPAEEL smart glove enhances hand rehabilitation using textile-based sensors, which improve comfort and effectiveness during prolonged use [30].

Within wearable technology, **soft robotic devices** represent a significant advancement. These devices combine flexible materials with sophisticated sensors, enabling them to interact naturally with the human body. This makes them highly suitable for rehabilitation and assistive technologies, where adaptability and responsiveness are critical. A core component of these soft robotic systems is the **tactile sensor**, which detects pressure and touch. Tactile sensors are vital for measuring grip strength, providing feedback for robotic prosthetics, and improving the user-device interaction by making it more responsive and adaptive.

In addition to tactile sensors, **Electromyography (EMG)** and **Surface Electromyography (sEMG) sensors** are essential for medical and therapeutic applications in wearable and soft robotic devices. These sensors measure electrical activity in muscles, which is key to understanding muscle function and health:

- **EMG** is invasive and requires needle insertion into the muscle, often used in clinical diagnostic settings.
- **sEMG**, on the other hand, is non-invasive, making it more practical for continuous monitoring in wearable devices. In rehabilitation, sEMG helps in diagnosing muscle disorders, monitoring recovery, and controlling prosthetics or exoskeletons to aid individuals with mobility impairments [31,32].

Capacitive sensors also play a critical role in wearable devices. They detect changes in capacitance due to proximity or touch, making them useful for interactive technologies like touchscreens. Capacitive sensors can be integrated into wearable devices such as gloves to detect hand gestures, adding another layer of interactivity. These sensors are particularly advantageous in human-device interfaces, enhancing usability [40].

In **smart textiles**, textile sensors and **stretch sensors** are essential for wearable technology. Textile sensors can be woven into fabrics to monitor physiological signals such as heart rate, temperature, and hydration. These sensors are designed for continuous monitoring, with attributes like stretchability, washability, and flexibility, making them ideal for daily wear. **Stretch sensors**, a subset of textile sensors, measure deformation in fabrics, which is useful for monitoring joint movements and for adaptive clothing that responds dynamically to the wearer's movements [22,50].

Combining these various sensors, wearable technology and soft robotic devices can provide a more holistic approach to health monitoring and rehabilitation. For instance, a smart glove designed for hand rehabilitation may integrate tactile sensors to monitor grip strength, sEMG sensors to track muscle activity, and stretch sensors to adapt to hand movements [27,34]. This multi-sensor integration enhances both the accuracy and responsiveness of the device, providing real-time, actionable feedback that improves therapeutic outcomes and the overall user experience.

2.5 Hysteresis Background and Neural Network Applications

Hysteresis in tactile sensors poses a significant challenge in robotics, where precision is critical for control and decision-making. Various methodologies have been proposed to address this issue, but many of these methods face practical limitations that reduce their effectiveness in real-world applications.

One approach involves adapting the external control loop of the sensor system to compensate for hysteresis by estimating errors between desired and measured forces. While this technique shows promise in enhancing accuracy and performance in robotic systems [80], it can be computationally intensive, requiring continuous recalibration and adaptation, which may not be feasible for fast or real-time applications.

Researchers have also explored the use of Recurrent Neural Networks (RNNs) to model hysteresis patterns in piezoelectric actuators, capturing the nonlinear relationship between input voltage and output displacement. Although RNNs can improve positioning accuracy [81], their implementation is complex and may suffer from long training times and difficulty in generalising to new input conditions, limiting their practical application. The Generalised Prandtl–Ishlinskii Model (GPIM) has been employed for real-time hysteresis compensation by training the model with experimental data, significantly enhancing force measurement accuracy [82]. However, GPIM requires extensive and precise training data, and its effectiveness diminishes when the system operates outside the conditions it was trained. This makes it less adaptable in dynamic environments where conditions frequently change. Innovative designs, such as soft tactile electronic skin, aim to minimise hysteresis by reducing mechanical and electrical memory effects [83].

Methods like Gaussian processes with sensory Markov properties, which model and estimate hysteresis behaviour, offer improved force measurement accuracy [85]. However, they often require significant computational resources and may not perform well in low-power or embedded systems where processing capability is limited.

In smart-material systems, an inverse feedforward controller based on the Preisach model has been introduced to control hysteresis nonlinearities by generating an inverse compensation signal [86]. Although this method can reduce hysteresis, it often depends on precise modelling, which is challenging when dealing with the complex nonlinearities of soft materials used in tactile sensors.

Similarly, while modified Prandtl–Ishlinskii models have been developed to capture asymmetric hysteresis behaviour in piezoelectric actuators [88], they require detailed characterisation of the actuator's behaviour, which may not be feasible for all sensor types, especially those that experience highly variable input conditions.

Methods such as radial basis function neural networks, fuzzy neural networks, and hybrid neural networks have been explored for hysteresis compensation in soft sensors [89-95]. While these methods can effectively reduce hysteresis in controlled environments, they tend to lack robustness in real-world applications, where factors such as sensor degradation, environmental changes, and varying loads introduce additional complexities.

In the context of conductive fibre-based tactile sensors, a Backpropagation Neural Network (BPNN) has been successfully employed to mitigate hysteresis nonlinearity, improving sensor accuracy [96]. However, the BPNN approach, like other neural networks, can require extensive data for training and may be sensitive to variations in the input data, reducing its effectiveness when applied to dynamic, real-time tasks. Alternative sensing methods, such as capacitive, piezoelectric, optical, resonant, Hall effect, and strain gauge-based compensation, offer unique advantages in terms of accuracy and sensitivity [97]. However, these methods often involve trade-offs in terms of sensor size, power consumption, or complexity, making them less practical for widespread use in wearable devices or low-power applications. Despite the progress made with these methodologies, practical and effective solutions for hysteresis compensation remain elusive, particularly in dynamic, real-world scenarios.

Many approaches either require too much computational power, are overly complex, or lack the robustness needed for adaptive environments. The current study proposes a novel approach using BPNNs to address these challenges, building on previous research findings while aiming to provide a more robust and practical solution for hysteresis correction in tactile sensors. This method is expected to offer enhanced accuracy in real-time applications, contributing valuable insights into improving hysteresis compensation in tactile sensors used in wearable technology and robotics. Chapter Four will explore these methodologies in more detail, critically evaluating their effectiveness and presenting new strategies to mitigate hysteresis.

This chapter provides an extensive review of various sensors, focusing on their use in wearable technology and soft robotics. While the chapter outlines numerous hysteresis correction methods, a critical evaluation reveals notable trade-offs and gaps in their practical implementation.

For example, **machine learning approaches** like Recurrent Neural Networks (RNNs) demonstrate effectiveness in capturing nonlinear hysteresis behaviour, yet they often require large training datasets and suffer from high computational demands. These requirements limit their feasibility in real-time applications, particularly in low-power or embedded systems used for wearable devices. Moreover, the challenge of generalising RNNs to new and dynamic input conditions raises concerns about their adaptability in unpredictable environments, such as rehabilitation settings.

The **Generalised Prandtl–Ishlinskii Model (GPIM)**, while promising in improving force measurement accuracy, depends heavily on the quality and extent of training data. In scenarios where the operational conditions deviate from the training parameters—such as varying user behaviours in rehabilitation—the model’s performance deteriorates. This lack of robustness in dynamic environments underscores the need for adaptive models capable of real-time recalibration.

Innovative sensor designs, such as **soft tactile electronic skin**, aim to address hysteresis by minimising mechanical memory effects. However, these solutions often introduce compromises, such as reduced sensitivity or increased material complexity, which limit scalability and integration into existing rehabilitation systems. While these designs push the boundaries of sensor capabilities, their high production costs and technical challenges remain barriers to widespread adoption.

Comparatively, **capacitive sensors**, **piezoelectric sensors**, and **strain gauges** offer unique advantages, including high sensitivity and compact size. However, their susceptibility to environmental noise, such as temperature fluctuations, limits their reliability in rehabilitation devices. For instance, piezoelectric sensors may exhibit performance degradation under prolonged use, posing challenges in long-term rehabilitation applications. Despite these advancements, **real-world case studies** integrating these methodologies into upper limb rehabilitation devices are sparse. For example, while some studies report successful implementations of neural network models for prosthetic control, there is limited evidence detailing their adaptability to diverse patient groups, such as stroke survivors or individuals with Parkinson's disease. Furthermore, there is a lack of comparative studies evaluating how different sensor types perform under identical rehabilitation tasks, such as gripping or fine motor control exercises. Such analyses would offer valuable insights into their suitability for specific clinical applications.

Finally, while the chapter references numerous studies, it does not fully explore the broader implications of these findings. For instance, the trade-offs between computational efficiency and accuracy in hysteresis compensation methods are critical for ensuring practical utility in resource-constrained systems. Addressing these trade-offs is essential for advancing sensor technologies beyond experimental setups to robust, real-world applications.

2.6 Conclusion

In conclusion, this chapter provides a comprehensive overview of the design, assembly, and implementation of a soft tactile sensor. By leveraging fabric-based materials and innovative circuitry, the sensor demonstrates remarkable adaptability and accuracy in capturing pressure variations. However, as with any sensor technology, addressing challenges, such as hysteresis is imperative to the enhancement of reliability and precision. In the subsequent section, the details of hysteresis will be explored, as well as how it affects tactile sensors. This will help in advancing the understanding into how to make the sensors work even better by improving their performance.

Chapter Three:

Design and Implementation of a Soft Tactile Sensor

3.1 Introduction

Tactile sensors are crucial in various fields, from robotics to healthcare, by enabling the detection and measurement of physical interactions with surfaces. Among the different types of tactile sensors, soft tactile sensors are notable for their adaptability and versatility, particularly in scenarios where interaction with delicate or irregular surfaces is required. In this chapter, the intricate process of designing and implementing soft tactile sensors are explored, determining the innovative methodologies and materials that underpin their functionality. Soft tactile sensors represent a significant advancement in sensor technology, offering a flexible and adaptable solution for capturing tactile information across a wide range of applications. Their ability to conform to irregular surfaces and withstand deformation makes them indispensable in fields such as wearable technology, human-robot interaction, prosthetics, and biomedical engineering. Hence, understanding the design principles and fabrication techniques behind soft tactile sensors is paramount for unlocking their full potential in real-world scenarios.

This exploration begins by exploring the materials used in the fabrication of soft tactile sensors; examining the properties and characteristics of key components, such as conductive fabrics and threads, that enable the sensor to detect and respond to pressure changes. By understanding the underlying principles of piezoresistivity, it is possible to appreciate how these materials interact to convert mechanical stimuli into electrical signals, laying the foundation for sensor functionality. Beyond materials, the assembly process of soft tactile sensors is also examined, investigating the complexities of integrating sensor components with textiles to create a functional sensing platform. From selecting the appropriate stitching techniques to optimising contact points and circuit paths, each step in the assembly process is carefully orchestrated to ensure the sensor's reliability and performance.

With the sensor assembled, the focus is on devising experiments and analysing the signals, noting how the sensor reacts to real-life situations. By making special sleeves and using microcontrollers such as Arduino, it is possible to collect and study the data from touch in a controlled setting. The data is carefully gathered and studied to learn more about how well the sensor works in different situations, helping the possibility to improve it. As the readout circuitry is explored, how the electrical signals are turned into useful information is explained; and by employing voltage dividers and multiplexing circuits, it is possible to enhance the sensor's capabilities and streamline data acquisition processes. Additionally, through detailed circuit diagrams and code implementations, how the sensor system works inside is explained, in order to copy and build on what has been found.

3.2 Designing a Soft Tactile Sensor

The proposed design sensor utilises fabric-based sensors due to their simple design, ease of fabrication. With the ability to stretch and bend easily, these sensors adapt well to soft surfaces, making them ideal for various applications. In the following section, the fabrication and design of the tactile sensor are explored, outlining my innovative approach and the key considerations driving the current study's design choices.

1. Use of Materials

The fabric sensor employed in this study operates based on the piezoresistive effect, which induces a decrease in the electrical resistance of a piezoresistive material upon applying pressure. The sensor consists of two main components:

- **EeonTex™ knitted conductive fabric:** This commercially available fabric is knitted, conductive, stretchable, has a thickness of 0.38mm, and has a mass per unit area of 113.78g/m². The fabric exhibits an elongation of 40% at break and a wrap recovery of 85% after stretching. It primarily comprises 72% nylon and 28% spandex, with a proprietary conductive coating. [99]
- **Silver-plated conductive thread:** To establish conductive connections with measuring devices, a silver-plated conductive thread is used. MADEIRA yarn (detox 290 ± 6 HC 40) is employed for sewing. [100].

These materials work synergistically to create a tactile sensor that detects and converts pressure changes into analogue electrical signals, typically in voltage.

2. Sensor Assembly

The assembly of the sensor involved integrating the EeonTex™ fabric with silver-plated conductive thread to create a functional device for measuring muscle activities. The choice of materials was pivotal: the EeonTex™ fabric provides stretchability and conductivity, while the silver-plated thread, with its low resistance and high conductivity, ensures reliable electrical connections and optimises the sensor's performance.

Prior to the commencement of my PhD, initial exploratory work on stitch designs for integrating conductive textiles was conducted by an MSc student in the Robotics Laboratory. Although this work was not published, it provided valuable insights into sensor integration and highlighted early challenges in maintaining consistent electrical conductivity during fabric deformation. Building on these foundational experiments, my research introduced a novel approach using Arduino technology for real-time data processing, significantly enhancing the precision and functionality of the sensor system.

In the PhD phase of this project, my work introduced a significant advancement through the integration of Arduino technology, marking a shift from the earlier design trials. This addition enabled real-time data processing, allowing for more precise control and interpretation of sensor data, which was not achievable with previous methods. The use of Arduino technology in the PhD phase greatly enhanced the analytical capabilities of the sensor, improving accuracy and enabling more effective measurement of muscle activity.

The sensor was assembled by connecting the tactile fabric with textiles using silver-coated conductive thread, which is fully silver-plated and made of 100% polyamide. This thread, with a linear resistance of less than 300Ω/m, was chosen for its low resistance characteristics, crucial for optimising the sensor's contact points and circuit paths. Data on the resistance versus force relationship was collected manually and

analysed using MATLAB to generate plots that visualise the sensor's performance (see Figure 3.1)

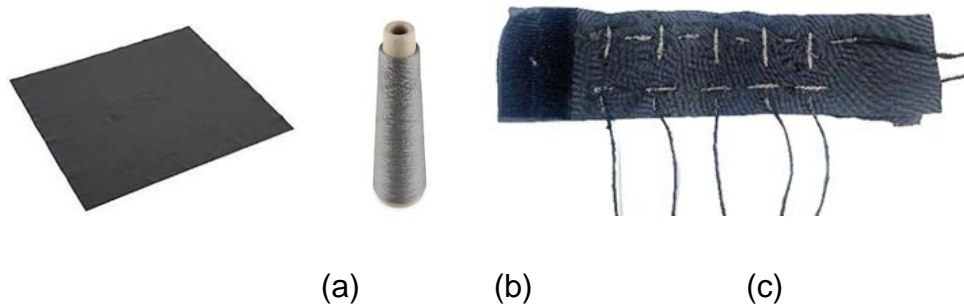


Figure 3.1: *Materials used for sensor development: (a) conductive stretchable fabric; (b) silverplated conductive thread; (c) Fully designed tactile sensor*

Figure 3.1 (a) above displays the EeonTex™ knitted conductive fabric, which contains conductive fibres that allow electrical current to flow through it. This fabric is used in various applications, such as smart textiles, wearable technology, and sensor systems. Figure 3.1(b) displays the silver-plated conductive thread made by coating a base thread with a layer of silver, which is often used with conductive fabrics to create wearable electronics and other devices. The objective of the specific design of the sensor is the detection of the electric resistance signals when applying forces, while Figure 3.1 (c) shows the fully designed soft tactile sensor with ten sensing points.

3. Experimental Setup and Signal Analysis

The experimental setup was designed to evaluate the sensor's ability to recognise hand movements under real-world conditions, focusing on upper limb rehabilitation, which is a critical but often under-resourced area in stroke recovery. A custom-designed sleeve was developed to house the sensors comfortably around the upper limb, enabling precise signal capture during movement, while linking this wearable technology with Arduino for real-time data processing and analysis.

4. Novel Sensor Configuration

- **Sleeve Design:** The sleeve was embedded with tactile sensors and securely attached to the upper limb. These sensors were connected to an Arduino controller via analogue pins, allowing for continuous data collection and analysis. This Arduino integration represents a key novelty of the study, as it enabled the transition from basic sensing experiments to real-time monitoring and interpretation, making the setup applicable for dynamic, real-world applications like rehabilitation.
- **Sampling Rate:** The Arduino controller, maintaining a sampling rate of 1 kHz, allowed for fine-grained signal capture during hand movements. This high frequency ensured precise and accurate recording of tactile sensor data, supporting the goal of using the system for sensitive and responsive applications in upper limb therapy.
- **Tactile Sensor:** The sensor, measuring 10 x 30 cm², consisted of ten individual sensing points, strategically placed to capture muscle activity during rehabilitation exercises. The sensor was secured using double-sided sticky tape and non-conductive fabric to ensure consistent placement, a crucial factor for maintaining data integrity during prolonged or repetitive movements.
- **Signal Integrity:** Conductive thread was used to reinforce sensor placement and improve signal transmission, ensuring reliability during movement. This enhancement directly contributed to better data accuracy, making the system suitable for precise muscle monitoring, a critical requirement in rehabilitation.

5. Readout Circuitry and Data Processing

The integration of the Arduino platform with multiplexing circuits for data handling is a core innovation in this study, enabling the system to process multiple tactile sensors with minimal hardware input. This configuration made the setup efficient for real-world applications, where multiple points of data need to be processed without excessive complexity.

- **Multiplexing Circuits:** These circuits allowed multiple sensor inputs to be managed efficiently without overloading the Arduino's analogue input capacity.

By dynamically switching between the sensing points, multiplexing circuits maximised the data captured, ensuring comprehensive monitoring of hand movements and muscle activity.

- Custom Arduino Code: A unique Arduino code was developed to process and interpret the sensor data in real-time. This innovation allows for immediate feedback and monitoring, critical in rehabilitation scenarios where real-time analysis is necessary to track patient progress and adjust therapy as needed.

6. Novelty in Application: Upper Limb Rehabilitation

The true novelty of this work lies in the combination of tactile sensors, Arduino-based real-time data processing, and the specific application in upper limb rehabilitation. While previous methods for capturing hand movements have been either too slow or limited in their real-world applicability, this setup provides a practical and real-time solution for healthcare professionals to monitor and analyse muscle activity during rehabilitation. This is particularly beneficial for stroke survivors who require precise, responsive feedback systems to improve motor control and facilitate recovery.

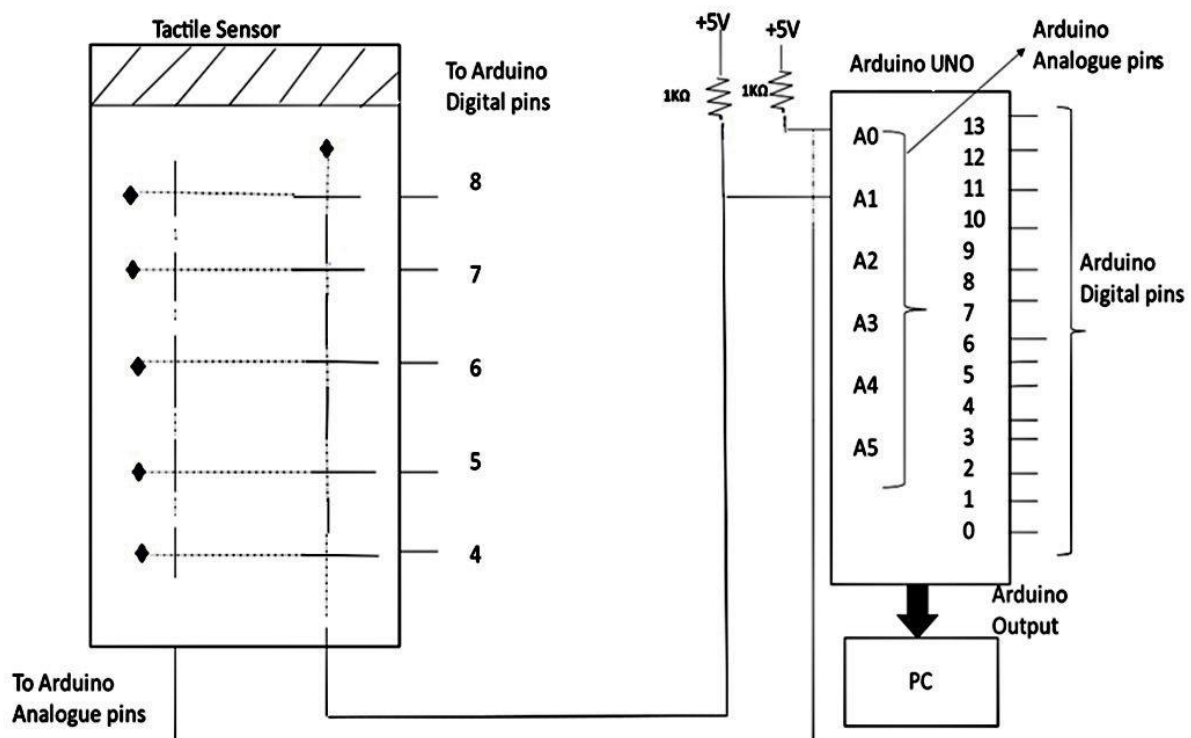


Figure 3.2: Block diagram depicting the thread arrangement in the sensor and full circuit connections

The block diagram in Figure 3.2 illustrates the detailed arrangement of the circuit connections and threads within the sensor system. The threads are organised into a dual-column and five-row configuration, with each row acting as a sensing element. The key aspect of this configuration is the use of a voltage divider circuit to measure resistance changes, which occur as pressure is applied to the tactile sensors.

7. Voltage Divider Operation

The voltage divider circuit is formed by connecting the tactile sensor in series with a known external 1kΩ resistor. When pressure is applied to the sensor, its resistance changes, causing a corresponding variation in the output voltage across the 1kΩ resistor. The voltage divider equation for this setup is given by:

$$V_{out} = V_{in} \times \frac{R_{sensor}}{R_{sensor} + R_{fixed}}$$

Where:

V_{out} Is the voltage across the known resistor (read by the Arduino's analogue pins A₀ and A₁).

V_{in} Is the supply voltage (5V in this case).

R_{sensor} Is the variable resistance of the tactile sensor.

$R_{fixed} = 1\text{k}\Omega$ is the known resistor value.

8. Digital Pin Switching and Circuit Operation

The digital pins (A4 to A8) on the Arduino are used to control the five rows of the sensor configuration by switching the lower rail of the voltage divider between 0V and 5V. By toggling these digital pins on and off, the Arduino selectively activates the different sensor rows, ensuring that each sensor is read in sequence. This switching process allows multiple sensor points to be read without the need for numerous analogue input pins, significantly simplifying the hardware design.

When a digital pin is set to 0V, the corresponding row is connected to the lower rail of the voltage divider, allowing current to flow through the sensor and the 1kΩ resistor. The resulting voltage across the 1kΩ resistor is then measured by the analogue input pin. When the digital pin is set to 5V, the circuit is effectively turned off, preventing current from flowing through that particular sensor.

9. Converting ADC Values to Resistance

The analogue input pins (A0 and A1) of the Arduino read the voltage output (V_{out}) from the voltage divider and convert it to a digital value using the built-in Analog-to-Digital Converter (ADC). The ADC output is a 10-bit value (ranging from 0 to 1023) that corresponds to the input voltage range of 0V to 5V.

To convert the ADC values to the resistance of the tactile sensor, the following equation is used:

$$R_{sensor} = R_{fixed} \times \left(\frac{V_{in}}{V_{out}} - 1 \right)$$

R_{sensor} Is the calculated resistance of the sensor,

V_{out} Is derived from the ADC value: $V_{out} = \left(\frac{ADC \text{ Value}}{1023} \right) \times V_{in}$

$V_{in} = 5V$,

$R_{fixed} = 1K\Omega$.

To reflect the updated data processing approach, Figure 3.3 has been modified to plot sensor resistance values over time (pressure) rather than raw ADC values. This conversion offers a more intuitive understanding of the sensor's behaviour, as the resistance changes are directly linked to the pressure applied during testing. The plot displays real-time fluctuations in resistance as hand movements are performed, offering detailed insight into the sensor's response to varying forces. This adjustment provides a clearer representation of how the sensor interacts with the physical forces applied during the experiment, thereby improving the overall analysis of the sensor's performance.

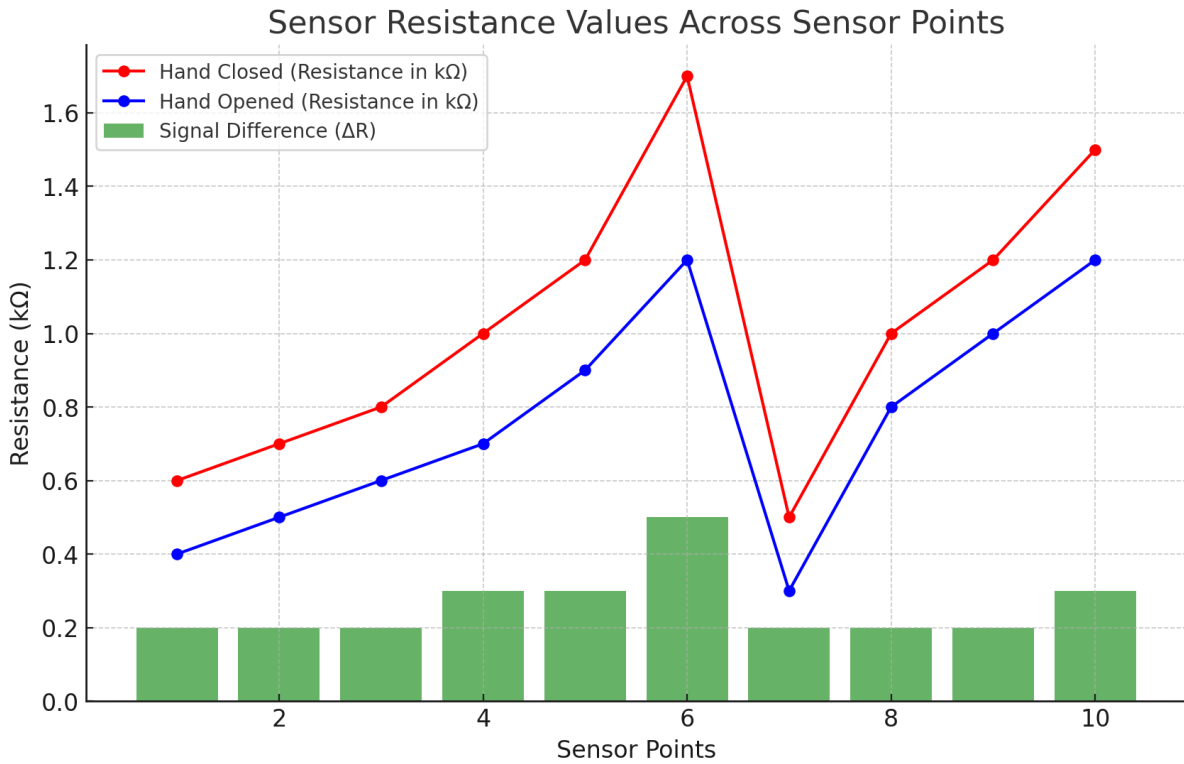


Figure 3.3: Tactile Sensor Output

The graph in Figure 3.3 represents the sensor output, measured in resistance ($k\Omega$), as the hand dynamically transitions between open and closed positions. The red line shows the average resistance values across ten sensing points during the closed-hand state, with each point reflecting the pressure exerted by the underlying muscles. The most significant resistance change was observed at point six ($1.7 k\Omega$), followed by point ten ($1.5 k\Omega$) and point four ($1.2 k\Omega$). The smallest change was at point seven, registering at $0.8 k\Omega$.

In contrast, the blue line depicts the sensor output during the open-hand state, showing variations in resistance under muscle pressure. Similar to the closed-hand state, point six exhibited the largest resistance change ($1.2 k\Omega$), while point seven recorded the least change, with a resistance value of $0.3 k\Omega$. The green bars illustrate the differences in resistance between the open and closed states, providing a visual comparison of the sensor response in both conditions.

The hand postures were dynamic throughout the data collection, meaning the hand actively moved between open and closed positions. This dynamic movement allowed the sensors to capture real-time variations in resistance as the hand transitioned between states, offering more comprehensive data than static measurements.

To validate the tactile sensor's functionality, it was tested under various conditions where participants alternated between rapid and slow hand movements. The sensor, attached to the forearm, recorded the resistance changes, and the collected data were saved in Excel files for further analysis (see Figure 3.4).

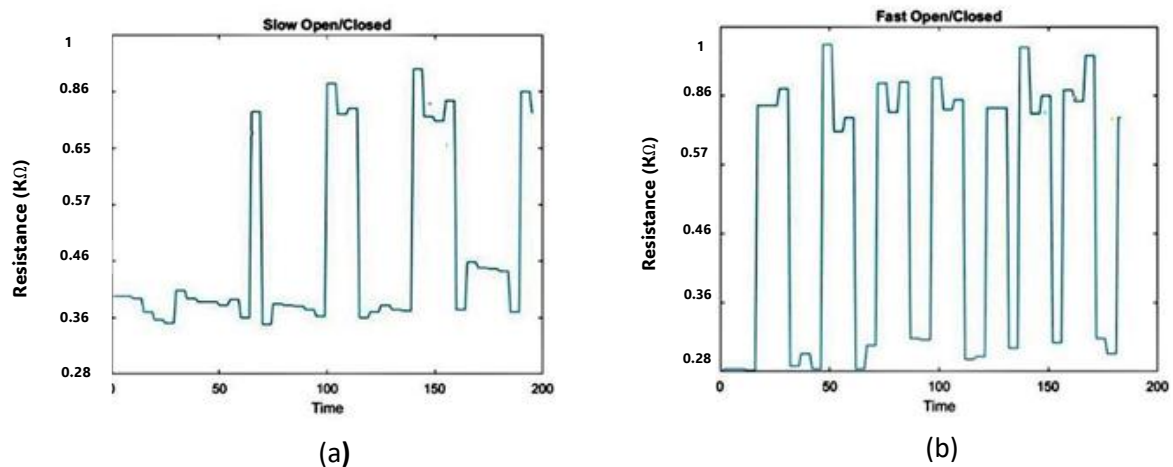


Figure 3.4: (a) The sensor output during slow opening/closing of hand; (b) The sensor output during fast opening/closing of hand

Figure 3.4 displays the sensor output variations in terms of resistance during hand movements. The y-axis shows resistance values in kilohms (kΩ). The left graph (a) illustrates the sensor response during slow hand movements, while the right graph (b) shows the response during fast movements. In both cases, the resistance values fluctuate as the hand opens and closes, with the slower movements producing smoother transitions and the faster movements resulting in more abrupt changes.

The data shows that resistance values vary significantly with hand movement speed. For slow movements, resistance values range from approximately 0.28 kΩ to 0.86 kΩ. For fast movements, the resistance fluctuates within the same range, but the frequency of changes is higher, reflecting the quicker transitions between open and closed states.

Table 3.1: Statistical Analysis of Sensor Outputs During Slow and Fast Hand Movements

Movement Type	Mean	Standard Deviation	Confidence interval	Time interval (sec)
Slow movement	0.691	0.077	92%	40
Fast movement	0.509	0.090	94%	20

Table 3.1 provides a statistical overview of sensor output (resistance in k Ω) during slow and fast hand movements. For slow movements, the mean resistance is 0.691 k Ω with a standard deviation of 0.077 k Ω , while for fast movements, the mean is 0.509 k Ω with a standard deviation of 0.090 k Ω . The confidence intervals for slow and fast movements are 92% and 94%, respectively. Data was collected over 40 seconds for slow movements and 20 seconds for fast.

This analysis aimed to assess the sensor's performance at different movement speeds by examining mean resistance, variability (standard deviation), and reliability (confidence intervals).

The table shows that sensor output is influenced by movement speed. Higher mean resistance during slow movements suggests more pronounced muscle contractions, while increased variability in fast movements reflects more fluctuation in sensor readings. These results underscore the need to account for movement speed in sensor data analysis, as it impacts both output magnitude and consistency.

3.3 Conclusion

This chapter has explored a carefully engineered tactile sensor designed to detect muscular contractions. Constructed using EeonTex conductive fibres known for their impressive bidirectional stretch and elastic properties, the sensor is primarily made of a nylon and spandex fabric blend coated with a conductive thread. The positive characteristics of this fabric in various electronic tactile applications have been well-documented in previous studies. The study results indicate that the sensor effectively detects arm muscle movements. Positioned on the forearm, it consistently registered responses during both slow and rapid hand movements. Notably, distinct signals were

observed for varying movement speeds; faster actions yielded more signals compared to slower ones. This straightforward, user-friendly device accurately correlates with muscle contractions, exhibiting versatility across different settings and offering cost-effectiveness, making it suitable for various industries. One important aspect of this sensor is that it does not require the usual electrodes. Its special design means it does not rely on complicated processing to detect muscle contractions. The fact that it can accurately detect muscle movements without being invasive makes it highly suitable for applications such as healthcare and body-controlled devices.

Chapter Four:

Modified Nonlinear Hysteresis Approach of a Tactile Sensor

4.1 Introduction

Soft tactile sensors based on piezoresistive materials play a pivotal role in a multitude of applications, owing to their capability to provide large-area sensing. These sensors have found utility in fields such as soft robotics, wearable technology, medical devices, consumer electronics, and gaming, revolutionising the way people interact with technology and the world. However, despite their wide-ranging applications, these sensors face a significant challenge – hysteresis. Hysteresis is a phenomenon that affects the accuracy of tactile sensors, making it imperative to seek innovative solutions for its mitigation. Subsequently, this chapter introduces a novel approach that employs a backpropagation (BP) neural network to address the hysteresis nonlinearity in conductive fibre-based tactile sensors. Hysteresis, in the context of tactile sensors, refers to the discrepancy in sensor response when subjected to the same force, depending on whether the force is increasing or decreasing. Specifically, this nonlinearity can significantly impact the precision and reliability of tactile sensor readings.

To evaluate the effectiveness of the proposed method, four sensor units were designed, each of which underwent force sequences to collect corresponding output resistance. The critical aspect of the approach was the utilisation of a backpropagation network trained with these sequences, effectively correcting the resistance values. The training process demonstrated exceptional convergence, fine-tuning the network's parameters to minimise the error between predicted and actual resistance values. Consequently, the trained BP network accurately predicted the output resistances, showcasing its potential to mitigate hysteresis nonlinearity. Moreover, the validation experiments underscore the primary contribution of this study, as the proposed method reduced the maximum hysteresis error from 24.2% of the sensor's full-scale output to a more manageable 13.5%. This substantial improvement establishes the approach as a promising solution for enhancing the accuracy of soft tactile sensors based on piezoresistive materials. While complete hysteresis elimination in tactile sensors may not be entirely feasible, my method effectively

modifies the hysteresis nonlinearity, leading to significantly improved sensor output accuracy. This discussion is further explored in subsequent sections, explaining various aspects of hysteresis, important ideas behind hysteresis modelling and neural networks, the creation of soft tactile sensors, results and discussions, system sensitivity analysis, and a detailed analysis and discussion of the findings.

4.2 Types of Hysteresis in Tactile Sensors

Understanding the various types of hysteresis in tactile sensors is of paramount importance for improving sensor performance and accuracy [73]. Hysteresis, in the context of tactile sensors, can manifest in diverse forms, each with unique characteristics and influences on sensor behaviour. Indeed, a comprehensive grasp of these hysteresis types is essential for devising effective compensation strategies; thus, this section explores rate-dependent, displacement-dependent, and material-dependent hysteresis.

a. Rate-Dependent Hysteresis:

Rate-dependent hysteresis, often encountered in tactile sensors, is distinguished by its sensitivity to the rate at which forces are applied and removed. This hysteresis type can lead to discrepancies in sensor readings when forces are dynamically changing [78]. For instance, in robotic applications, where rapid and precise force control is crucial, rate-dependent hysteresis can result in inaccuracies. Understanding this form of hysteresis is pivotal for designing sensors that respond accurately to varying force application speeds (see Figure 4.1).

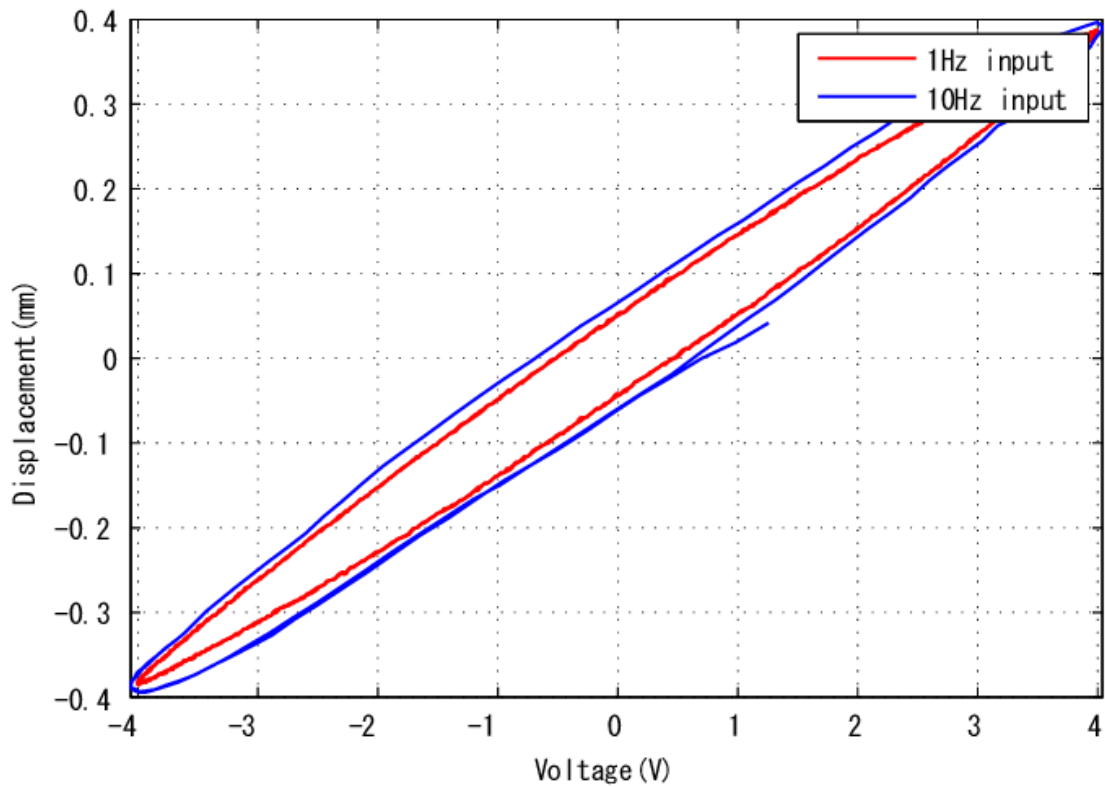


Figure 4.1: Rate -Dependent Hysteresis[78]

b. Displacement-Dependent Hysteresis:

Displacement-dependent hysteresis is closely tied to the displacement range of tactile sensors. This hysteresis type influences the sensor's response based on how far it is compressed or stretched. In applications where tactile sensors are subjected to varying degrees of deformation, such as soft robotics or medical devices, the impact of displacement-dependent hysteresis on sensor accuracy becomes apparent [80]. By uncovering the characteristics of this hysteresis type, researchers and engineers are able to tailor their compensation techniques to match the specific operational requirements of tactile sensors (see Figure 4.2).

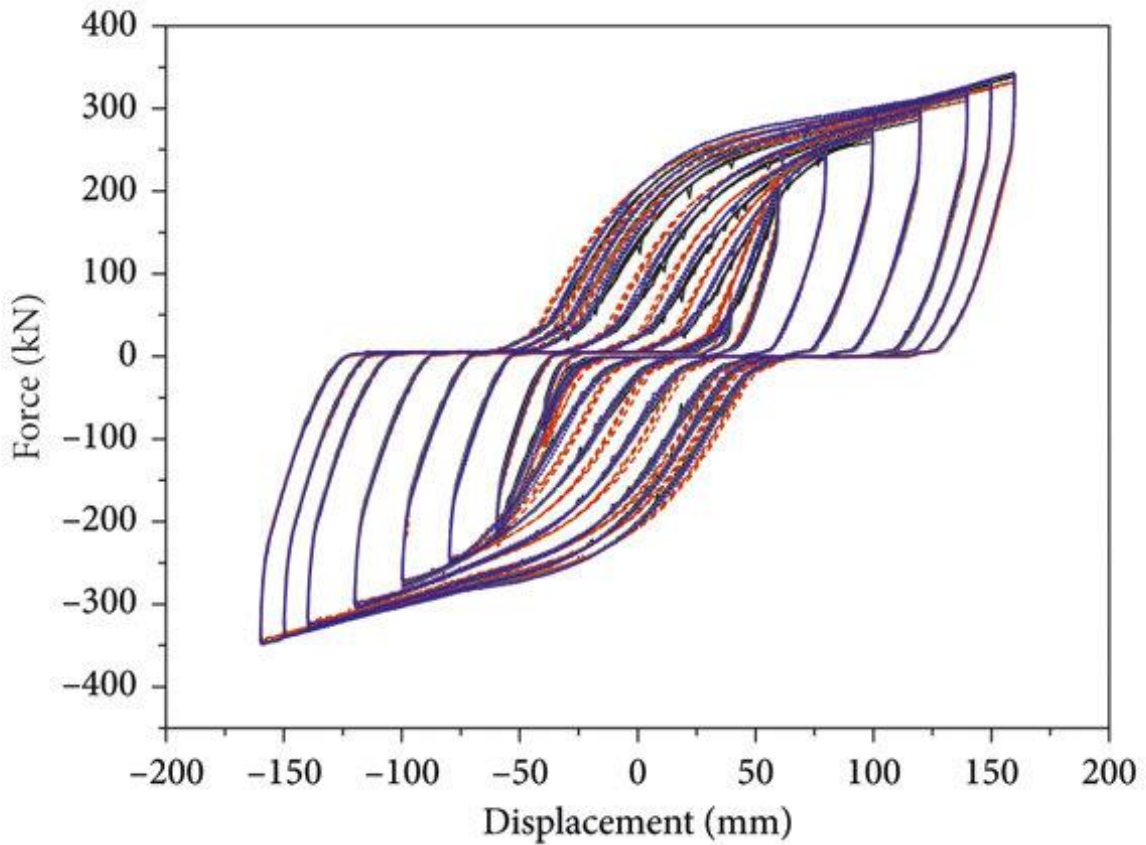


Figure 4.2: *Displacement-Dependent Hysteresis*[80]

c. Material-Dependent Hysteresis:

Material-dependent hysteresis pertains to the properties of the materials used in the construction of tactile sensors. The materials themselves can introduce nonlinearity and memory effects, influencing the sensor’s response to external forces. By understanding the role of materials in hysteresis, researchers can make informed decisions in selecting or modifying materials to minimise the impact of this type of hysteresis [79-81]. Real-world examples and experiments further illustrate the significance of material-dependent hysteresis in tactile sensor design and application (see Figure 4.3).

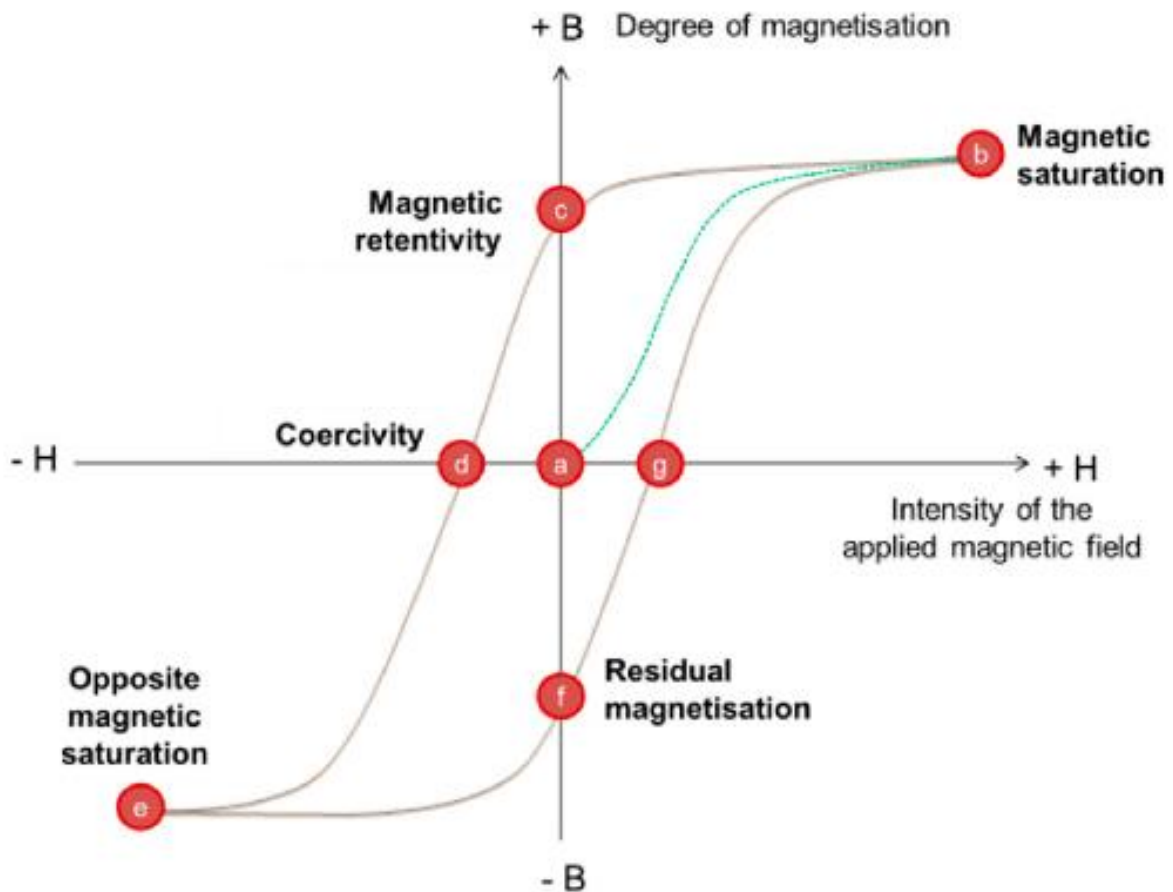


Figure 4.3: Material-Dependent Hysteresis[25]

As the current study proceeds, these insights lay the groundwork for the proposed approach to hysteresis mitigation in conductive fibre-based tactile sensors.

4.3 Key Concepts

Subsequent sections explore the theoretical background underlying hysteresis modelling, curve-fitting models, and neural networks. Additionally, how these methods are used in the proposed approach are explored, with a simple diagram and a step-by-step algorithm shown to make it clear.

a. Curve-Fitting Model(s)

Curve-fitting models serve as indispensable tools in the analytical toolbox, enabling the exploration of relationships between variables by examining diverse data points. Their effectiveness in predicting outcomes and uncovering patterns depends on both

the quality of the data and selecting the right model. [99]. In the current study, the spotlight falls on the pivotal role of curve-fitting models, specifically employing a polynomial curve-fitting model to address hysteresis nonlinearity inherent in tactile sensors. The selected polynomial curve-fitting model can be expressed mathematically using Equation (1):

$$R = a_0 + a_1F + a_2F^2 + \dots + a_nF^n \quad (1)$$

Where R is the corrected output; and F is the raw input, in the context of the polynomial curve-fitting model, the coefficients a_0 , a_1 , and a_n , exist in the space of real numbers. These coefficients play a pivotal role in tailoring the model to the specific characteristics of the hysteresis nonlinearity. This process involves determining the coefficients by minimising the sum of the squared errors between the corrected output and the actual output, effectively fine-tuning the model to enhance the occurrence. Hence, the polynomial curve-fitting model is like a versatile tool for understanding how the raw data from a tactile sensor relates to the corrected output. By including terms such as (F^2, F^3, \dots, F^N) the model becomes good at handling the tricky aspects of hysteresis. Moving on to the next sections, the main focus is on checking whether this curve-fitting model effectively handles the challenges of hysteresis, making the tactile sensor readings more dependable overall.

b. Neural Network

Neural networks (NN) are computational models that learn complex patterns and relationships from data. With their interconnected layers and mathematical operations, NN enables accurate predictions and valuable insights in various domains. In the present study, a Backpropagation Neural Network (BPNN) was employed to modify the hysteresis nonlinearity of the tactile sensor [96].

The BPNN algorithm consists of two phases: forward and backward. In the forward phase, the input (force sequence) is propagated through the network to generate the corresponding output resistance of the tactile sensor. During the backward phase, the error between the predicted output and the actual output is propagated backwards through the network to adjust the weights of the nodes [97]. This training process helps the BPNN minimise the difference between predicted and actual output resistance.

Once trained, the BPNN can accurately predict the output resistance for any given force sequence.

The neural network's effectiveness in managing hysteresis nonlinearity lies in its ability to iteratively learn from input-output data pairs and refine its predictions through weight adjustments. The entire process can be summarised as shown in Figure 4.4 and Equation (2) below.

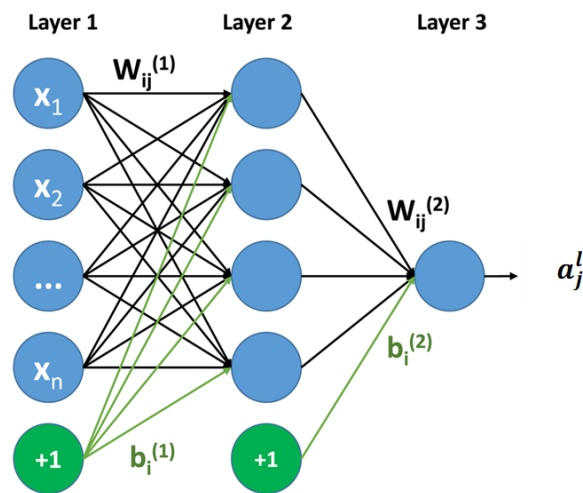


Figure 4.4: Neural Network Architecture

$$a_j^l = \sigma(\sum_i w_{ji}^l a_i^{l-1} + b_j^l) \quad (2)$$

In this example, a_i^{l-1} represents the output of node i in layer $l-1$; w_{ji}^l is the weight connecting node i in layer $l-1$ to node j in layer l ; a_i^{l-1} is the output of node i in the previous layer; b_j^l is the bias of node j in layer l ; and σ is the activation function. In the backward phase, the error between the actual output and the desired output is propagated backwards through the network to adjust the weights of the nodes. The error δ_j^l of each node j in layer l measures how much that node contributes to the overall network error. It is defined as the partial derivative of the total error E for the input z_j^l of node j in layer l .

$$\delta_j^l = \frac{\partial E}{\partial z_j^l} \quad (3)$$

The weight updates are then determined based on this network error. The weights are adjusted in a direction that reduces the error by an amount proportional to the error and the previous layer's output. This is known as the delta rule, which is represented by the following Equation (4):

$$\Delta w_{ji}^l = -\eta \delta_j^l a_i^{l-1} \quad (4)$$

Here Δ is the learning rate, which controls the size of weight updates. The biases are updated similarly:

$$\Delta b_j^l = -\eta \delta_j^l \quad (5)$$

These weight and bias updates are applied to the network after processing each input to reduce the error gradually over time. By iteratively adjusting the weights and biases, the network can learn the mapping between the input and the desired output.

The algorithm can be summarised as follows:

- Initialise the weights and biases of the network randomly.

For each input in the training data:

- Perform the forward phase to generate the output of the network;
- Calculate the error between the actual output and the desired output;
- Perform the backward phase to adjust the weights of the network;
- Calculate the error between the actual output and the desired output;
- Repeat step 2 for a specified number of epochs or until the network reaches a satisfactory level of performance. (see Algorithm 1 below).

Algorithm 1 Neural Network Training

Require: *training_data*: Matrix of input training data

Require: *desired_output*: Matrix of corresponding desired output data

Require: *num_epochs*: Number of training epochs

Ensure: Trained neural network weights and biases

```
1: Initialize the network weights and biases randomly
2: for epoch = 1 to num_epochs do
3:   for i = 1 to size(training_data, 1) do
4:     input_data = training_data(i, :)
5:     output_data = desired_output(i, :)
6:     Perform the forward phase
7:     predicted_output = neural_network(input_data)
8:     Calculate the error between the predicted output and the desired output
9:     loss = loss_function(output_data, predicted_output)
10:    Perform the backward phase
11:    gradients = backward_phase(loss, neural_network)
12:    Update the weights and biases of the network
13:    neural_network = update_weights(neural_network, gradients)
14:  end for
15: end for
16: return Trained neural network weights and biases
```

The selection of BPNN is highly strategic in effectively mitigating hysteresis nonlinearity in conductive fibre-based tactile sensors. This algorithm offers several advantages that align well with the specific challenges posed by hysteresis in this context. Initially, BPNN exhibits remarkable generalisation capabilities, making it exceptionally suitable for understanding complex relationships between input and output variables. Given the complex and nonlinear nature of hysteresis, BPNN's ability to capture complex mappings is crucial for achieving accurate corrections [82,97]. Moreover, the proposed tactile sensor system demands a modelling approach that strikes an optimal balance between simplicity and efficiency, while still delivering precise predictions. BPNN adeptly fulfils this requirement by offering stability and robustness during the training process. Its robustness in handling noisy or incomplete datasets assures reliable predictions, even in real-world scenarios. Additionally, BPNN excels at accurately approximating values, making it ideal for consistently precise tactile measurements.

While more complex neural architectures, such as Convolutional Neural Networks (CNNs) or Long Short-Term Memory networks (LSTMs), exist, the inherent complexity

of the tactile sensor system makes BPNN a suitable and powerful option for addressing nonlinear hysteresis. While BPNN has found application in diverse domains, its specific adaptation for mitigating hysteresis in conductive fibre-based tactile sensors might remain poorly understood. Therefore, this study significantly contributes to the literature by showcasing the efficacy of BPNN in this specialised domain. The application of BPNN leads to heightened accuracy and reliability in practical implementations, spanning domains, such as soft robotics, wearables, and medical devices. Figure 4.5 below shows the block diagram that combines various models, including the hysteresis model, curve-fitting model, and Backpropagation Neural Network (BPNN). The choice of models is influenced by factors, including the nature of the problem and the available data. In this context, the BPNN emerges as a specialised solution for addressing nonlinear hysteresis in conductive fibre-based tactile sensors. Illustrated in Figure 4.5, the diagram depicts the collaborative functioning of these models. This combined approach recognises the special strengths of each model, intending to make the most of the benefits of all, a common method in scientific modelling.

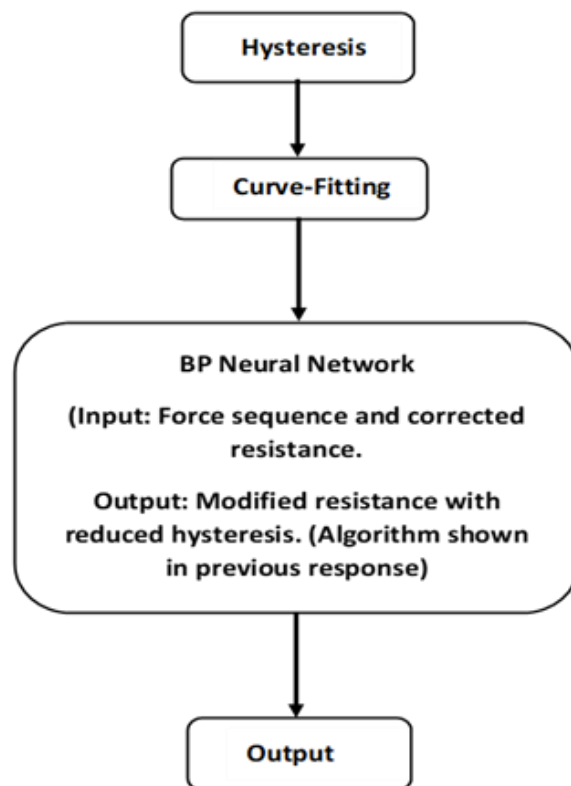


Figure 4.5: A generic flow chart showing the integration of the hysteresis model, curve-fitting model, and NN

The integration of the hysteresis model, curve-fitting model, and BPNN provides a comprehensive approach for modelling a system where force is the input and resistance is the output. The hysteresis model captures the non-linear dynamics and the memory effects of the system by the hysteresis model in response to force. The curve-fitting model approximates the mathematical relationship existing between force and resistance. The BPNN learns from the curve-fitting model's output to improve resistance predictions using backpropagation. This integrated system takes force as input, processes it through the hysteresis model, refines the output with the curve-fitting model, and further enhances it with the BPNN, thereby generating accurate predictions of resistance based on the force applied.

4.4 Neural Networks and Their Relevance to Addressing Hysteresis in Sensor Data

Neural networks are a popular selection for compensating for hysteresis in tactile sensors, as they are able to effectively learn the complex nonlinear relationships between input and output data. Tactile sensors are used to detect and measure parameters, such as physical forces, pressure, and vibrations. Specifically, hysteresis, a common problem encountered in tactile sensors, can cause measurement inaccuracies. Hysteresis occurs when the sensor's output does not return to its original state after the input has changed, causing a lag in the sensor's response [96-98]. Neural networks can learn to compensate for this hysteresis by analysing the sensor's input-output data and building a model to predict the correct output based on the input. They can learn the nonlinear relationship between input and output data, allowing them to compensate for hysteresis accurately [97].

Though other methods can also be used to compensate for hysteresis in tactile sensors, such as physical calibration or mathematical modelling, these methods may be less effective in capturing the complex nonlinear relationship between input and output data. Neural networks offer a flexible and powerful solution for hysteresis compensation in tactile sensors [99]. Nonlinear hysteresis in a tactile sensor can result in degraded system performance and instability [100]. In the experiment, a BPNN was used to eliminate nonlinear hysteresis, as an Artificial Neural Network (ANN) is simple

and sufficient to boost performance and reduce instability, albeit within the tactile sensor. BPNNs have a high precision approximation, robust fault tolerance, and nonlinear solid mapping capabilities [101-106]; therefore, BPNN was used due to its better generalisation and strong nonlinear mapping abilities, which makes it a popular choice in various fields.

The BPNN was trained to predict the static resistance value based on the current and historical resistance values (R_t and R_{t-1} , respectively), together with the estimated resistance value, which was used as a target. Figure 4.6 below shows that the neural network used in the current study consisted of an input layer that has the current resistance R_t at a time t , the historical resistance R_{t-1} at a time $t-1$, and a corrected resistance R_{est} as a target, the output layer is a static resistance R_{static} for training and two hidden layers. Each hidden layer has five neurons; the transfer function is the sigmoid function. The Levenberg-Marquardt algorithm (LMA), a popular optimisation method for training neural networks, is a variation of the Gauss-Newton algorithm, which is known for fast convergence and good stability. Using the LMA algorithm to train the BPNN, the model could learn the complex relationships between the input and output variables and make accurate predictions [107].

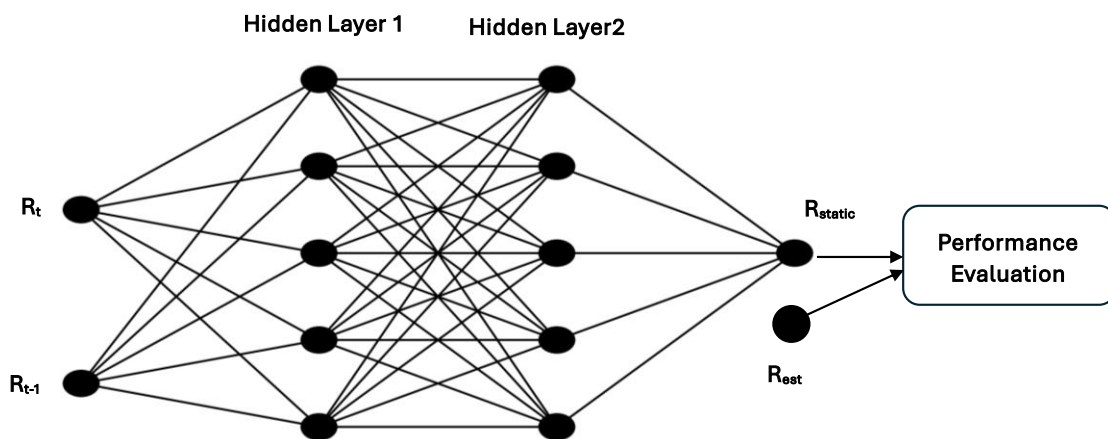


Figure 4.6: Neural Network Architecture for Resistance Prediction

Overall, the use of BPNN in the proposed sensor offers more accuracy and reliability, and different neural network techniques can be helpful in various applications, where precision and measurement accuracy are required. To assess the effectiveness of

employing a backpropagation (BP) neural network in mitigating hysteresis nonlinearity in conductive fibre-based tactile sensors, four sensor units with different layer configurations (1, 3, 6, and 12) were designed.

This section introduces a hysteresis compensation technique using BPNN to enhance the accuracy of soft sensors by modifying hysteresis nonlinearity, thereby overcoming the limitations posed by hysteresis. The BPNN was trained using collected force sequences and the corresponding resistances, aiming to reduce the maximum error caused by hysteresis, as demonstrated through experimental validation. The choice to use BPNN for hysteresis compensation is grounded in its ability to model complex and nonlinear relationships, making it an ideal candidate for addressing hysteresis in the context of soft sensors. The following sections provide a detailed account of the materials used, the methodology for training the BPNN, and the experiments conducted. The results obtained and subsequent discussions contribute to a comprehensive understanding of the proposed hysteresis compensation technique. The training process demonstrated favourable convergence, achieving a high level of accuracy in predicting resistances based on force inputs.

4.5 Modelling the Hysteresis Nonlinearity

Soft tactile sensors based on piezoresistive materials have drawn significant attention in recent years on account of their wide-ranging applications in robotics, medical devices, consumer electronics, and gaming. The accuracy of these sensors, however, is often hindered by hysteresis, which is a nonlinear phenomenon wherein a sensor's output is influenced by its current input and previous history. Hysteresis can introduce notable measurement errors and compromise the reliability of the sensor. Several methods have been proposed to address hysteresis and modify the hysteresis nonlinearity of piezoresistive sensors, including curve-fitting models and neural network approaches [76]. Even though hysteresis approximation using BPNN has already been employed, the novelty of the proposed method lies in its specific application to a conductive fibre-based tactile sensor.

In the current study, the Back Propagation Neural Network (BPNN) was employed to address hysteresis nonlinearity in a specific type of sensor, introducing a new application within the domain of conductive fibre-based tactile sensors. Unlike in

previous research, the uniqueness of this approach lies not only in the individual components or techniques employed, but in their combination and application within an unexplored context. While the use of BPNN for hysteresis approximation may not be ground-breaking on its own, its application to conductive fibre-based tactile sensors offers a novel perspective in this specialised field of tactile sensing. The selection of BPNN over alternatives, such as Convolutional Neural Networks (CNN) reflects a deliberate decision to balance accuracy and simplicity. While CNNs excel at capturing complex spatial relationships, the emphasis on achieving a balance resulted in preferring the straightforward yet effective architecture of BPNN for addressing the hysteresis phenomenon in the tactile sensor system, with the goal to find a solution that effectively mitigates hysteresis, while maintaining practicality and deployability. The BPNN stood out due to its capacity to model nonlinear hysteresis and complex relationships common in tactile data. Its architecture strikes a balance between accuracy and complexity, avoiding unnecessary complexities that might hinder understandability. The model's stability in handling noisy data aligns with the aim for reliable predictions. While alternatives are valuable, the BPNN aligns closely with the objective of a pragmatic and precise solution.

By utilising the BPNN to adjust the sensor's resistance based on polynomial curve approximations, there were significant improvements in how accurate and consistent the sensor's readings are. This decision effectively addressed hysteresis, resulting in an optimally performing tactile sensor system. Figure 4.7 describes the experimental setup used to design four distinct types of sensor units with varying layers, along with the process of collecting output resistances by applying force sequences. These force sequences and the corresponding corrected resistances were employed as inputs to train the BPNN, resulting in favourable convergence and high accuracy. Through validation experiments, a reduction in the maximum error caused by hysteresis was demonstrated in the proposed method, wherein the sensor's full-scale output was reduced from 24.2% to 13.5%



Figure 4.7: Flow Diagram of the Experiment Setup and Hysteresis Error Reduction

4.6 Design a Soft Tactile Sensor

Fabric-based sensors have been selected due to their simplicity in design, ease of fabrication, and cost-effectiveness, providing stretchability and adaptability to soft surfaces. The subsequent discussion on the fabrication and design of the tactile sensor was previously detailed in section 3.1. For a comprehensive understanding of the materials used and the assembly process of the tactile sensor, please refer to section 3.2 - "Design of a Soft Tactile Sensor". The section explores the materials employed, including the EeonTex™ knitted. All the necessary pieces of samples were prepared with dimensions of $1 \times 1 \text{ cm}^2$. Figure 4.8 below shows the overall diagram of the designed soft tactile sensor.

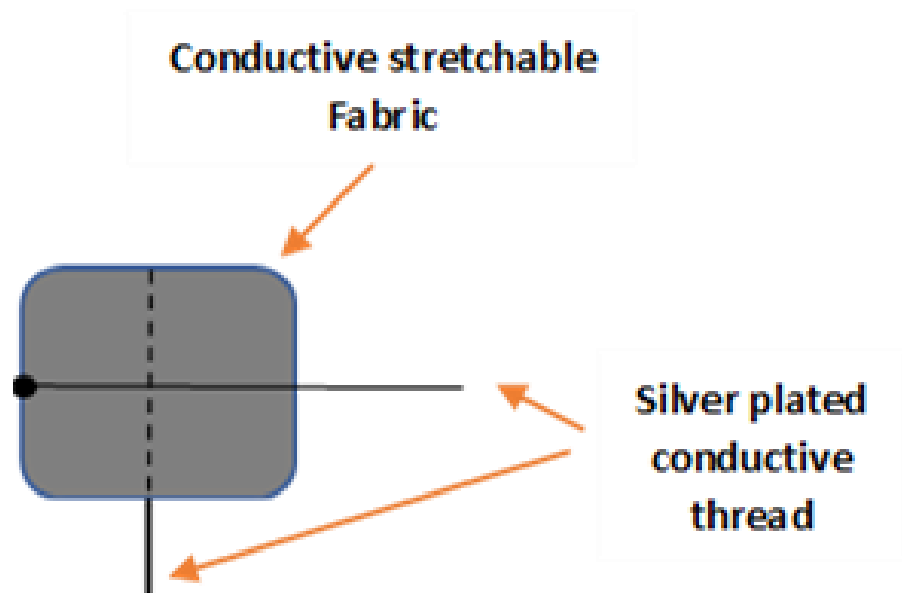


Figure 4.8: The soft tactile sensor

4.6.1 Single-Layer and Multi-Layer Sensors

- **Single-Layer Sensor**

Application: Single-layer sensors are used in scenarios where the applied forces are relatively low and within a narrow range. This configuration offers high sensitivity, making it ideal for detecting small and precise changes in force. It is particularly

beneficial in delicate touch detection or environments requiring high responsiveness to slight pressure changes. While sensitive, the single-layer sensor has limited capacity for measuring higher forces and can reach saturation quickly, making it less suitable for applications involving larger forces.

- **Multi-Layer Sensors (Three, Six, Twelve Layers)**

As the number of layers increases, the sensor's ability to measure a broader range of forces improves. Multi-layer sensors distribute the applied force across multiple layers, increasing the sensor's force capacity. This design is suitable for applications where higher forces are expected, such as seating pressure monitoring or medical beds. It is ideal for environments that require the sensor to withstand and accurately measure larger forces without saturating. The increased thickness of multi-layer sensors enhances their structural integrity and ensures consistent performance under higher loads. Despite the additional layers, these sensors maintain good sensitivity while expanding their force measurement range, making them versatile for various applications that require durability and a wide measurement spectrum. For each sensor, forces were applied using an instrument positioned directly above the sensor, which is installed on the digital electronic weight scale (see Figure 4.10). Subsequently, the change in resistance was measured using a multi-metre.

The choice between single-layer and multi-layer sensors depends on the specific application requirements. Single-layer sensors offer high sensitivity for detecting small forces, while multi-layer sensors provide a broader range for measuring higher forces, making them ideal for more demanding environments that require durability and versatility in force measurement.

4.6.2 Experimental Setup

In the current study, four tactile sensor samples (one, three, six, and twelve layers) were used, as shown in Figure 4.9. The sensor was designed in layers three, six, and twelve to increase the range of applying force to be measured. An increase in the number of layers implies an increase in the capacity of the tactile sensor to apply force, which can be used in other applications, such as in the patient's seat or bed.

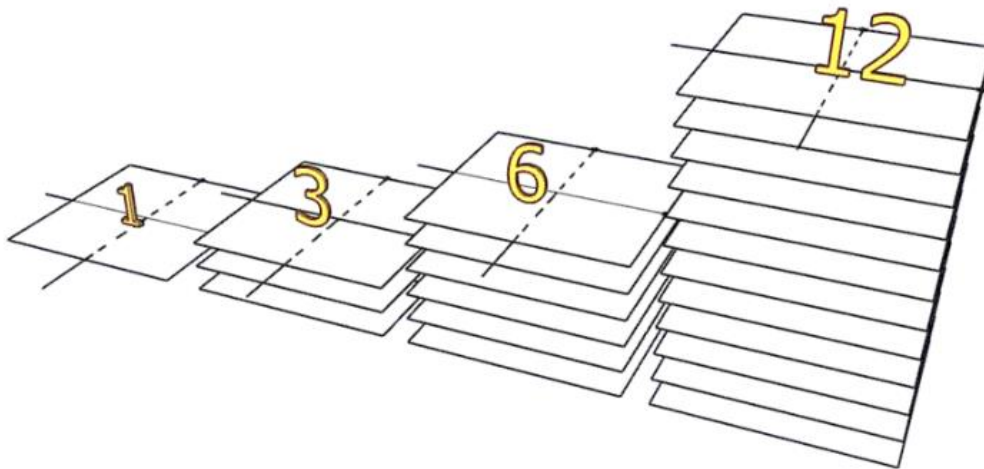
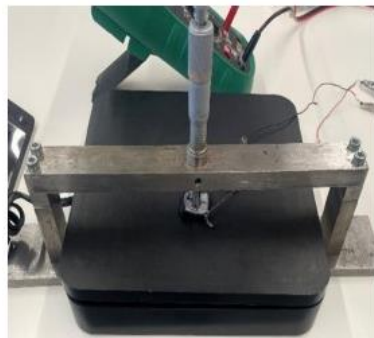


Figure 4.9: Tactile sensors with different layers

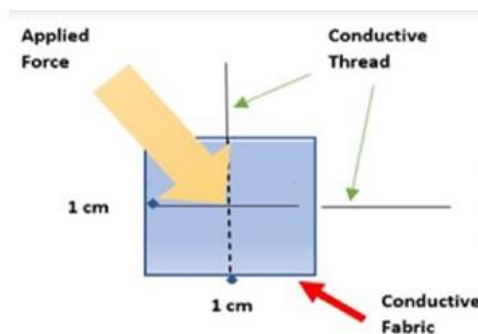
The following section outlines the characteristics and applications of the single-layer and multi-layer sensors used in the experiment.



(a) The Experimental Setup



(b) Force being applied to the sensor



(c) Functional diagram

Figure 4.10: (a) The Experimental Setup; (b) Force being applied to the sensor; (c) Functional diagram

Figure 4.10 (a) illustrates the placement of the tactile sensor on a weight scale, where force is manually applied using a force measurement instrument. The instrument allows for precise application of pressure or tension to the sensor, simulating real-world conditions. The sensor is positioned to detect changes in resistance as force is exerted.

Figure 4.10 (b) shows the process of measuring the resistance change in the sensor. A controlled and gradual force is manually applied through the instrument to ensure consistent pressure, allowing the sensor's response to be recorded. Figure 4.10 (c) provides a functional diagram, which outlines the mechanism for applying force. This involves a manual system that exerts force evenly, ensuring that the tactile sensor's performance is tested across a range of pressures.

4.6.3 Calibration Analysis

The sensor calibration was performed by applying incremental forces until sensor saturation was reached. The calibration equation derived from the experimental data is:

$$y = -0.2468 x + 3.3033 \quad (6)$$

$$(R^2 = 0.919) \quad (7)$$

Where

x : represents the compression force(N)

y : represents the sensor output(K Ω)

R : denotes the regression value.

Figure 4.11 demonstrates this relationship, illustrating the linear calibration between applied force and sensor resistance, with the regression line and corresponding.

Sensor Calibration: Force vs. Resistance with Best-Fit Line

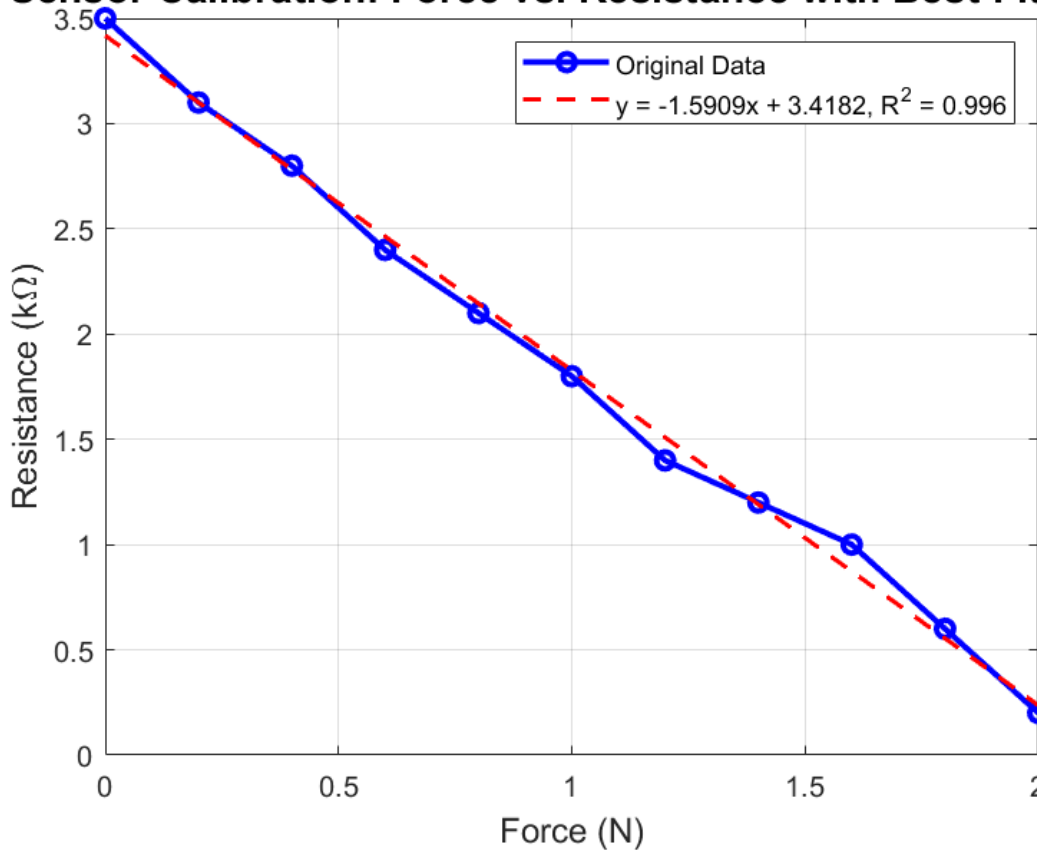


Figure 4.11: Calibration of Tactile Sensor: Force vs. Resistance

The graph shows the linear relationship between force and resistance, along with the calibration equation and the R^2 value. This placement is appropriate since it directly follows the explanation of the calibration equation.

4.6.4 Loading-Unloading Cycle and Hysteresis

To study the behaviour of the tactile sensor output, a measurement method was used to record the sensor's response to a sequence of forces exerted manually. The forces were applied manually by pressing an object onto the sensor, increasing the applied force incrementally. This manual application involved careful control to ensure consistency in the pressure applied during each cycle.

Specifically, four to six consecutive loading-unloading cycles were performed, with different points of return for the same ascending curve and different starting points for the same descending curve. This method allowed both the descending and ascending behaviour of the sensor to be characterised. During the experiment, forces were increased in 0.1 N increments. The sensor's response was recorded after a brief interval of 2 seconds, allowing the sensor to stabilize before the next force level was applied.

These hysteresis curves represent the average output produced by the tactile sensor at each point after the cycle was repeated five times. The interval between each new force level and the resistance measurement was set to 2 seconds to ensure the accuracy of the readings.

To quantify the hysteresis exhibited by the sensor, the hysteresis error was determined by measuring the difference in the sensor's output resistance for the same applied force when exerted on both the ascending and descending branches of the cycles. The maximum force applied varied depending on the type of object used. For example, using the index fingertip on a thin ring, the maximum force was 59.5 ± 21.4 N while using all four fingers on a straight bar, the maximum force was 268.7 ± 77.2 N. This variation in maximum force (F) provides essential data for understanding the sensor's response to different levels of force.

For the one-layer sensor, a force of 0-2 N was applied. The load was increased until the sensor output reached its saturation level. Then, the load was reduced from 2 N to 0 N, and the change in resistance was determined. This experiment was repeated with random force ranges of 0-1.27 N, 0-1 N, 0-1.96 N, 0-0.5 N, and 0-1.7 N. Figure 4.12 below shows the hysteresis in the one-layer sensor. The maximum and average hysteresis errors are referenced to the highest output value to obtain a percentage of the error relative to the full scale. The maximum error due to hysteresis is 24.2% of the full-scale output.

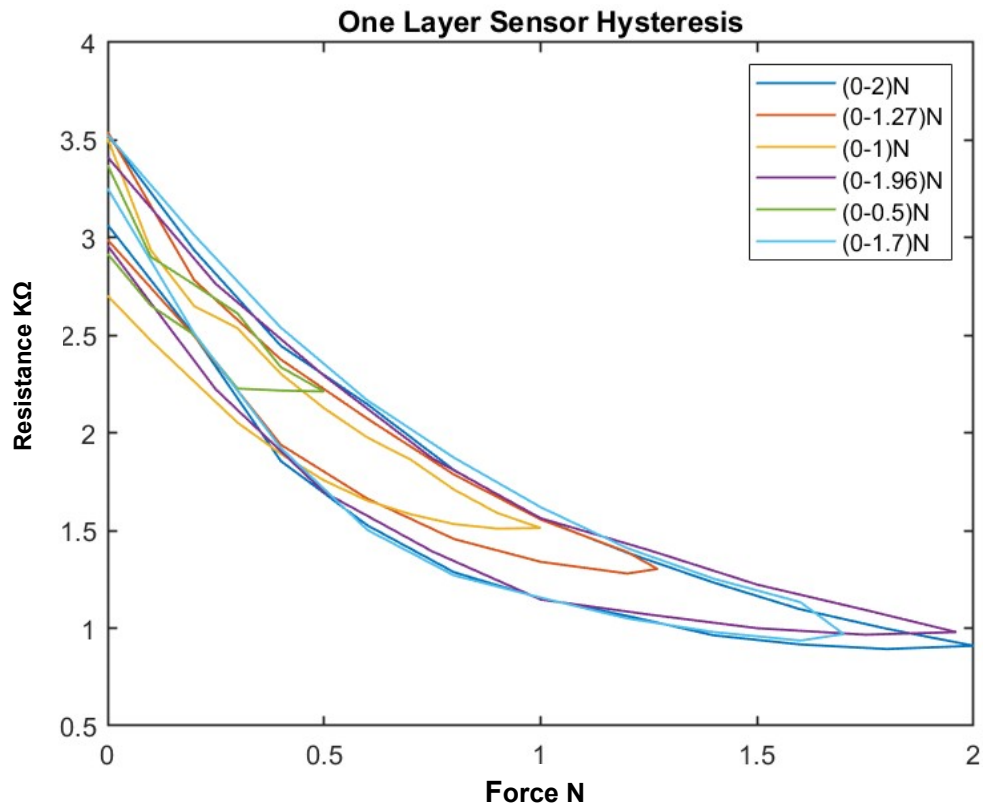
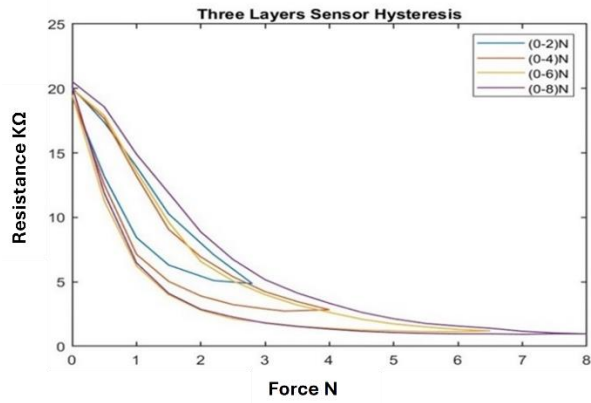
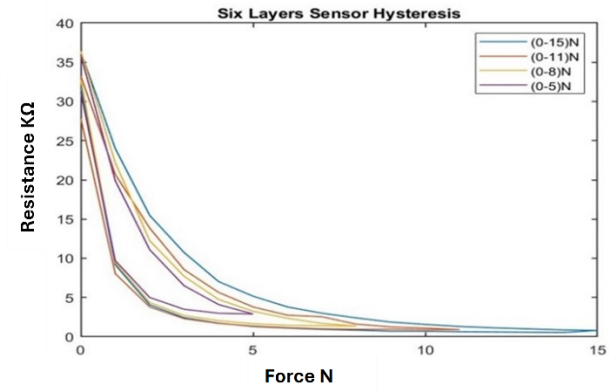


Figure 4.12: *The hysteresis phenomenon in the One-Layer Sensor*

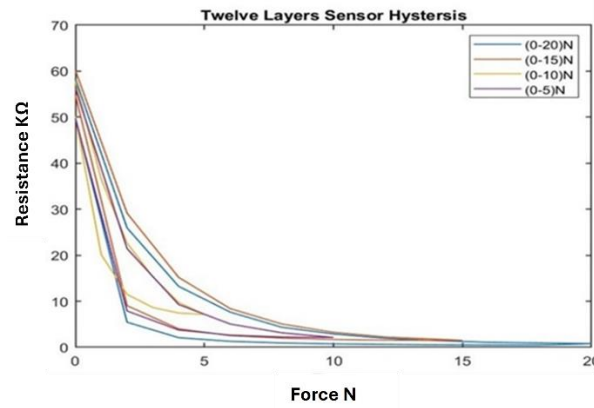
Figure 4.12 demonstrates the hysteresis behaviour of the sensor when it is compressed to a maximum force, and then released multiple times. The sensor exhibits a different number of loops, indicating variation in the sensor's hysteresis behaviour depending on the sensor's compressed and released layer. The number of loops increases as compressions and releases increase, indicating that the force history influences the sensor's hysteresis behaviour. For the three-layer sensor, force ranges of 0-2.8 N, 0-4 N, 0-6 N, and 0-8 N were applied and the associated resistance was recorded over several experiments, reporting the average resistance over the individual experiments as a function of force. The experiment was repeated with the 6- and 12-layer sensors and the associated hysteresis was plotted accordingly. Figure 4.13 below shows the hysteresis for the three-, six- and twelve-layer sensors.



(a)



(b)



(c)

Figure 4.13: (a) The hysteresis phenomenon in the Three-Layer Sensor; (b) The hysteresis phenomenon in the Six-Layer Sensor; (c) The hysteresis phenomenon in the Twelve-Layer Sensor

Both figures 4.12 and 4.13 show that the hysteresis curve of the proposed sensor exhibits a multi-loop behaviour in different layers of the sensor. Hence, this implies that the output resistance of the sensor depends not only on the current force applied but also on the force history. Additionally, Figure 4.13 above indicates the hysteresis behaviour of the sensor when it is compressed and released multiple times in the same layer. The findings emphasise that the output curve of the proposed sensor is influenced by both the current force applied and the force history. This underscores the significance of considering the hysteresis during the design and interpretation of results from tactile sensors. To address this challenge, a BPNN is proposed in the current study to adjust the sensor's resistance based on estimated values obtained from the polynomial curve. This approach helps to enhance the accuracy and reliability of readings, enabling more precise interpretations of the sensor's output.

4.7 Results and Discussion

Modified Hysteresis: Simulation and Experiments

In the current study, multiple sensor units were developed with different layers, and the output resistance was determined by applying force sequences on the sensors. These force sequences, along with the corresponding corrected resistance values, were utilised to train a BPNN. This network exhibited good convergence and demonstrated high accuracy during the training process. A tactile sensor is used to verify the hysteresis model based on BPNN; with the target part is determined by approximating a curve from the hysteresis graph, and for each layer, the approximated curve's line is plotted as a desired resistance. Figure 4.14 shows the approximated curve plotted for a one-layer sensor, which likely represents the relationship between the sensor's actual resistance values with the desired values represented by the curve. Subsequently, the accuracy of the hysteresis model can be evaluated and then any necessary adjustments can be made.

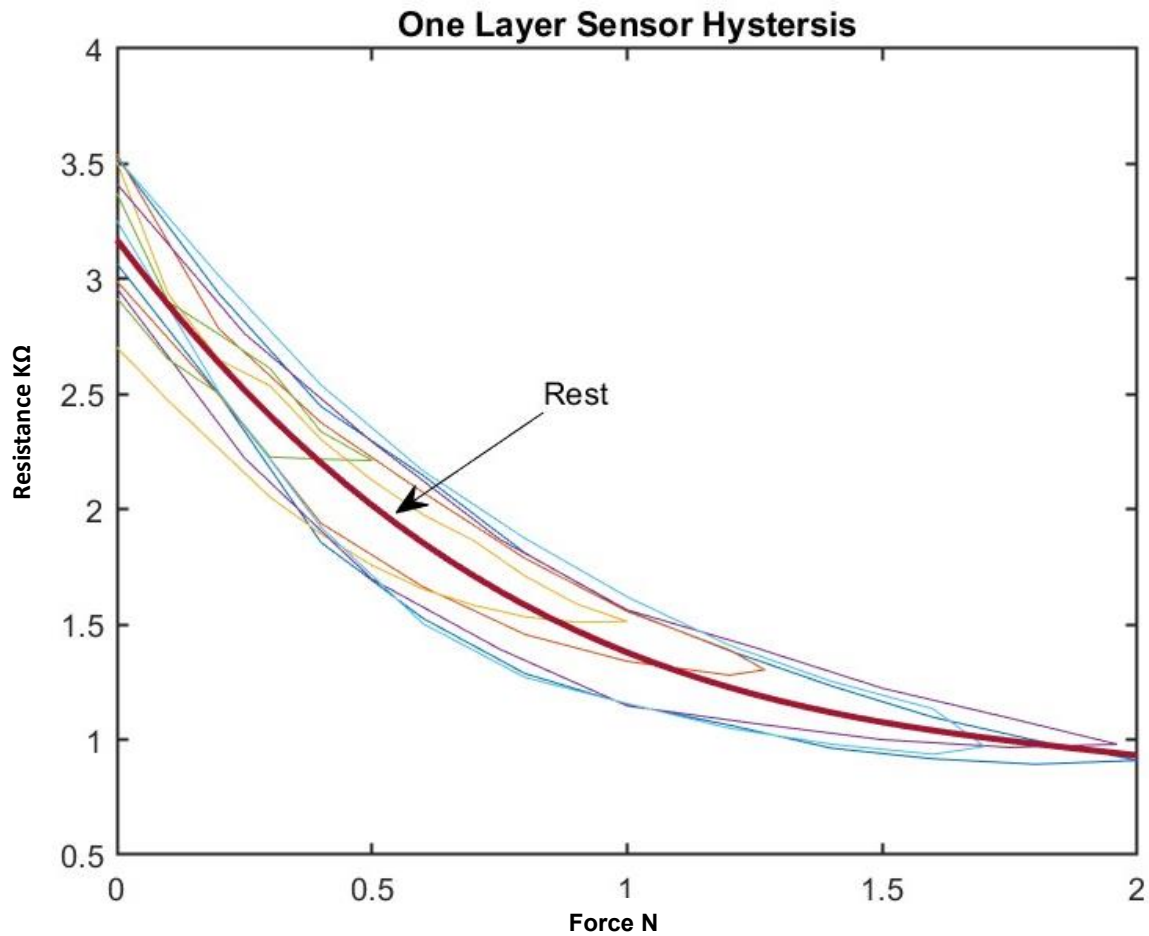


Figure 4.14: The Approximated Curve Plotted for the One-Layer Sensor

A third-degree polynomial curve was used to fit the hysteresis curve in a one-layer tactile sensor, which provided the best practical results. After fitting the polynomial curve, the force values were substituted into the polynomial to determine the corresponding estimated resistance values. These estimated resistance values were then used as the target input for the BPNN. BP is a popular neural network training algorithm used to adjust the network weights and minimise the difference between the predicted and actual values [106]. In this case, the target input was the estimated resistance value obtained from the polynomial regression, and the neural network was trained to predict this value based on the input force values.

The proposed model captured the nonlinear relationship between the force and resistance values by combining the polynomial regression and neural network techniques and making accurate predictions. This approach can be helpful in various

applications where complex relationships between variables are challenging to models employing traditional techniques. Fitting a polynomial curve to hysteresis data is a common approach, although it has limitations, as the relationship is complex. In such cases, neural networks excel by capturing nonlinear patterns, extracting hidden features, generalising to new data, and handling diverse inputs. Their flexibility and ability to model complex relationships make neural networks a preferred choice when traditional methods struggle in machine learning [103].

Once a polynomial curve is fitted to the hysteresis data, the estimated values can be used as inputs for a neural network, which are powerful machine learning models that can learn complex patterns and relationships in data. By using the estimated values from the polynomial curve as inputs for the neural network, the variables can make better predictions.

$$R_{est} = -0.24F^3 + 1.38F^2 - 2.93F + 3.17 \quad (8)$$

Here, 'F' represents the applied force ranging from 0 to 2N, encompassing 41 samples of force. Equation (6) has been derived based on this relationship, establishing a clear link between the estimated resistance (R_{est}) and the applied force F in the current investigation. The earlier tested procedure of the one-layer sensor was repeated for all four layers. Figure 4.15 shows the subsequent results of approximated curves of all different layer sensors.

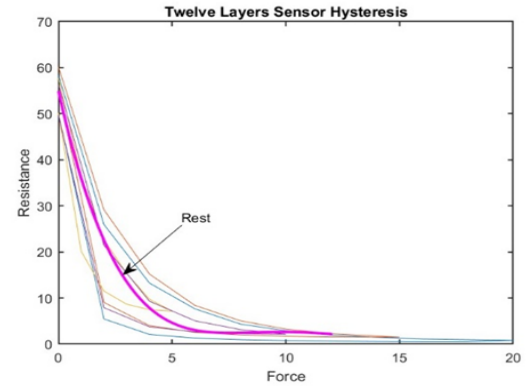
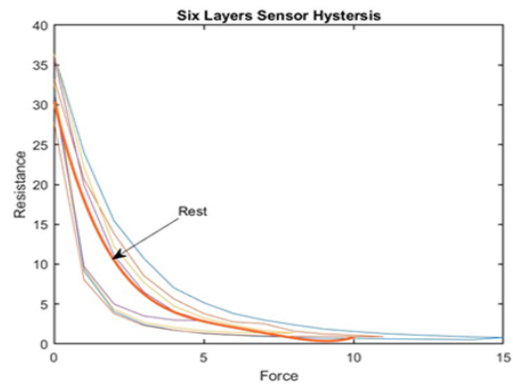
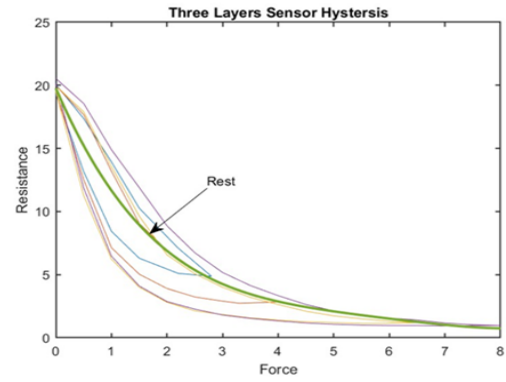
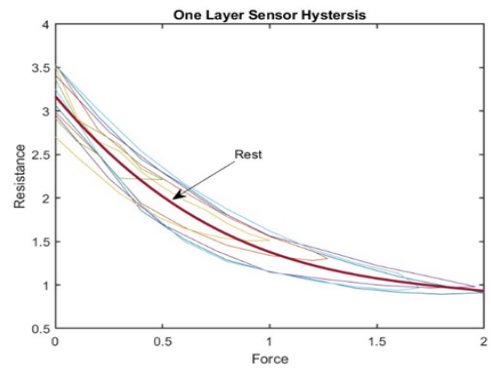


Figure 4.15: Approximated Curves of all different Layer Sensors

The corrected curve equation for all four layers of sensors can be found in the graphs shown above, and by using the same procedure of layer one sensor the desired target in the BPNN can be found.

$$R_{\text{est}} = 0.01F^4 - 0.26F^3 + 2.36F^2 - 10.21F + 19.77 \quad (9)$$

The range of values for F in equation (7) is between 0 and 8N, with 90 samples of force used to derive this equation.

$$R_{\text{est}} = 0.01F^4 - 0.33F^3 + 3.32F^2 - 15.34F + 30.41 \quad (10)$$

Values for F in equation (8) range from 0-15 N. Overall, 142 samples of force are used to derive this equation.

$$R_{\text{est}} = 0.01F^4 - 0.23F^3 + 3.43F^2 - 22.18F + 54.94 \quad (11)$$

The range of values for F in this equation is between 0 and 20 N, with 240 samples of force used to derive this equation. Three equations (2-4) represent the estimated curve equation for the three-, six-, and twelve-layer sensors. The equations provide an estimate of the value of R (representing a dependent variable) based on the force F applied, an independent variable. Each equation exhibits different characteristics in terms of the power of F and the sign of the coefficients. This helps to determine the relationship between F and R. The power of F in the equations captures complex and nonlinear relationships between F and R, accommodating different curves and intricate patterns. By considering the powers of F ranging from 2 to 4, these equations can capture the nonlinearity and complexity present in the relationship between F and R. Positive coefficients indicate a direct relationship, while negative coefficients suggest an inverse relationship. These coefficients are established through an analysis involving curve fitting, and their values hinge on both the dataset characteristics and the selected statistical methodology.

4.8 Analysis and Discussions

The validation for the tactile sensor was performed by applying force, removing it from the sensors, and measuring the corresponding changes in resistance. The observed resistance changes were subsequently compared to the theoretically expected resistance changes, with the validation process specifically focusing on evaluating the performance and accuracy of the tactile sensor itself. Figure 4.16 below shows the validation of the system by using the same force data set that was used initially to train in the NN model for one layer and the other sensor.

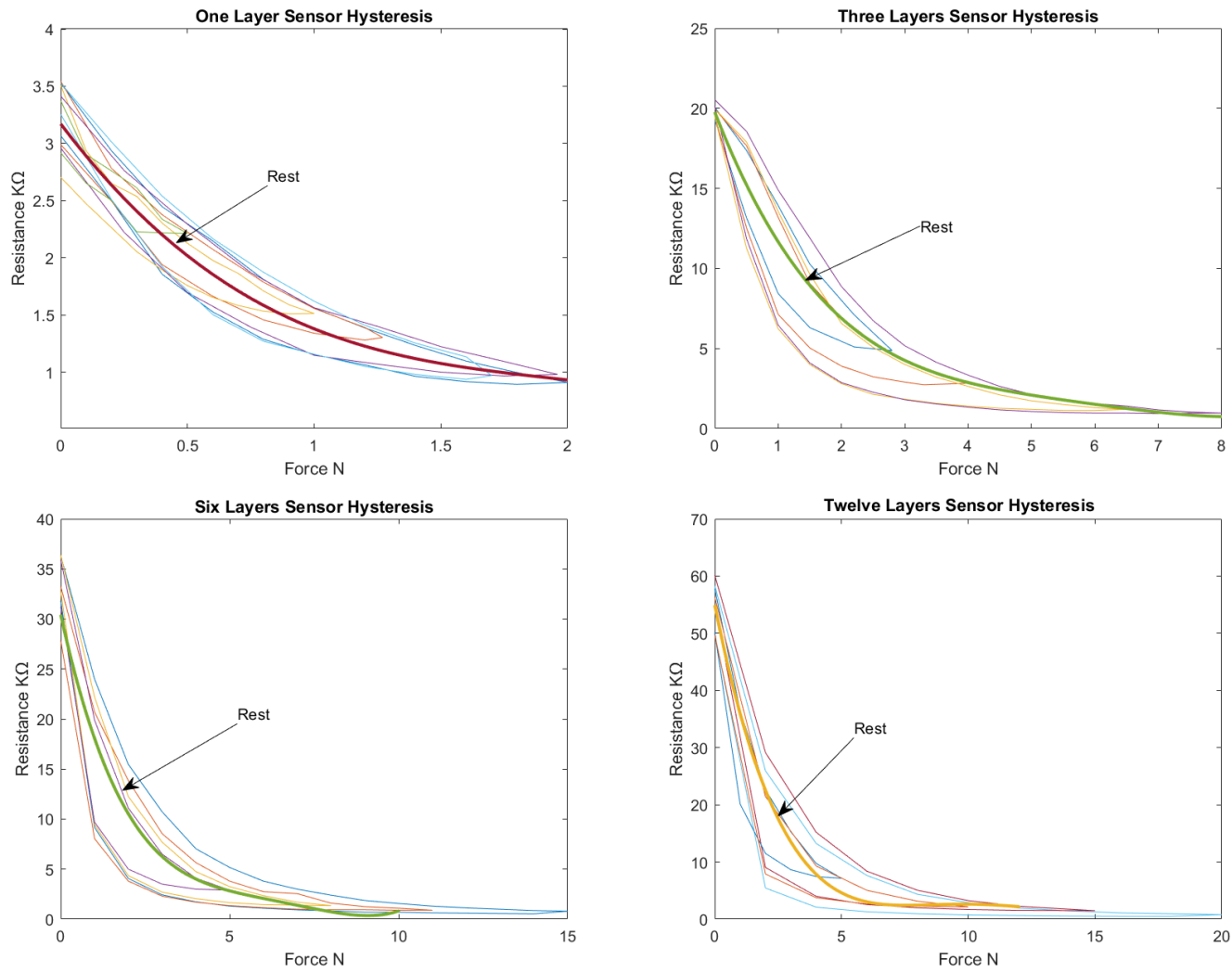


Figure 4.16: Graphs showing the validation of the system of different Layers of Sensor

As shown in Figure 4.16 above, the tactile sensor has been specifically designed to accurately measure changes in resistance in response to applied or removed force. Through the validation process, the tactile sensor has demonstrated its capability to produce reliable and accurate results within the maximum force domain of 2N for the layer one sensor. Hence, the validation results indicate that the tactile sensor consistently provides measurements that closely align with the actual values of measurements. This alignment signifies that the predicted results generated by the neural network closely match the expected values based on the training data. Notably, the output results of the BPNN, which fall perfectly on the target curve 'R_{est}' after training, serve as a good indicator of the accuracy and reliability of the tactile sensor. Furthermore, the use of the same dataset for training and validation purposes facilitates a direct comparison between the predicted and actual results. When the predicted results closely resemble the actual results, the accuracy and reliability of the tactile sensor are confirmed in measuring resistance change.

The above findings highlight the overall reliability and accuracy of the tactile sensor in measurements, which consistently provide highly dependable results and demonstrate high alignment between predicted and actual values. Accurately capturing resistance changes, reliable performance within the specified force range, and close alignment with actual results validate the reliability and accuracy of the tactile sensor in measuring resistance changes. It may be highlighted that using the same data set for training and validation can potentially lead to overfitting, where the model becomes highly specialised to the training data and may struggle to generalise to new data. To address this concern, the model was validated using new and independent data sets. The tactile sensor was tested with new sets of 25, 30, and 60 random forces, and the resulting output resistance was recorded and compared to the expected values (see Figure 4.17). This type of testing ensures that the model can accurately predict resistance values even when presented with new and previously unseen data.

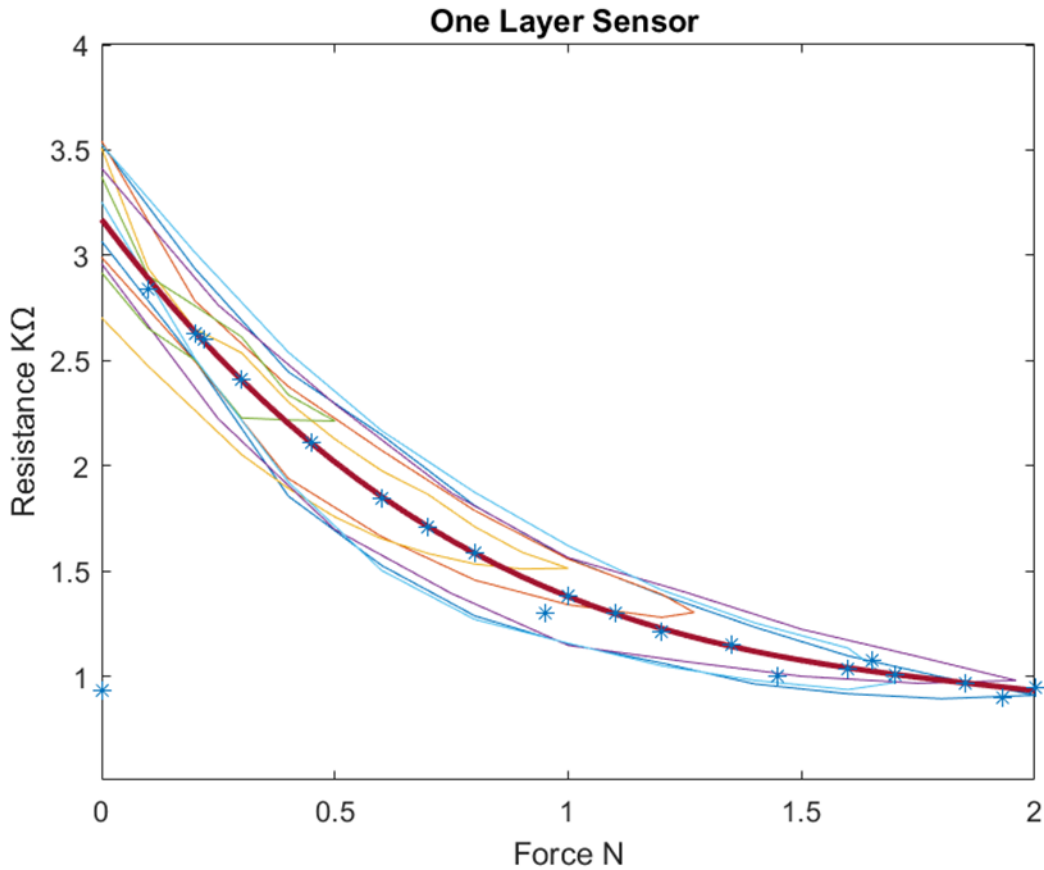
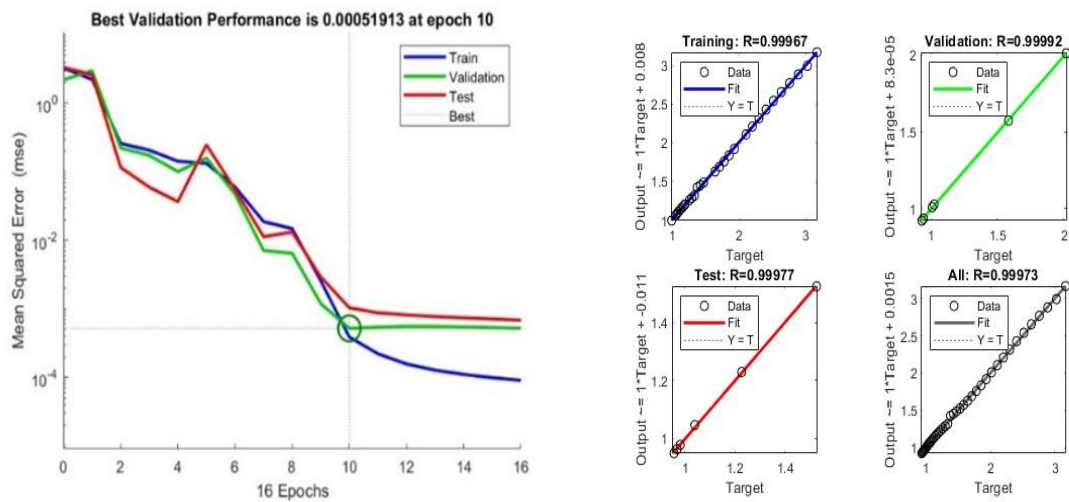


Figure 4.17: Validation of the system with new experimental results

Close alignment of the output results of the BPNN with the target curve R_{est} after training is a positive indicator of the effectiveness of the training process. This suggests that the neural network has learned the underlying patterns and relationships between force and resistance, resulting in accurate predictions. This alignment between the predicted results and the target curve indicates that the neural network, and subsequently the tactile sensor, performs well in accurately estimating resistance values. Continuing testing and validation are essential to ensure the ongoing accuracy and reliability of the tactile sensor, which includes testing the tactile sensor under various conditions and using different data sets that were not included in the training process of the BPNN, to ensure its ability to generalise to new situations and data.

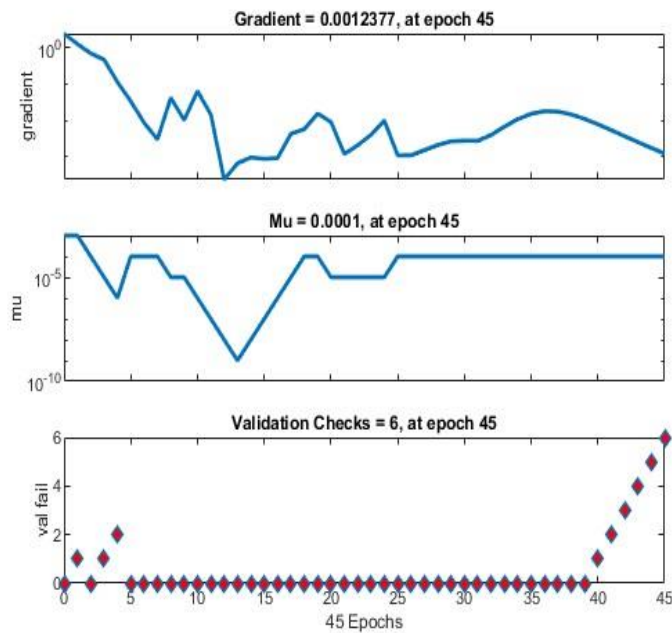
In addition to assessing the performance and accuracy of the BPNN, the evaluation of the robustness of the tactile sensor is also important. Robustness refers to the ability of a sensor to consistently maintain its performance and reliability despite uncertainties or variations in the input. Further, to evaluate the robustness of the tactile sensor,

various factors, including the gradient, mu, and validation check values were considered for neural network training. Analysis revealed that at epoch 45, the gradient was 0.001, mu was 0.0001, and the validation check value was 6. These values provide useful insights into the stability and adaptability of the neural network during the training process (see Figure 4.18).



(a)

(b)



(c)

Figure 4.18: One Layer Sensor (a) Neural network performance; (b) Neural network regression; (c) Neural network training

Furthermore, the validation performance of the BPNN (see Figure 4.18(a)) indicates the system's ability to maintain a low validation error ≈ 0 , which is a high level of accuracy at a specific epoch. This suggests that the neural network is able to consistently provide accurate predictions of the tactile sensor's resistance despite encountering potential variations in the input force.

Table 4.1: Regression Results and Accuracy Statistics of Datasets

Dataset	R-Value
Training	0.999967
Validation	0.99992
Test	0.999977
Overall	0.99973

Data shown in Figure (4.18)(b) and the regression values shown in Table 4.1 reveal that the proposed system exhibits remarkable robustness. The high Regression (R-values) across all datasets (training, validation, test, and overall) indicates a strong correlation between the predicted resistance values and the actual values. This consistency in performance demonstrates the system's ability to handle variations in input effectively. Overall, the system's robustness is the combination of a low validation error, high correlation coefficients, stability during training, and consistent performance on new datasets. These findings also highlight the system's ability to reliably measure changes in resistance based on the applied force, even in the presence of uncertainties or variations in the input. The system's robustness enhances its practical utility and strengthens its potential for various applications.

By conducting a comprehensive analysis of the system's performance, accuracy, and robustness, valuable insights are gained into its behaviour and capabilities. These insights are able to inform regarding the sensor system's design, optimisation, and application, thereby contributing to improved reliability and performance of the system in real-world scenarios. Figure (4.18) (a) shows the validation performance of the BPNN, with the best validation performance of 0.000051913 at the epoch, indicating that the neural network can accurately predict the sensor's resistance based on the

input force applied. Figure (4.18) (b) shows the neural network regression values, with R values indicating the correlation between the predicted and actual resistance values in training, validation, and test datasets. The R values in training, validation, and testing are all above 0.9999, indicating a strong correlation between the predicted and actual resistance values. The overall R-value of 0.99973 also indicates a strong linear correlation between predicted and actual values. Overall, these results suggest that the proposed system performs well and accurately predicts the sensor's resistance. Table 4.2 provided below displays the results of the BPNN evaluation for sensors with varying numbers of layers; with the performance of the BPNN was assessed using the mean squared error (MSE) and correlation coefficient (R) metrics

Table 4.2: Comparison of Neural Network Performance with Different Numbers of Sensor Layers

Layers	Observation	MSE	R
1	6	9.41E-05	0.996
1	11	0.0039	0.9975
1	14	0.0515	0.9992
1	18	0.0263	0.9988
1	21	0.0058	0.9997
1	29	9.9327E-05	0.999
1	46	0.0261	0.9972
3	6	6.7356E-05	0.999
3	11	0.0045	0.9983
3	14	0.0515	0.9992
3	18	0.1109	0.9997
3	21	0.0028	1
3	29	0.1510	0.9973
3	46	0.0114	0.9984
6	6	0.0001	1
6	11	0.0055	0.9997
6	14	0.0107	0.9998
6	18	0.1736	0.9995
6	21	0.0051	1
6	29	0.0051	1
6	46	0.0042	0.9994
12	6	0.0034	0.9992
12	11	0.0222	0.9985
12	14	0.0842	0.9989
12	18	0.9985	0.9993
12	21	0.2538	0.9965
12	29	0.9731	0.9728
12	46	0.2597	0.9964

The results shown above in Table 4.2 are based on testing different types of sensors with different numbers of layers. The sensors were evaluated using MSE and R.

Mean squared error is a measure of the difference between the predicted values and the actual values; with the lower the MSE, the better the performance of the sensor. Moreover, the results show that the performance of the sensors varies depending on the number of layers. Generally, increasing the number of layers in the sensor improves its performance, as shown by the decreasing values of MSE and increasing R values. However, in some cases, the sensor's performance decreases as the number of layers increases. These results provide valuable insights for designing and optimising sensors for various applications. Further, the results obtained from testing the BPNN for a tactile sensor with varying layers demonstrate that the proposed method is effective in modifying hysteresis nonlinearity in soft tactile sensors based on piezo resistance materials. The BP algorithm adjusted the neural network weights and produced good convergence and high accuracy in compensating for the effect of hysteresis. The BPNN presented in this chapter exhibits promising potential for enhancing tactile sensors by considering the sensor's range as a variable.

In addition, the significance of certain sensor designs and materials that have garnered substantial acceptance within the research community is acknowledged, even though the primary focus in this chapter centres on the application of the BPNN approach for sensor analysis. Valuable insights and innovative approaches to sensor technology are offered by these studies, as outlined in the provided papers, which complement and enrich the landscape of the current research. This study contributes significantly by proposing a methodology to enhance tactile sensor performance by effectively capturing the nonlinear relationship between force and resistance values. This is achieved through a synergistic combination of polynomial regression and neural network techniques. The resultant models offer enhanced interpretability and ease of understanding compared to the intricate mathematical models, such as Preisach or Prandtl-Ishlinskii, rendering them more suitable for practical implementation across a spectrum of fields including robotics, medical devices, consumer electronics, and gaming. However, the selection of the appropriate modelling technique depends on various factors, such as the specific application, the complexity of the hysteresis behaviour, and the availability of data.

The BPNN presented in this chapter exhibits promising potential for enhancing tactile sensors by considering the sensor's range as a variable. To comprehensively evaluate its versatility, it is worth noting that alternative methods may have yielded distinct results. The decision to utilise a BPNN was driven by its capability to capture complex relationships and adapt to variations in sensor range, providing a comprehensive approach to sensor enhancement.

4.9 Conclusions

This investigation significantly advances the understanding of conductive fibre-based tactile sensors by addressing the unique challenges these sensors present. By leveraging the capabilities of Backpropagation Neural Networks (BPNN), the study effectively modifies the hysteresis nonlinearity, enhancing the accuracy and performance of these sensors in force measurement and control applications. The proposed method successfully reduced the maximum hysteresis error from 24.2% to 13.5%, which, while still present, represents a substantial improvement.

In comparison to other hysteresis compensation methods, such as the Generalized Prandtl–Ishlinskii (GPI) model [108], which typically reduces hysteresis by 10–15%, the 13.5% achieved here is competitive and highlights the robustness of the BPNN approach. More advanced models, like the Modified Prandtl–Ishlinskii [109], can sometimes achieve even lower hysteresis, but they often come with greater complexity and implementation challenges. The use of BPNNs in this context is particularly valuable because of their adaptability and effectiveness in managing the nonlinear characteristics of conductive fibre-based sensors.

The development of multiple sensor units with different layers and the application of force sequences to collect output resistance for BPNN training showcased good convergence and high accuracy. Validation with new datasets confirmed the BPNN's ability to effectively address nonlinearities, resulting in a significant reduction in hysteresis. The implications of this work are far-reaching, with potential impacts in robotics, prosthetics, and human-computer interfaces, where precise and reliable sensors are crucial. The improved accuracy of these tactile sensors marks a significant step forward, adding valuable insights to the field and paving the way for further advancements in real-world applications.

While the remaining 13.5% hysteresis error is still notable, it compares favourably with other contemporary methods, positioning the BPNN approach as a strong contender in the ongoing quest to improve tactile sensor technology. Future research might explore hybrid approaches that combine the strengths of neural networks with operator-based models, further pushing the boundaries of what can be achieved in hysteresis reduction.

Chapter Five: Validation and Evaluation of a Fabric-Based Tactile Sensor in Comparison with an sEMG Sensor

5.1 Introduction

In the domain of assistive technology and rehabilitation robotics, the integration of diverse sensors has become crucial for a detailed understanding of user intentions. From pressure and bend sensors on wrists to advanced readings such as surface electromyography (sEMG) and electroencephalography (EEG), these sensors enable the discernment of user intent, which is vital for aiding individuals with mobility challenges. While EEG holds promise for individuals with total paralysis, its complexity—requiring numerous electrodes and complex signal processing—poses significant challenges to practical implementation. Conversely, sEMG readings offer reliable signal acquisition and are widely used to decode user intent. Some systems even combine sEMG with voice recognition for more accurate intent detection. However, there remains a notable gap in the integration of diverse sensors and feedback modalities for intent detection in robotic development, as evidenced by prior research [4-10].

This chapter focuses on the validation and evaluation of a novel fabric-based tactile sensor compared to a commercially available sEMG sensor (Myoware EMG) for measuring muscle activity. The primary objectives are to:

1. Determine the efficacy of the fabric-based tactile sensor in generating output signals that distinguish between various exercises.
2. Assess the reliability of the signals produced by the tactile sensor during simple exercises, and compare these results with the sEMG system.

The study involves collecting electromyography (EMG) signals from the Biceps and Flexor Carpi Ulnaris muscles during dynamic exercises, using both the fabric-based tactile sensor and the sEMG sensor. These signals will be analysed to evaluate the sensor's accuracy, consistency, and potential applications in rehabilitation. This chapter also details the experimental setup, validation criteria, and statistical analysis methods used to evaluate the sensors' performance, ensuring the integrity and reliability of the collected data and results.

Through this validation study, the research highlights the advantages and limitations of the tactile sensor system, providing insights into the feasibility of fabric-based tactile sensors as an alternative to more expensive commercial sEMG systems. Additionally, the broader implications for rehabilitation practices and potential areas for future research will be explored.

Tactile sensors are pivotal in measuring object properties and contact events through direct sensor-object interaction. Over the years, tactile sensor technology has made significant progress, particularly in assisting robots with object manipulation. Their applications span diverse fields, including medical diagnostics, invasive surgeries, and rehabilitation. Moreover, they have demonstrated efficacy in executing complex tasks, sometimes outperforming human hands in certain scenarios [83, 85]. Textile-based sensors, with their unique textile structure, offer versatility in fabrication techniques and materials, enabling electrical conductivity. These sensors can be designed at various levels, such as yarn, fibre, or coatings, using methods like sewing, embroidering, painting, or integrating conductive yarns [10]. They find wide-ranging applications in wearable devices and possess desirable properties such as stretchability, flexibility, and sensitivity.

In general, this chapter evaluates the advantages and limitations of tactile sensors in measuring muscle activity. The study involves collecting EMG signals from the Biceps and Flexor Carpi Ulnaris muscles during dynamic exercises. Two types of sensors were compared: the commercial superficial electromyography (sEMG) sensor (Myoware EMG) and the fabric-based tactile sensor, as discussed in Chapter Three. The primary objectives were:

1. To determine the efficacy of the tactile sensor system in generating EMG output signals capable of distinguishing between different exercises, and
2. To assess the reliability of the signal produced by the tactile sensor, particularly in the context of simple exercises.

This experimental approach aims to provide insights into the capabilities and limitations of tactile sensor systems for assessing muscle activity. The chapter covers the tools, equipment, and procedures used, including the experimental design, data collection methods, statistical and analytical techniques, and validation criteria. The discussion also addresses participant demographics, informed consent procedures, validation analysis, and the presentation of raw data in tables, graphs, or other representations. The chapter concludes with an interpretation of outcomes, a comparison with existing literature, a summary of the main findings, and recommendations for future research.

5.2 Materials and Methods

This section outlines the experimental methodology employed in the current study. The approach is detailed in Section 5.2.1, covering the experimental steps. Section 5.2.2 provides an overview of the equipment used and its design considerations. Lastly, Section 5.2.3 focuses on the analysis method, explaining the filtration techniques and the evaluation of study indicators.

5.2.1 Experimental Setup and Exercise Protocol

The experimental study aimed to gather data from the Biceps muscle in the arm and the Flexor Carpi Ulnaris muscle in the forearm and wrist using two different devices. The first device, an sEMG sensor, measured EMG signals directly. The second device, a tactile sensor, detected pressure from muscle activity, which was then converted into an electrical signal using piezoelectric technology. The primary objective was to compare the EMG signals from the sEMG sensor with the pressure data from the tactile sensor to evaluate the feasibility and reliability of the custom system. The experiment involved over 60 different cases with the participation of 10 subjects (8 males and 2 females). The average characteristics of the participants were as follows: age, 40 ± 15 years; weight, 61.8 ± 13.1 kg; height, 170 ± 6.2 cm. Figure 5.1 illustrates the protocol and steps followed by each volunteer.

Step 1 involved explaining the experiment and potential risks to the volunteers. Each participant provided informed consent by signing a form (informed consent 'Recruitment Email' was obtained from all participants as outlined in Appendix A under the Ethics Application ID: 8194) that detailed the experiment's specifics. Volunteers

had the freedom to withdraw from the experiment at any time. Additionally, while the informed consent form contained all necessary information, specific exercise instructions were provided individually to each volunteer.

Step 2 encompassed the execution of the exercises, as depicted in Figure 5.1. The exercises were selected based on expert opinion and in consideration of the active involvement of the Biceps muscle in the arm and the Flexor Carpi Ulnaris muscle in the forearm and wrist. Data collection was standardised for all participants, ensuring consistency. For each movement, the muscles were held in both flexed and extended positions, and data was collected for 30 seconds in each state. This procedure was applied to all movements to ensure uniformity in the data across all participants and trials.

The exercises were as follows:

1. Arm Flexion/Extension: This exercise, proven reliable in previous studies, involved flexing and extending the arm. Data was collected for 30 seconds in both the fully flexed and fully extended positions to ensure consistency.
2. Hand Open/Close: This exercise focused on the opening and closing of the hand, serving as a basic and straightforward movement suitable for beginners [37]. Data was collected when the hand was fully opened for 30 seconds and then fully closed for 30 seconds.
3. Wrist Flexion/Extension: This exercise involved flexion and extension movements of the wrist. Data was collected for 30 seconds in both the fully flexed and fully extended positions of the wrist. Table 5.1 describes the full arm movement.

By following this data collection protocol, where movements were held for 30 seconds in both the flexed and extended states, the study ensured consistency across all participants, improving the reliability and comparability of the recorded data.

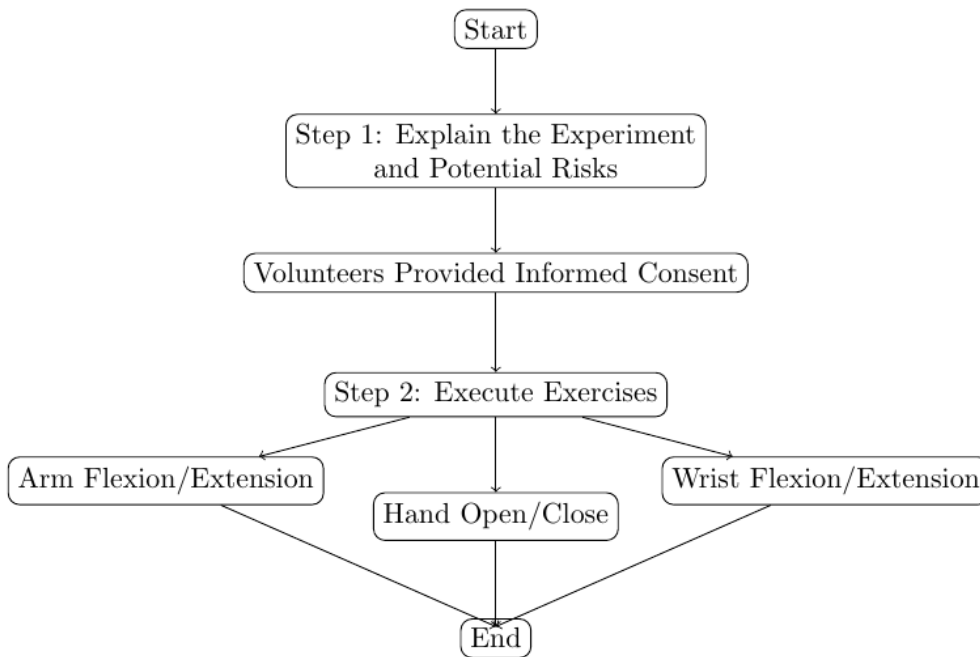


Figure 5.1: Diagram of the experiment

Table 5.1: Description of Full Arm Movement

Exercise	Number of Repetition	Duration (sec)	Description
Arm Flexion/Extension	2	30	
Hand Open/Close	2	30	
Wrist Flexion/Extension	2	30	

In Table 5.1 above, both sets of exercises are explained. Further details of each exercise are included in the same line.

5.2.2 Equipment and Sensor Systems' Description

The testbed was built using two different systems, sEMG and soft tactile sensor systems. The first system was a sEMG sensor system, and the second system comprised a set of tactile sensors. Both devices were placed separately on the same region of the muscle to obtain a signal from the same muscle during exercise. The muscles selected were the Biceps muscle in the arm, as well as the Flexor Carpi Ulnaris muscle in the forearm and wrist due to its high number of motor units [37–41]. Figure 5.2 below shows how the testing equipment was installed, the sEMG system and its wire connection with the computer and with the muscle using three electrodes. On the right side of Figure 5.2 is shown the tactile sensor. The tactile sensor needs to be placed on the muscle directly and aligned with the muscle fibres, which communicate with the computer using a wire connection.

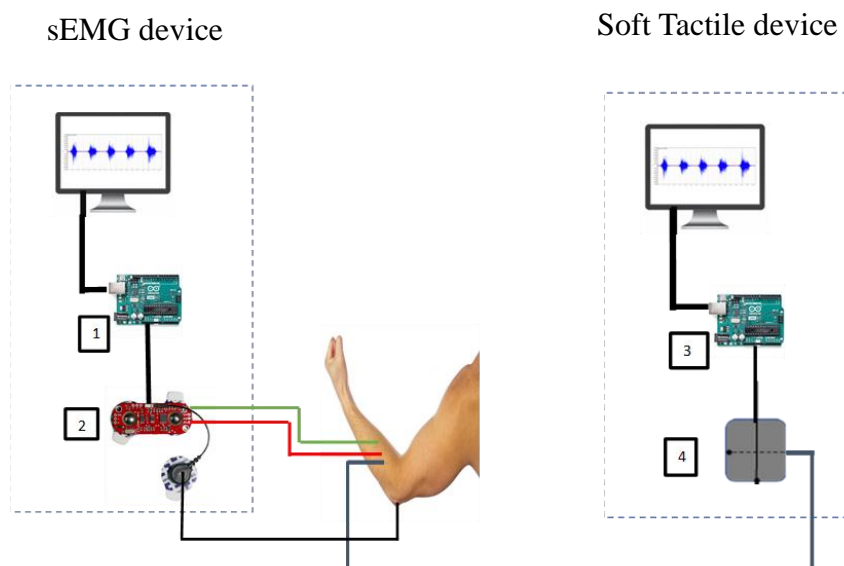


Figure 5.2: Equipment of the testbed used in the experiments. 1. & 3. Arduino Uno board. 2 Myoware EMG Muscle Sensor (SEN-13723 ROHS). 4. Soft Tactile sensor

a) sEMG System

The sEMG system consisted of three components: a laptop running Matlab [15], an Arduino board (numbered 1 in Figure (5.2)), and the sEMG sensor itself (numbered 2 in Figure (5.2)). The Arduino board played a crucial role in handling communication with the sensors, capturing and recording the data, and transmitting it to the computer for storage and subsequent analysis. For the sEMG sensor to function effectively,

three electrodes were required. The first electrode was positioned near the middle of the muscle body, represented by the red line in Figure 5.2. The second electrode was aligned with the direction of the muscle fibres and placed close to the muscle's end, as indicated by the green line in Figure 5.2. The third electrode was placed near a bony area, serving as a reference (represented by the black line in Figure 5.2) to handle any crosstalk signals from adjacent muscles [14]. These electrode placements were necessary to ensure accurate and reliable signal acquisition from the targeted muscle region. This test involved locating the targeted muscle and identifying the direction of the muscle fibres. Following this, the skin was prepared by removing any dirt and ensuring it was free of hair. To achieve hairlessness, a disposable razor was used, and the area was then cleaned using alcohol and sterile gauze. Once the skin preparation was complete, the three electrode pads were applied to the designated locations.

b) Fabric-Based Soft Tactile Sensor:

The fabric-based soft tactile sensor operates on the piezoresistive effect, where its electrical resistance changes when pressure is applied [110-113], utilising EeonTex™ knitted conductive fabric (comprising 72% nylon and 28% spandex with a proprietary conductive coating) and silver-plated conductive thread (MADEIRA yarn with linear resistance $<300\Omega/m$). To ensure fabric elasticity, a long-running loose stitch (saddle stitch) is used for sewing. When pressure is exerted on the EeonTex™ fabric, its resistance decreases due to the piezoresistive effect, with the silver-plated conductive thread capturing and transmitting these resistance changes. Meanwhile, the electronic system connects the sensor to a data acquisition module or microcontroller to measure resistance changes as voltage variations proportional to applied pressure. The fabric tactile sensor is primarily used to measure the force exerted by muscles during contraction and relaxation phases. This parameter directly reflects the mechanical pressure or tension generated by muscle activity and provides insights into muscle behaviour and activity patterns during various movements or exercises. Signal processing involves analog-to-digital conversion, signal filtering, and subsequent data analysis.

The physical prototype comprises the specified materials and is optimised for detecting resistance signals under applied forces, with $4\times 4\text{cm}^2$ sensor samples for

testing and validation (see Figure 4.8). The Arduino board played a critical role in managing communication with the sensors, recording the data, and transmitting it to the computer for storage and subsequent analysis. A summary of the features of this sensor system is provided in Table 5.2. This sensor has been widely utilised in various studies [114-125], owing to several reasons. The sensor response parameter in fabric-based tactile sensors involves changes in voltage or resistance corresponding to the force exerted by muscles during contraction and relaxation phases. As muscles contract or relax, they apply force to the sensor, resulting in variations in its electrical properties, which manifest as changes in voltage or resistance. Calibration is also essential to establish the correlation between the sensor's response and the parameter being sensed, which is the force exerted by muscles.

Fabric-based tactile sensors detect variations in voltage or resistance due to mechanical pressure or tension from muscle activity. These variations are precisely captured by placing the sensor on the targeted area and ensuring its stability during data collection [126-132]. Using computer interfaces, such as Matlab, the signals detected by the sensor are recorded and analysed. This meticulous recording procedure ensures accurate reflection of muscle activity, facilitating comprehensive calibration for reliable muscle force measurement. It is crucial to maintain sensor stability during data recording to minimise inaccuracies caused by sensor movement, which can lead to fluctuations in the detected signals and potential errors in analysis. Ensuring the sensor remains stationary throughout the recording process is vital in maintaining data quality and validity. The soft tactile sensor is notably evident for its ability to conform to diverse surfaces and shapes [130-142]. This unique characteristic makes it ideal for applications involving contact with curved or non-uniform objects, as it excels at capturing and measuring tactile information from complex surfaces.

Despite its low thickness and mass per unit area, the sensor displays high sensitivity, as demonstrated in the experiments where it accurately detected subtle changes in pressure or touch intensities [143-145]. Previous studies [16,147-156] also support this outstanding sensitivity, making the sensor well-suited for precise tactile feedback required in areas such as robotics, prosthetics, and human-machine interaction studies. The sensor's stretchability, evident in its elongation at break and warp recovery characteristics, allows it to adapt to deformations and variations in shape,

providing reliable tactile feedback during dynamic interactions. An additional advantage lies in the sensor's tuneable surface resistivity, allowing for the adjustment of its electrical properties. This feature proves valuable in applications requiring different levels of sensitivity or response, offering customisation based on specific needs. The soft tactile sensor's versatility is also a key asset, finding applications in wearable devices, human-computer interfaces, robotic systems, and medical applications, making it a popular choice among researchers and developers [151,157].

Overall, the combination of conformability, sensitivity, stretchability, tuneable surface resistivity, and versatility has led to the widespread adoption of the soft tactile sensor in various studies. Its flexibility and adaptability make it a valuable tool for capturing and analysing tactile information, contributing to advancements in robotics, human-computer interaction, and biomedical engineering [154-163].

Table 5.2: Specifications of Soft Tactile Sensor

Parameters	Value
Conductive stretchable fabric thickness (mm)	0.38
Mass per unit area (g/m ²)	113.78
Elongation at break (%)	40
Warp recovery after stretching (%)	85
Tunable surface resistivity (Ω /sq)	10 ⁴ to 10 ⁷

This tactile sensor distinguishes itself by not only identifying tactile input, but also by discerning movement intentions and monitoring muscle activities in various sections of the upper limb, including the arm, forearm, and wrist. The innovative approach involves integrating this sensor into a wearable sleeve designed to be comfortably worn on these three segments of the upper limb. The underlying concept stems from the idea that muscle contractions induce changes in the shape and volume of surrounding tissue, resulting in mechanical pressure variations promptly detected by the sensor. The approach is innovative in comparison to conventional wearable sensors, which typically focus on either monitoring muscle activity or predicting movement intentions. Through this concept, it is proposed to integrate a specialised

sensor into a wearable sleeve designed for the arm. Additionally, what sets this sensor apart is its distinct ability to evaluate both muscle activity and intended movements concurrently, representing a shift from conventional sensor functionalities. This novel approach holds the potential to enhance the level of understanding of arm functionality, which could find applications in various fields such as aiding in rehabilitation, sports research, and optimising human-machine interactions. This represents a significant stride in incorporating intelligent sensors into clothing for comprehensive monitoring of the human body.

5.2.3 Analysis Method

After completing all the exercises and saving the signals from both the sEMG and soft tactile sensor devices, the data analysis process commenced; and it is important to address the potential impact of noise on the EMG signal from both medical and scientific/technical perspectives. From a medical standpoint, an EMG signal distorted by noise could lead to an inaccurate diagnosis of muscle behaviour. Similarly, from a scientific and technical standpoint, a signal contaminated by noise is unable to ensure an accurate interpretation of the results, thereby compromising the reliability of research findings [47-49].

The choice to employ signal filtering is based on the characteristics of the signal itself, as indicated in reference [50]. In the current research, signal filtering was a crucial step in enhancing the quality and reliability of data obtained from the soft tactile sensor systems. Filtering was implemented to eliminate noise and artefacts, improving the clarity and accuracy of the muscle activity signals used for analysis.

A bandpass Butterworth filter was employed, which is widely used in signal processing for its ability to isolate signals within a specific frequency range while suppressing unwanted frequencies outside that range. The filter was configured with a fourth-order filter and a frequency range of 40-100 Hz, carefully chosen to align with the characteristics of the tactile sensors and the frequencies at which muscle activity and tactile information are most prominent.

The application of this filter ensured that signals captured by the tactile sensors focused on pertinent physiological phenomena while reducing noise interference.

The decision to use filtering is based on established signal-processing practices [47]. It was essential to apply this step before conducting further analysis to ensure accurate and reliable data interpretation. Without proper filtering, signal noise could have led to inaccuracies, potentially affecting the integrity of the research findings.

Accordingly, in the current study, a robust analysis methodology was carefully selected that was inspired by established practices in the field [98]. The analysis process involved key stages: Signal Processing, Maximum Voluntary Contraction (MVC) Computation, which refers to the maximum amount of force that a muscle can generate voluntarily under specific conditions, and Normalisation, and Assessment of Indicators; all of which ensured reliable and meaningful results from two independent measurement systems.

a.Enhancing Data Accuracy through Advanced Signal Processing Techniques:

In the current experiment, signal filtering played a crucial role in improving the quality and reliability of the data collected from both the sEMG and soft tactile sensor systems. While signal filtering is a well-known concept in signal processing, its significance to these devices cannot be overstated. The sEMG and soft tactile sensor systems are highly sensitive instruments intended to capture intricate patterns of muscle activity and tactile feedback, respectively. However, these sensitive sensors are vulnerable to different types of noise, such as electromagnetic interference and baseline wander. Without effective noise reduction, this interference can obscure the true signals of interest, potentially leading to inaccurate conclusions.

b.MVC Computation and Normalisation

For each exercise, Maximum Voluntary Contraction (MVC) values were individually calculated to establish personalised baselines. This allowed equitable comparisons between individuals and exercises, considering variations in strength levels and muscle capabilities.

c.EMG Signal Normalisation for Biceps and Flexor Carpi Ulnaris Muscles:

To ensure an accurate comparison of EMG signals, normalisation was performed for each exercise related to the Biceps muscle in the arm and the Flexor Carpi Ulnaris

muscle in the forearm and wrist. This step was necessary due to significant differences in the output ranges of the different equipment sets used. Figure 5.3 illustrates the steps involved in signal normalisation during dynamic exercises, such as Arm flexion/extension, Hand open/closed, and Wrist flexion/extension. The signal was first acquired and then subjected to denoising during the signal processing stage. Subsequently, the dynamic EMG signal was normalised using the following formula:

$$\text{Signal Normalisation} = \frac{EMG \text{ Signal} - EMG_{min}}{EMG_{max} - EMG_{min}} \quad (1) \text{ (where the signal normalisation}$$

range is [0, 1])

This normalisation formula was selected based on its ability to standardise the EMG signals, making them comparable across different exercises and individuals [159]. This accounts for variations in signal amplitudes and ensures uniformity in the interpretation of muscle activation levels. These normalised signals are then utilised to derive MVC values from both the sEMG sensor and the soft tactile sensor separately. The choice of this normalisation formula arises from its efficacy in standardising EMG signals across different exercises, facilitating accurate comparison and analysis of muscle activity levels.

d. Comparison of MVC Values with Literature Values:

The MVC values in this study for the Biceps Brachii ranged from approximately 60% to 100% of maximum voluntary force, which is consistent with literature values for isometric or dynamic movements of this muscle. Studies report EMG signal amplitudes for the Biceps Brachii typically between 150 μV and 500 μV , depending on movement type and equipment sensitivity [164,165]. The MVC data collected in this study align well with these ranges, indicating the reliability of the methodology.

For the Flexor Carpi Ulnaris, MVC values ranged from 30% to 70% of maximum voluntary force, which also corresponds with published data for gripping and wrist flexion tasks [166]. This alignment with the literature reinforces the accuracy of the MVC computation and signal normalisation methods used in the study.

Overall, the normalised MVC values fall within the expected range reported in the literature, validating the use of the chosen methodology for assessing muscle activity through both sEMG and tactile sensors. The consistency of MVC values across studies confirms the robustness of the data collection and normalisation protocols.

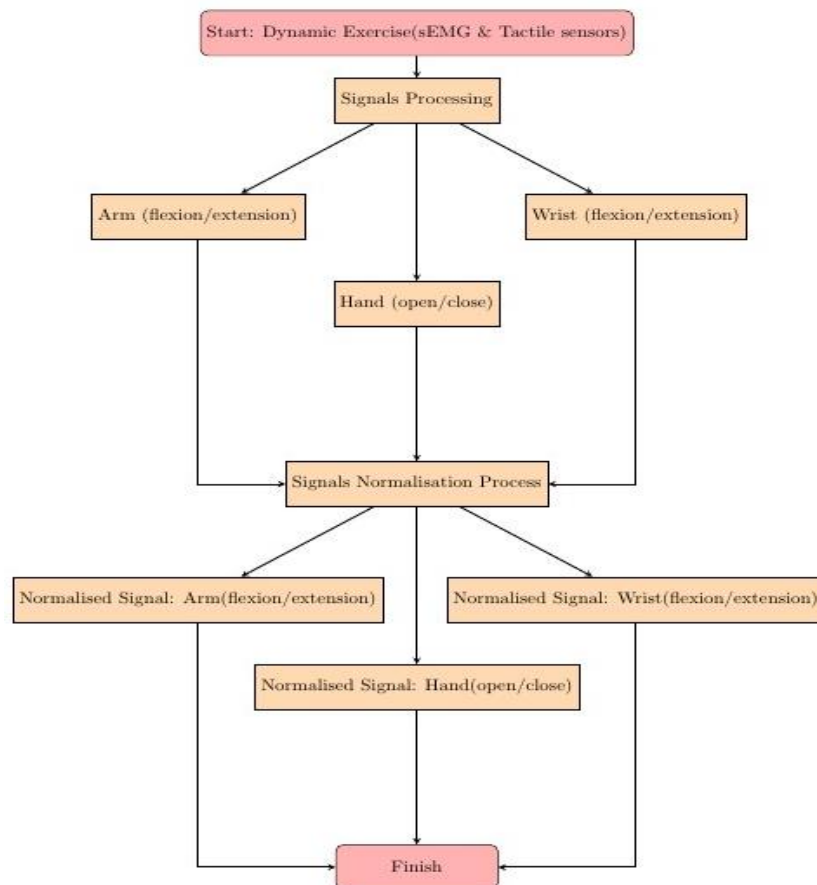


Figure 5.3: Diagram followed to normalise the sEMG & soft Tactile sensor signal from the dynamic exercises

Figure 5.3 above illustrates the normalisation process employed to standardise the data obtained from both the sEMG and soft tactile sensor systems during dynamic exercises. This diagram outlines the essential steps taken to ensure that signal amplitudes from these two distinct sensors are directly comparable, enabling accurate analysis and interpretation of muscle activity across various exercises. Further, the normalisation process is crucial in the current study as it helps to accommodate the diverse strengths and muscle capabilities of the participants. By dividing the recorded signal amplitudes by the corresponding Maximum Voluntary Contraction (MVC) values unique to each exercise, it is possible to establish a normalised dataset that ensures fair comparisons across individuals and exercises. It is also essential to acknowledge

that different normalisation methods may indeed influence the outcomes from the study. However, by adopting a standardised approach and documenting the normalisation procedures, the aim is to minimise potential biases and ensure the reliability of the results.

5.3 Validation Indicators

In the current research, validating the signals from the soft tactile sensor against those from commercial sEMG systems holds significant weight. To ensure the validation process's thoroughness and accuracy, a series of carefully chosen validation indicators were selected. Each indicator serves a distinct purpose that directly corresponds to the objectives of the study.

- **Kendall Correlation Coefficient (Kendall's Tau):** Kendall's Tau was selected as an indicator due to its non-parametric nature [167-169]. In this context, it is necessary to deal with complex muscle activity patterns that may not adhere to specific distributions. Kendall's Tau enables the possibility to assess the strength and direction of association between paired observations, which is particularly valuable when comparing ranked variables. This indicator enables the exploration of ordinal relationships and correlations between the tactile sensor and sEMG signals without making assumptions regarding the underlying data distributions.
- **Spearman's Correlation:** Spearman's correlation is employed to evaluate the monotonic relationship between two variables [169-172]. It is especially useful in scenarios where it is important to assess the degree of similarity between signals from different sources. By using Spearman's correlation, it is possible to quantify the degree of monotonic association between the tactile sensor and sEMG signals, providing insights into their overall agreement.
- **Energy Ratio:** To assess the similarity in energy between the two signals, the energy ratio indicator is employed [172,173]. This metric is particularly relevant in the application as it tests whether the EMG waves have a comparable form in both the tactile and commercial sEMG systems. Specifically, a high energy ratio suggests a strong similarity in the energy levels of the signals, indicating a consistent representation of muscle activity

- **Cross-Correlation Coefficient (CC):** The CC method is a well-established technique for comparing EMG signals [173-178]. Its application in my study enables us to measure the degree of correlation between the tactile sensor and sEMG signals. This indicator is valuable in capturing both positive and negative correlations, providing a comprehensive view of the signal agreement.
- **Pearson Correlation Coefficient:** The Pearson correlation coefficient, a widely recognised indicator for correlation analysis [179-182], was chosen to assess the linear relationship between the two variables. This metric allows the exploration of the linear association between the tactile sensor and sEMG signals, offering additional insights into their correlation.

- **Data Formatting and Correlational Analysis**

Data from 10 volunteers were used to perform the correlation analysis for each movement, including hand open/close, wrist flexion/extension, and arm flexion/extension. For each movement, the signals were processed and compared across volunteers using the following steps:

1. **Data Segmentation:** Data from each volunteer were segmented by movement type. Signals from the tactile sensor and sEMG system were collected separately for hand open/close, wrist flexion/extension, and arm flexion/extension.
2. **Correlation Analysis:** For each movement, the Kendall, Spearman, Pearson, Cross-Correlation, and Energy Ratio indicators were computed across all 10 volunteers. These indicators were calculated by correlating the signals from the tactile sensor and sEMG system for each movement.
3. **Statistical Summary:** After computing the correlations for each volunteer and each movement, the results were summarised by calculating the maximum (Max), minimum (Min), mean (μ), and standard deviation (σ) for each validation indicator. These statistical summaries provided insights into the consistency and variability of the correlation across the different volunteers.
4. **Result Interpretation:** The Max, Min, μ , and σ values for each indicator (Kendall, Spearman, Energy, Cross-Correlation, and Pearson) were then used to compare the performance of the tactile sensor relative to the sEMG system.

High Max and μ values indicated strong agreement between the two systems, while the Min and σ values helped identify the range and variability in the results across volunteers.

The following validation indicators were used to assess how well the tactile sensor system matched the commercial sEMG system, as summarised in Table 5.3:

Table 5.3: Summary of Validation Indicators for Tactile Sensor and EMG Sensor Comparison

Indicator Name	Equations	Citations
Kendall Correlation (KC)	$KC = \frac{\text{Number of Concordant Pairs} - \text{Number of Discordant Pairs}}{\text{Total Number of Pairs}(n(n - 1)/2)}$	[169]
Spearman Correlation (SP)	$SP = 1 - [(6 * \sum d^2)/(n * (n^2 - 1))]$	[172]
The energy between EMG signals (Energy)	$E = \int (x(t))^2 dt$	[173]
Cross Correlation (CC)	$CCC = \frac{n(\sum xy) - (\sum x)(\sum y)}{\sqrt{[n(\sum x^2) - (\sum x)^2][n(\sum y^2) - (\sum y)^2]}}$	[174]
Person Correlation (PC)	$PC = \frac{\text{cov}(x, y)}{\sigma(x)\sigma(y)}$	[181]
Statistical Measure		

Maximum Value (Max)	$\max(a_1, a_2, a_3, \dots, a_n)$	[22]
Minimum Value (Min)	$\min(a_1, a_2, a_3, \dots, a_n)$	[25]
Mean Value (μ)	$\mu = \frac{a_1 + a_2 + a_3 + \dots + a_n}{n}$	[27]
Standard Deviation (σ)	$\sigma = \sqrt{\frac{\sum_{i=1}^n (x_i - x')^2}{n - 1}}$	[32]

5.4 Participant Demographics, Informed Consent, and Validation Analysis

5.4.1 Participant Demographics and Informed Consent

The validation of the soft tactile sensor system was undertaken using volunteers who participated in the experiment. There were eight male and two female volunteers from different backgrounds, with an average age of 40 ± 15 years, an average height of 170 ± 6.2 cm and an average weight of 61.8 ± 13.1 kg. All the volunteers were informed in regards to the experiment and agreed to use all the data for scientific purposes. In addition, they were informed that the experiment could be stopped at any time as they wished, with no obligation to complete it.

5.4.2 Validation Analysis

This section presents a comprehensive analysis of the validation process, which involved a substantial dataset comprising more than 60 unique curves. Each curve was generated through the repetition of exercises by the participating volunteers. The primary objective of this analysis is to assess the performance of the tactile sensor system in comparison to the commercial sEMG system.

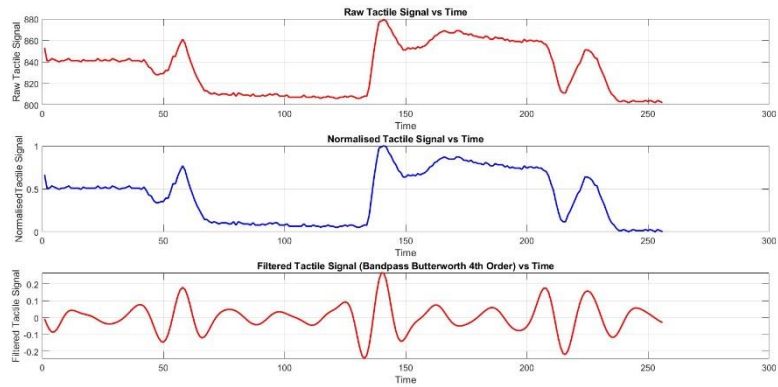
5.5 Experimental Findings and Sensor Performance Analysis

In the upcoming section, findings are shared from the current study, which is initiated by introducing the volunteers who took part in the experiment. Then, the results are presented, highlighting how the soft tactile sensor and sEMG sensor systems performed during different exercises. The results are subsequently divided into two main areas: signal filtering and assessment of physical exercises and indicators.

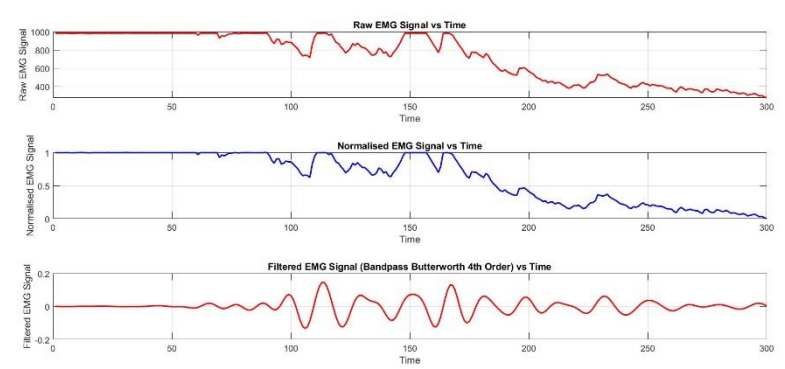
5.5.1 Signal Filtering

As previously described in Section 5.2.3, a bandpass Butterworth filter was applied to improve signal quality. This filtering process is illustrated in Figure 5.4, showing signals before and after applying the filter specifically for biceps flexion/extension, forearm open/closed hand, and wrist flexion/extension movements. This comparison demonstrates the effectiveness of the filtering technique in isolating relevant muscle activity across these targeted movements, highlighting the contrast between raw and filtered data for each case.

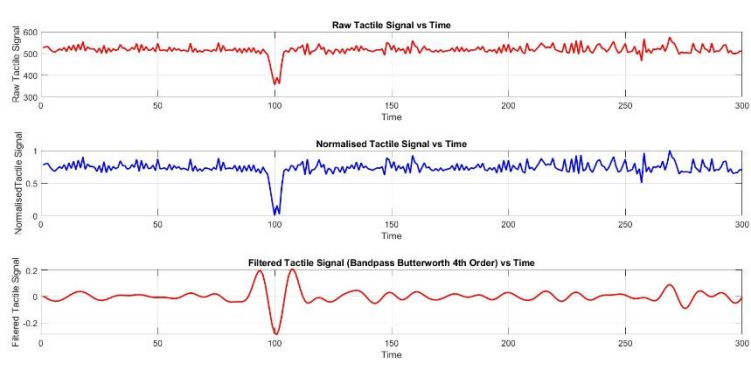
Biceps using Tactile sensor



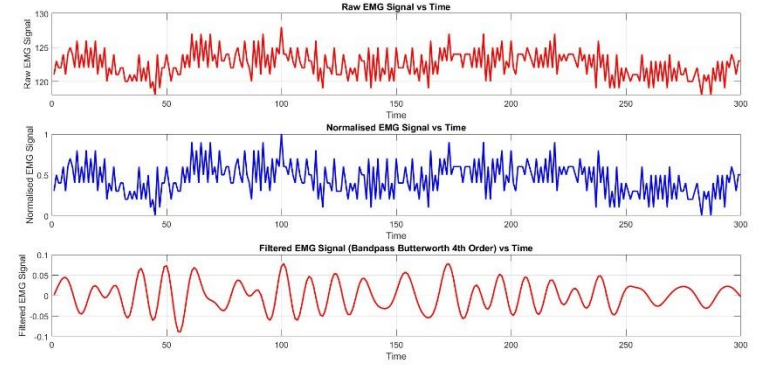
Biceps using sEMG sensor



Forearm using Tactile sensor



Forearm using sEMG sensor



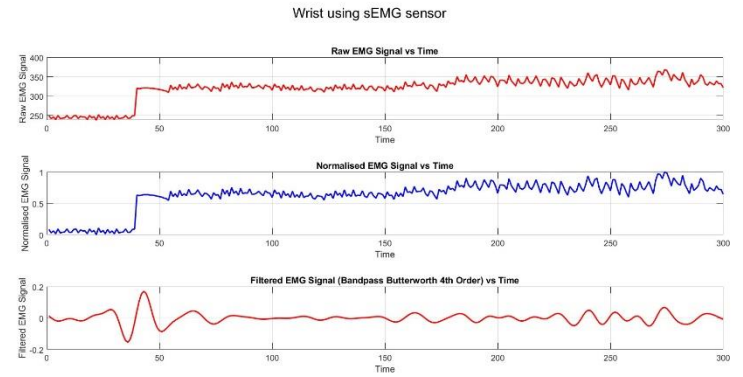
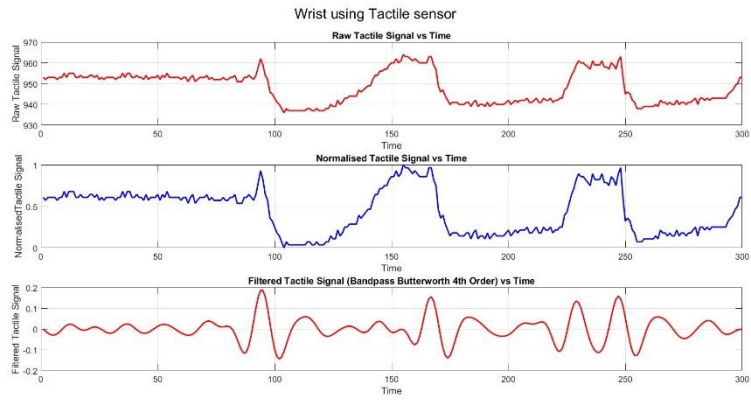
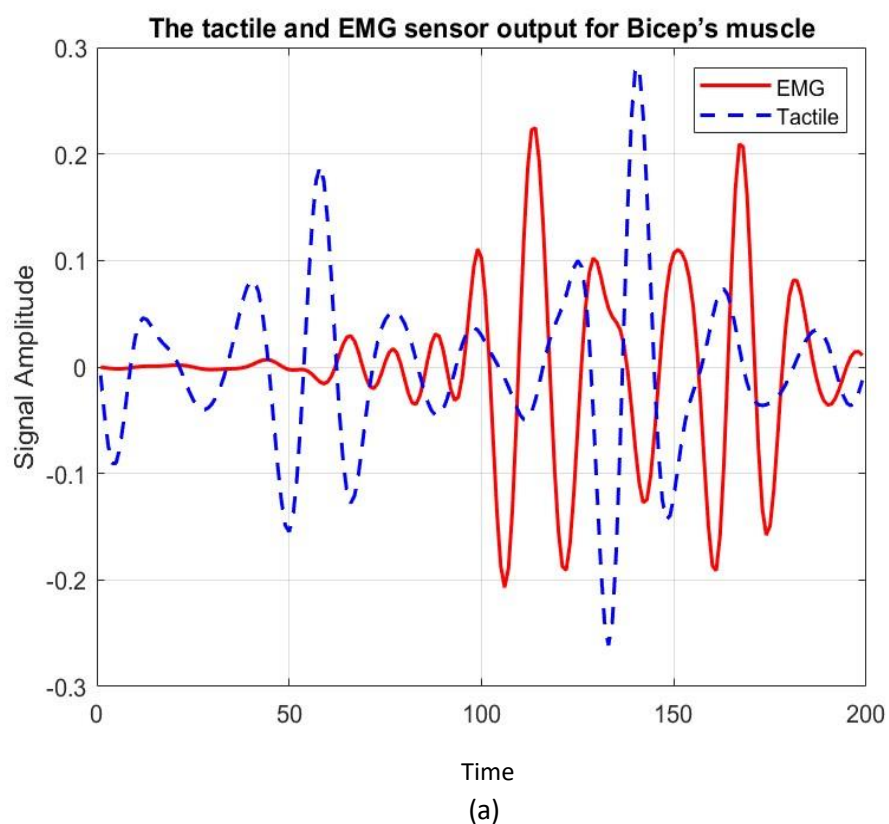


Figure 5.4: Comparison of Raw and Filtered Signals for Biceps, Forearm and Wrist Muscles

In Figure 5.4 the unfiltered signals before applying the filter exhibited high-frequency noise and fluctuations, which are commonly introduced by external interference or electronic noise. These unfiltered signals often showed sharp peaks, irregular patterns, and baseline wander, making it difficult to accurately interpret the muscle activity. For instance, in electromyography (EMG) signals, this noise could distort observations of muscle contractions.

After applying the 4th-order Butterworth bandpass filter, the signals became smoother and more consistent. The high-frequency noise was largely removed, allowing the true waveform that reflects genuine muscle activity to become more prominent. The key feature of the Butterworth filter is its maximally flat frequency response in the passband, preserving the true signal characteristics while filtering out the noise. Figure 5.5 illustrates the steps involved in signal filtering and its impact on data quality.



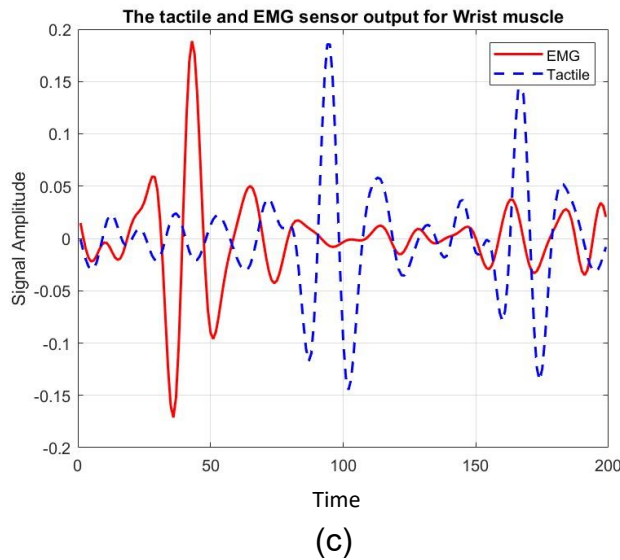
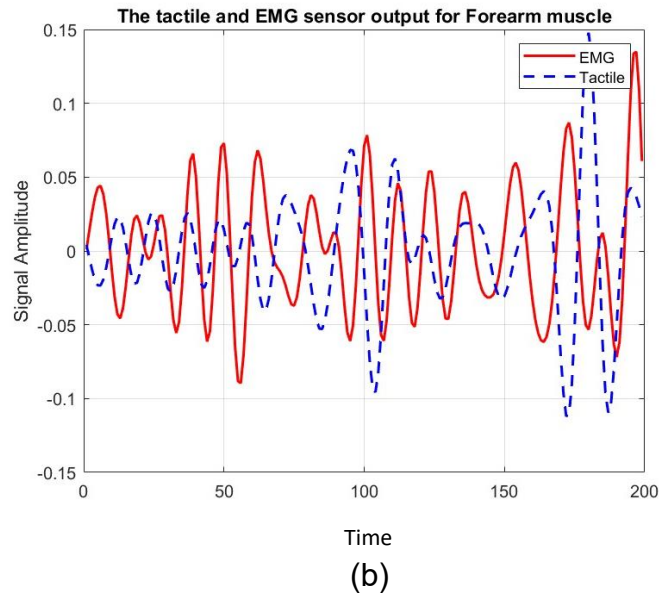


Figure 5.5: A visualisation of the filtered signals to illustrate the effectiveness of the noise reduction process. (a) The tactile and EMG sensor output for the Bicep’s muscle; (b) The tactile and EMG sensor output for the Forearm muscle; (c) Tactile and EMG sensor output for the Wrist muscle.

The analysis presented in Figure 5.5 illustrates the effects of applying a Butterworth filter (order 4) to refine tactile and EMG sensor data collected from various muscles, including the Bicep, Forearm, and Wrist. The figure shows the stabilisation of both tactile and EMG signals over time for each muscle group.

. This showcases that the application of the Butterworth filter enhances signal clarity by reducing noise interference, enabling more accurate analysis of muscle activity dynamics. Additionally, the figure demonstrates the differing response times and stabilisation patterns between tactile and EMG signals across different muscle groups.

5.5.2 Physical Exercises

Previous studies have established the correlation between muscle work activation levels and the output signal [25,43,180]. In this section, the focus is on demonstrating the compatibility of the tactile system with the commercial sEMG system, thereby confirming its reliability. To evaluate this, the maximum voluntary contraction (MVC) values are introduced derived from the physical exercises. These MVC values signify the muscle's maximum force output and act as a reference point for comparing the performance of both systems. In Figure 5.6 below, the distribution of maximum voluntary contraction (MVC) values are illustrated based on the exercise performed and the equipment utilised. This visual representation offers insight into the Maximum Voluntary Contraction (MVC) values recorded during the experiments. MVC measures the maximum force or effort a muscle or muscle group can generate during a specific contraction task. Throughout the current study, MVC values were gathered from all participating volunteers.

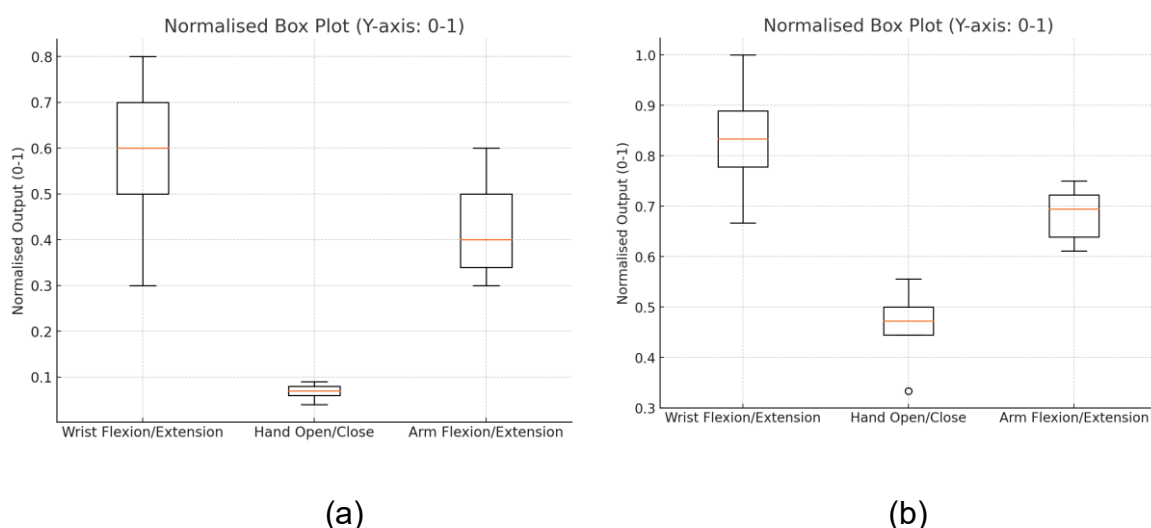


Figure 5.6: Illustration of the distribution of maximum voluntary contraction (MVC) values based on the exercise performed and the equipment used: (a) By using sEMG Sensor; (b) By using Tactile Sensor

In Figure 5.6 above the distribution of MVC values based on both the exercises conducted and the equipment used is presented, offering an overview of the MVC values recorded during my experiments. MVC represents the maximum force a muscle or muscle group is able to generate during a specific contraction task, and values were collected from all participants across the study. The comparison between the MVC values for wrist flexion/extension, hand open/close, and arm exercises using the sEMG and tactile sensor systems reveals distinct differences. Specifically, for wrist flexion/extension and hand open/close exercises, the sEMG sensor recorded higher values compared to the tactile sensor, indicating greater muscle activity detected by the sEMG system. Conversely, the tactile sensor exhibited lower MVC values across all exercises, suggesting a different level of sensitivity and response compared to the sEMG system. These variations underscore the importance of considering the specific requirements of each exercise when selecting the appropriate sensor technology, as differences in sensitivity and responses may impact the accuracy and interpretation of the recorded data.

5.5.3 Indicator Assessment

The results of the comparison between the commercial sEMG system and the soft tactile sensor system, based on the indicators, are presented in Table 5.4. These indicators provide valuable insights into the signal characteristics and the system's reliability when employed for simple exercises, as conducted in the experiment.

Table 5.4: Comparison of Statistical Indicators for sEMG and Tactile Sensor Systems. (KC): Kendall Correlation; (SP): Spearman's Correlation; (TE/sEMGE): Energy Comparison of Tactile and sEMG Sensor Systems; (CC): Cross-Correlation Coefficient; (PC): Pearson Correlation

Measurement Type	Statistical Measure	Wrist Flexion	Wrist Extension	Hand Open	Hand Close	Arm Flexion	Arm Extension
KC	Max	1	1	1	1	1	1
	Min	-0.4597	0.4358	-0.0996	0.5069	-0.4154	0.1399
	μ	0.2702	0.7179	0.4502	0.7534	0.2923	0.5699
	ϵ	0.8427	0.3257	0.6349	0.2847	0.8172	0.4966
SP	Max	1	1	1	1	1	1
	Min	-0.6089	0.5917	-0.1968	0.6805	-0.5808	0.1941
	μ	0.1956	0.7959	0.4016	0.8402	0.2096	0.5970
	ϵ	0.9289	0.2357	0.6909	0.1845	0.9127	0.4653
TE/sEMGE	Max	0.075133	0.061742	0.046046	0.059431	0.04965	0.0583
	Min	0.001624	0.024102	0.0058264	0.0034962	0.01004	0.0265
	μ	0.04019	0.036686	0.034947	0.036935	0.03082	0.03701
	ϵ	0.0262	0.005945	0.006792	0.004570	0.01109	0.00414
CC	Max	0.6695	0.9764	0.9632	0.9878	0.8723	0.9764
	Min	1.039e ⁻⁰⁴	0.0011	3.52e ⁻⁰⁴	0.0013	3.923e ⁻⁴	0.0011
	μ	0.3383	0.4875	0.4819	0.4928	0.4412	0.4875
	ϵ	0.2746	0.2733	0.3013	0.2842	0.2900	0.2733

PC	Max	1	1	1	1	1	1
	Min	-0.0953	0.6522	-0.0472	0.4062	-0.6182	0.3023
	μ	0.4523	0.8261	0.4764	0.7031	0.1909	0.6511
	σ	0.6324	0.2008	0.6046	0.3428	0.9342	0.4028

Table 5.4 presents a detailed comparison of the performance of the sEMG system and the soft tactile sensor system across six types of movements: wrist flexion, wrist extension, hand open, hand close, arm flexion, and arm extension. The table includes various statistical indicators such as Kendall Correlation (KC), Spearman's Correlation (SP), Energy Comparison (TE/sEMGE), Cross-Correlation (CC), and Pearson Correlation (PC). Each of these measures is reported with maximum (Max), minimum (Min), mean (μ), and standard deviation (σ) values.

Kendall Correlation (KC): Max values of 1 indicate a perfect correlation between the tactile sensor and sEMG signals for each movement type, demonstrating a strong agreement.

Negative Min values suggest some level of discordance between the two systems, indicating situations where the sensor outputs deviate from each other (e.g., in wrist flexion and arm flexion).

The mean (μ) and standard deviation (σ) provide a summary of consistency, showing how well the sensor systems agree overall, with wrist extension and hand close having higher mean correlations.

Spearman's Correlation (SP): Similar to Kendall, the Max values of 1 represent a perfect monotonic relationship, reflecting how the tactile sensor's output and the sEMG data change together across movements.

Negative Min values indicate inverse relationships for certain movements and the mean (μ) values show relatively strong monotonic correlation across movements, particularly for wrist extension and hand close.

Energy Comparison (TE/sEMGE): This indicator measures the energy similarity between the two systems. Higher Max values imply that the tactile sensor's energy output is comparable to the sEMG signals.

The Min values show lower energy alignment for certain movements, such as wrist flexion and arm flexion, while the mean (μ) and standard deviation (σ) indicate overall energy comparison consistency across volunteers.

Cross-Correlation (CC): Max values close to 1 indicate strong temporal similarity between the tactile sensor and sEMG system outputs, showing that the signals are highly synchronised in time, particularly for movements like hand close and wrist extension.

Min values near zero indicate less synchronisation in certain movements, while the mean (μ) and standard deviation (σ) reflect the overall temporal correlation performance.

Pearson Correlation (PC): Max values of 1 denote a perfect linear relationship, suggesting a strong direct correlation between the two systems for all movement types.

The Min values show some weak or negative linear correlations in movements like wrist flexion and arm flexion, while the mean (μ) values are generally high, with wrist extension and hand close showing the strongest linear correlations.

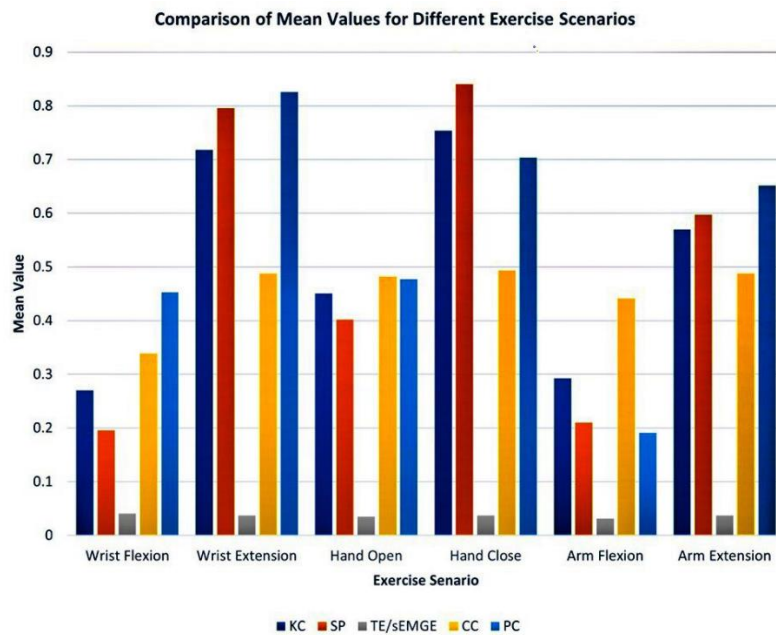


Figure 5.7: The Comparison of Mean Values for Different Exercise Scenarios

In Figure 5.7 above a visual representation of the mean values (μ) is presented for various exercise scenarios across different indicators. This chart provides a clear overview of the comparative analysis conducted in the current study.

5.6 Discussion and Implications

In the discussion and implications section, the aim is to explore the significance of the correlation measurements provided in the table. These measurements, including Kendall Correlation (KC), Spearman Correlation (SP), Energy, Cross Correlation (CC), and Pearson Correlation (PC), were computed between EMG signals acquired from both sEMG sensors and Soft Tactile sensors. This analysis covers various muscle movements, such as wrist flexion, wrist extension, hand open, hand close, arm flexion, and arm extension. By examining these correlation measurements, it is possible to gain insights into the consistency and reliability of the data captured by the two sensor types across different muscle movements. Additionally, it is possible to explore potential implications for the usability and effectiveness of each sensor types in monitoring and interpreting muscle activity during different activities.

a. Correlation Measurements

The examination of correlation measurements between signals recorded by the two types of sensors provides valuable insights into how they relate to each other and their potential applications in assessing muscle activity and movement. A detailed analysis of these measurements was conducted, which are summarised in Table 5.4 and visually represented in Figure 5.6 below. Analysing correlation measurements between different types of sensors helps to improve the understanding of their strengths and weaknesses in evaluating muscle activity and movement. By comparing correlation coefficients, such as Kendall Correlation (KC), Spearman Correlation (SP), Cross Correlation (CC), and Pearson Correlation (PC), it is possible to determine how well surface EMG (sEMG) sensors and Soft Tactile sensors align in capturing muscle activity patterns. In particular, higher correlations indicate better agreement between sensor outputs, suggesting higher reliability and accuracy. Furthermore, to understand which sensors perform best under specific conditions or movements is crucial for effective sensor selection.

b. Kendall Correlation (KC) and Spearman Correlation (SP)

The positive orientation of both KC and SP values across various muscle movements suggests a consistent trend of correlation between signals from the sEMG and Soft Tactile sensors. This consistency implies that the two sensor types are capturing

similar patterns of muscle activity during the analysed movements. However, it is important to note that the strength of correlation, as indicated by the magnitude of KC and SP values, may vary between different movements. For instance, movements with KC and SP values closer to 1 indicate a strong positive correlation between sensor signals, suggesting high agreement in muscle activity detection between the two sensor types. Conversely, movements with lower KC and SP values, albeit positive, may indicate weaker correlations and potentially more variability in the signals captured by each sensor type. Further, analysing the specific movements, where correlations are weaker, can provide insights into potential factors that influence sensor performance. What is more, differences in muscle group activation, movement complexity, or sensor placement could contribute to variations in correlation strength across different activities. Additionally, exploring the directionality of the correlation, especially in cases where KC and SP values are negative or close to zero, can offer valuable insights. Meanwhile, negative correlations may indicate inverse relationships between sensor signals, suggesting contrasting patterns in muscle activity detection.

c. Energy Measurements

Based on the data provided in Table 5.4, which illustrates measurements related to wrist flexion, wrist extension, hand open, hand close, arm flexion, and arm extension, insights can be derived into the energy levels inherent in the EMG signals across these movements. Across all measured movements, the maximum energy values appear to be relatively modest, suggesting that the EMG signals exhibit a generally low power level. However, it is crucial to interpret these energy values within context, which can be influenced by several factors, including the intensity of muscle contractions and the proximity of the sensors to the muscles being measured.

It is also important to comprehend that the minimum, mean, and standard deviation values for each movement provide a comprehensive view of the energy distribution within the EMG signals. These metrics offer valuable insights into the variations and characteristics of the muscle activity recorded during the movements analysed.

d. Cross-Correlation (CC)

The Cross-Correlation (CC) values in Table 5.4 quantify the degree of similarity between the electromyography (EMG) signals collected by the surface EMG (sEMG)

and Soft Tactile sensors across various movements. The correlation coefficients range from nearly zero to one, with higher values indicating greater resemblance between the sensor outputs. Upon analysis, it was found that the minimum CC values clustered around zero for all movements. For instance, in movements, such as wrist flexion and arm extension, the minimum CC values were approximately 0.001, indicating significant divergence between the signals captured by the two sensor types during these movements. Conversely, the maximum CC values differed by movement, suggesting that the strength of agreement between sensor outputs varied depending on the specific motion being performed. For example, in movements, including wrist extension and hand closing, the maximum CC values approached 0.9764, indicating a high degree of similarity between the sensor outputs. This suggests that the signals captured by both sensor types were closely aligned during these movements. Accordingly, by examining the range of correlation values for each movement, insights are gained into when and how these sensors capture comparable vs. distinct EMG patterns. Movements with higher CC values suggest greater similarity in sensor readings, while movements with lower CC values imply more variability between sensor outputs.

e. Pearson Correlation (PC)

The Pearson Correlation (PC) coefficients provided in Table 5.4 offer valuable insights into the relationship between the electromyography (EMG) signals captured by the surface EMG (sEMG) and Soft Tactile sensors. Upon examining the data, positive PC values could be observed ranging from approximately 0.2 to 0.9, indicating that heightened muscle activity detected by one sensor corresponds to increased activity measured by the other. This suggests a consistent alignment in the muscle activity patterns detected by both sensor types across various movements analysed. While these positive correlations are promising, it is essential to explore deeper into their implications and variations. It was also noted that while some movements exhibited strong correlations between the sensor outputs, with PC values approaching 0.9, others presented weaker correlations, with PC values of approximately 0.2 to 0.4, suggesting slight differences in muscle activation patterns. This variability underscores the importance of understanding the context-specific nature of sensor readings and their interpretive nuances.

Based on the correlation measurements provided in Table 5.4, the potential variability in correlation values is acknowledged across different movements and individuals. This variability is evident in the range of correlation coefficients observed for each movement and sensor type. For instance, the Pearson Correlation (PC) coefficients range from approximately 0.2 to 0.9 across various movements, indicating differences in the strength of correlation between EMG signals captured by surface EMG (sEMG) and Soft Tactile sensors. In relation to this variability, the plan is to conduct further statistical analysis to precisely quantify the extent of variability in correlation values, which involves comparing correlation coefficients using appropriate statistical tests to determine the significance of the observed differences. By conducting rigorous statistical analysis, the aim is to gain a deeper understanding of the factors that contribute to variability in correlation measurements, thereby enhancing the robustness and reliability of the findings.

In addition, based on the experimental data analysis conducted in the current study, several key outcomes and findings emerged, highlighting the performance and reliability of the sEMG and soft tactile sensor systems in capturing muscle activity and tactile feedback during dynamic exercises. The outcomes of the data analysis are presented below:

- **Strong Correlation between Sensors:** The analysis revealed a robust correlation between soft tactile sensors and surface electromyography (sEMG) recordings, indicating the reliability of tactile feedback as an indicator of muscle activity during dynamic exercises.
- **Validation of Measurement Techniques:** Validation techniques, including Kendall, Spearman, Energy, Cross-Correlation, and Pearson Correlation, confirmed the accuracy and consistency of data measurements, ensuring the reliability of the study's conclusions.
- **Documentation of Participant Demographics:** Detailed documentation of participant demographics enhanced the context for result interpretation, providing valuable insights into the representativeness of the study sample.
- **Implications for Various Fields:** The study's findings present significant implications for rehabilitation, sports science, and human-machine interfaces,

offering insights into motor rehabilitation, athletic performance optimisation, and improved human-computer interaction interfaces.

5.7 Muscle Activity Analysis and Rehabilitation Potential: Insights from Parkinson's Disease and Stroke Individuals

Parkinson's disease and strokes are neurological conditions known to profoundly affect motor function and coordination [2,18,182]. Understanding the specific motor control deficits associated with these conditions is essential in developing effective rehabilitation strategies. In this section we explore muscle activity patterns during hand movements in individuals with Parkinson's disease and stroke, utilising a newly designed soft tactile sensor and advanced signal processing techniques. The aim is to assess the efficacy of this sensor in capturing muscle activity in real patients and to characterise the motor control differences between individuals with Parkinson's disease, stroke survivors, and healthy controls. Specifically, the focus lies on analysing forearm and wrist muscle activity during tasks involving gripping an apple and manipulating a key, with emphasis on the dominant hand. To achieve the research objectives, participants who met the inclusion criteria for Parkinson's disease or stroke rehabilitation were recruited. Muscle activity signals were recorded during the specified tasks and processed using MATLAB to extract relevant information. The results were then plotted to visualise muscle activity patterns.

By comparing the results obtained from patients with Parkinson's disease and stroke individuals to those of healthy subjects, alongside testing my tactile sensor, the aim is to elucidate the distinct ways that each condition impacts motor control. This investigation holds promise for providing valuable insights into the underlying mechanisms of motor impairments in Parkinson's disease and strokes, thereby informing the development of targeted rehabilitation interventions to enhance motor function and improve the quality of life for affected individuals. Additionally, the statistical measurements presented in Table 5.5 offer a quantitative overview of muscle activity levels and variability across individuals, serving as a foundational reference for understanding the observed patterns. Furthermore, Figures 5.27 (Wrist Muscle Activity) and 5.28 (Forearm Muscle Activity) will be shown at the end of this chapter, visually depict the muscle activity patterns observed in the study, providing

additional insights into the differences in motor control mechanisms between individuals with neurological conditions and healthy controls.

5.7.1 Experimental Setup and Exercise Protocol

The experimental setup involved the recruitment of participants who met the inclusion criteria for Parkinson's disease or stroke rehabilitation, as well as a healthy subject. One participant had Parkinson's disease, aged 71, with a height of 181cm and weight of 81kg, while the other participant had experienced a stroke, aged 68, with a height of 170cm and weight of 75kg. The healthy subject was aged 65, with a height of 173cm and weight of 85kg. Specifically, all participants used their right hand for the experiment. The participants sat comfortably in standard chairs with armrests, positioning their right arm on a table. Tactile sensors were individually affixed to their forearms and wrists to capture muscle activity during specific hand movements. See Figures 5.7 to 5.11 for the details of the setup.

Each participant underwent ten repetitions of the experiment, with each repetition lasting 30 seconds. Initially, they gripped an apple, while baseline signals from forearm muscles were recorded at rest, followed by recording signals while gripping the apple. Subsequently, they manipulated a key for a simulated unlocking task, with baseline signals from wrist muscles recorded at rest before the task; the protocol was repeated ten times for each participant using their right hand. Recorded signals were processed using MATLAB, employing signal processing techniques, such as filtering to extract relevant information. The processed signals were then plotted using MATLAB, with each plot corresponding to a specific hand movement, facilitating visualisation and comparison of muscle activity patterns. The analysis of the plotted signals aimed to identify trends, variations, and abnormalities in muscle activity, providing insights into motor control and coordination differences between participants with Parkinson's disease, stroke survivors, and a healthy individual.

The study strictly adhered to the research's ethical guidelines to ensure participant safety, confidentiality, and privacy throughout the experimental process. Potential risks were minimised, and participants were provided with appropriate support and information. The tactile sensor samples measuring 4×4cm² for testing and validation purposes are referenced in Figure 4.8 from the previous chapter.

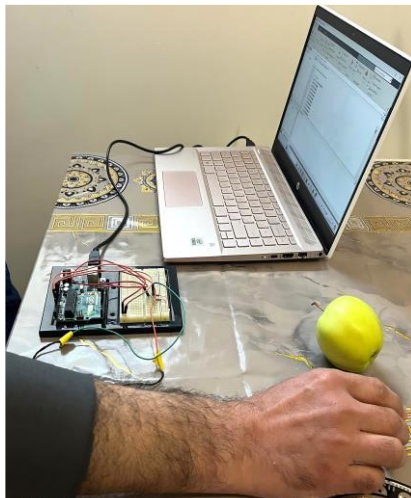


(a)

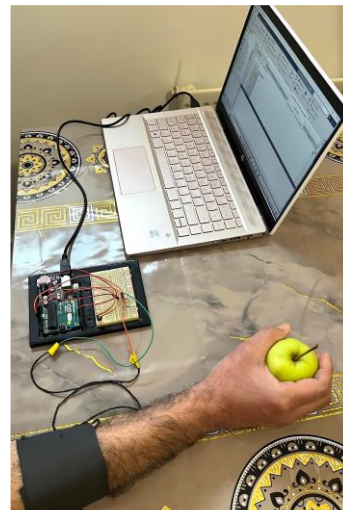


(b)

Figure 5.8: Wrist Muscle Activity Measurement Setup for Key Use in Parkinson's Patient. (a) Rest Wrist Muscle Activity; (b) Wrist Muscle Activity During Key Use



(a)



(b)

Figure 5.9: Forearm Muscle Activity During Grasping an Apple for Parkinson's Patient. (a) Rest Forearm Muscle Activity; (b) Forearm Muscle Activity During Grasping an Apple

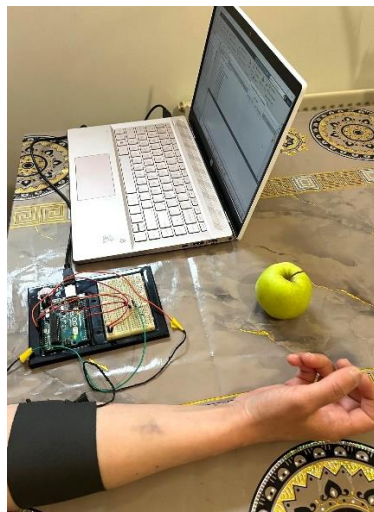


(a)

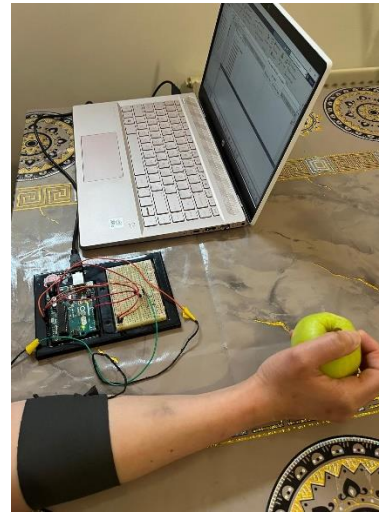


(b)

Figure 5.10: Wrist Muscle Activity During Key Use for Stroke Patient.
(a) Rest Muscle Activity; (b) Wrist Muscle Activity During Key Use



(a)



(b)

Figure 5.11: Forearm Muscle Activity During Grasping an Apple for Parkinson's Patient.
(a) Rest Forearm Muscle Activity; (b) Forearm Muscle Activity During Grasping an Apple

5.7.2 Experimental Results

Below are the plots depicting the raw signals followed by the filtered signals obtained from the experiments:

a) Raw Signal

The raw signals captured directly from the sensors during the hand movements of the participants are depicted in the plots. These raw signals represent the unprocessed data, showcasing the initial muscle activity patterns recorded during the gripping of the apple and manipulation of the key (see Figures 5.12 to 5.19).

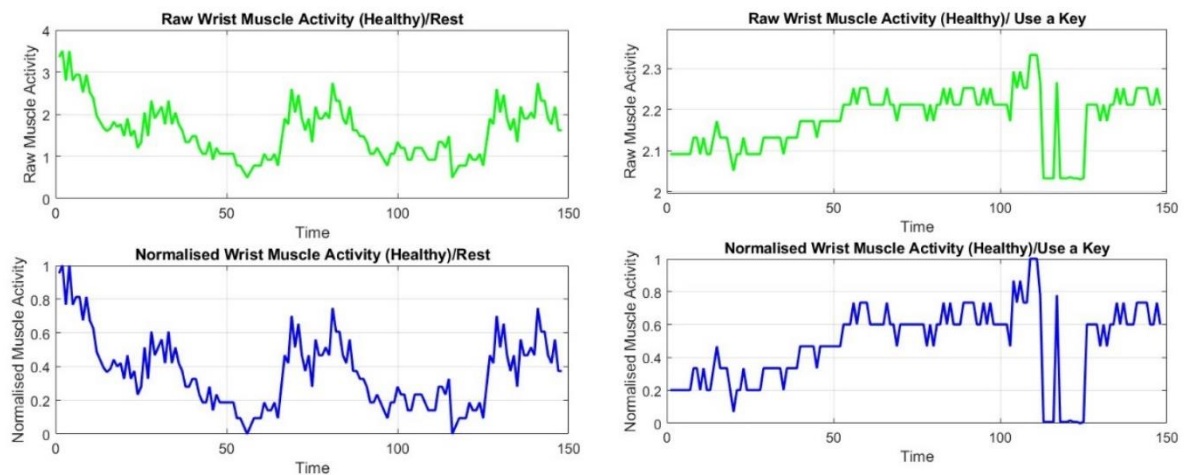


Figure 5.12: Wrist Muscle Activity During Key Use for Healthy Subject

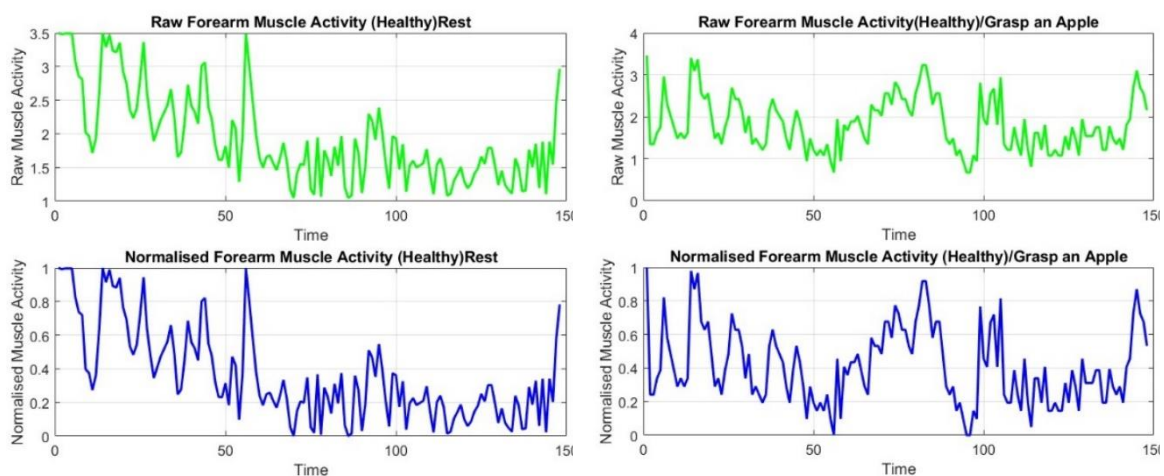


Figure 5.13: Forearm Muscle Activity During Grasping an Apple for Healthy Subject

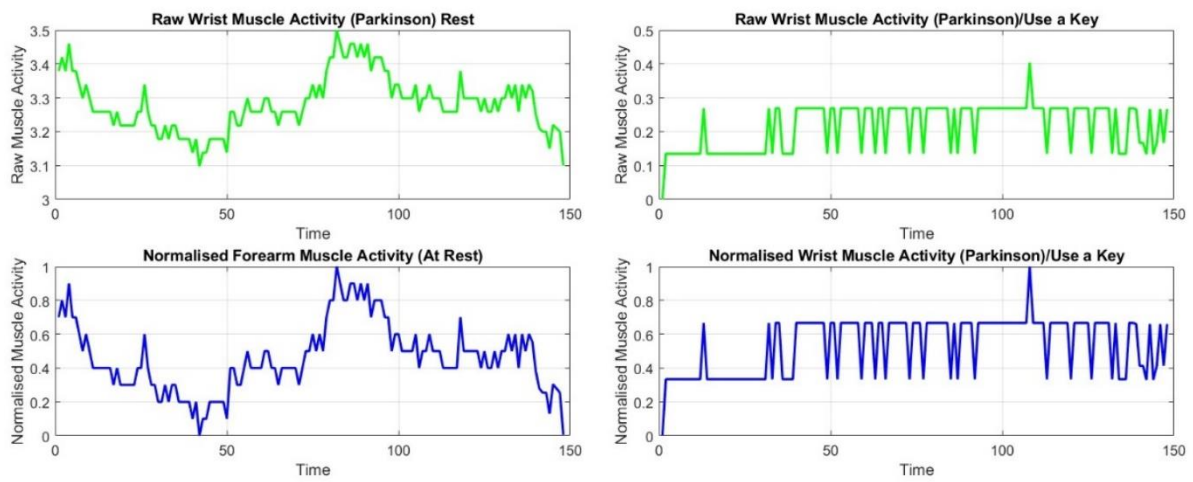


Figure 5.14: Wrist Muscle Activity During Key Use for Parkinson's Patient

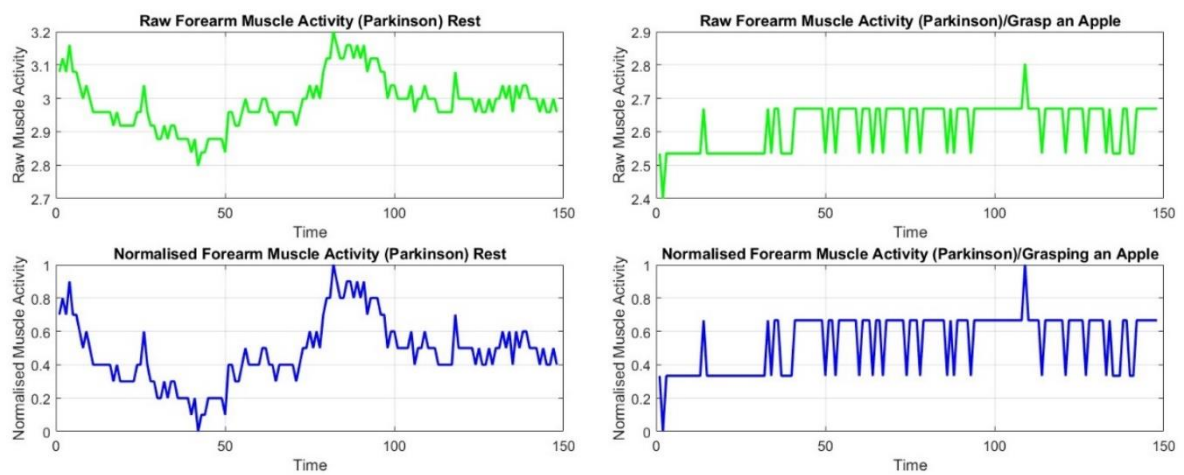


Figure 5.15: Forearm Muscle Activity During Grasping an Apple for Parkinson's Patient

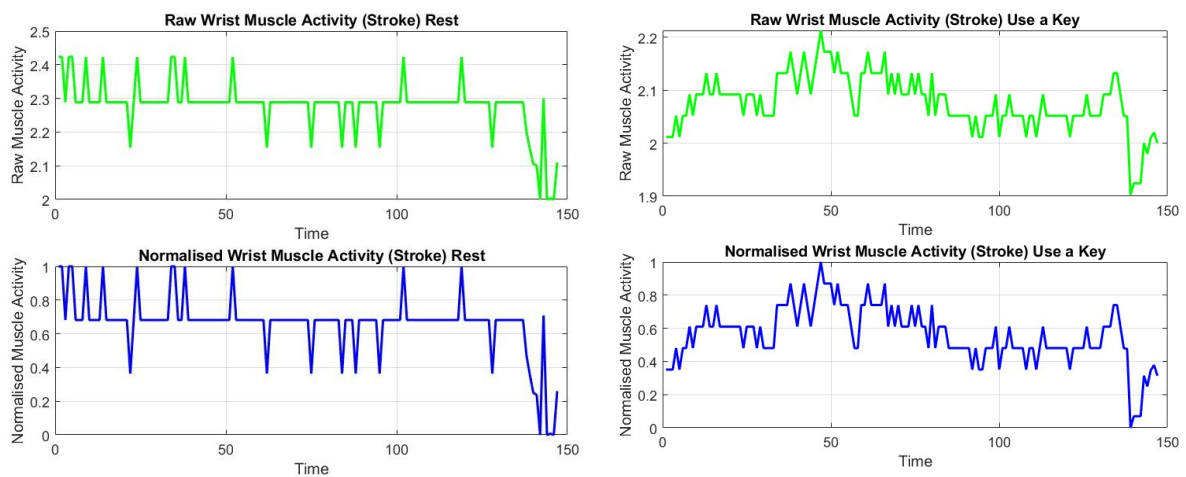


Figure 5.16: Wrist Muscle Activity During Key Use for Stroke Patient

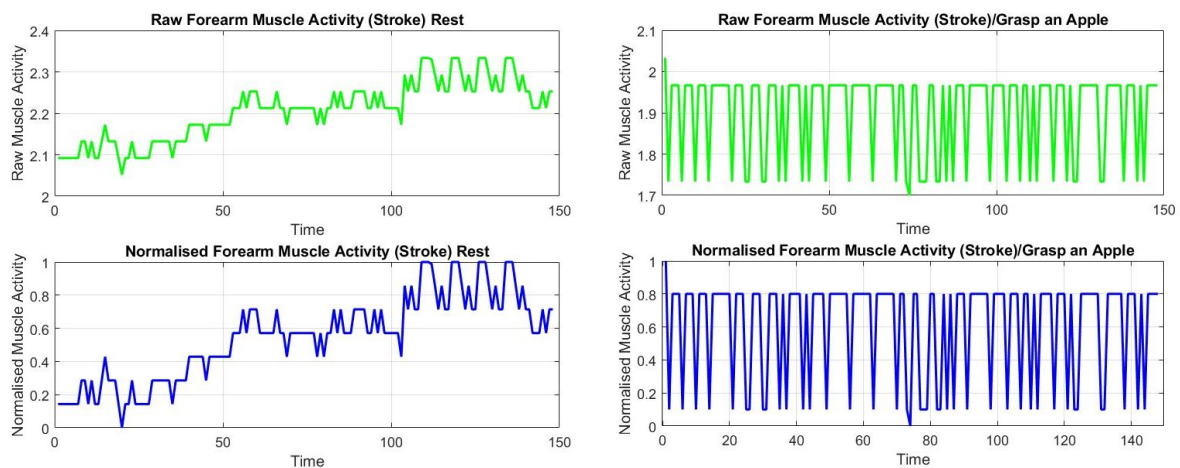


Figure 5.17: Forearm Muscle Activity During Grasping an Apple for Stroke Patient

The results are presented of fundamental tests conducted on the designed soft tactile sensor for detecting two types of muscle activities. Figures 5.12 and 5.13 illustrate muscle activity tests using the tactile sensor on a healthy subject. Subsequently, Figure 5.14 illustrates muscle activity tests using the sensor on a Parkinson’s patient,

depicting phases of rest and key use on the wrist muscle. Similarly, Figure 5.15 focuses on forearm muscle activity in a Parkinson's patient. Figure 5.16 demonstrates muscle activity tests on a Stroke patient, showcasing resting muscle activity and key use. Continuing from Figure 5.16, Figure 5.17 presents forearm muscle activity tests on a Stroke patient. In all graphs, the x-axis represents time, and the y-axis represents resistance to change in the tactile sensor, indicating muscle activity levels. To illustrate the disparity in muscle activities among all subjects, Figure 5.18 showcases the differences observed during distinct tasks.

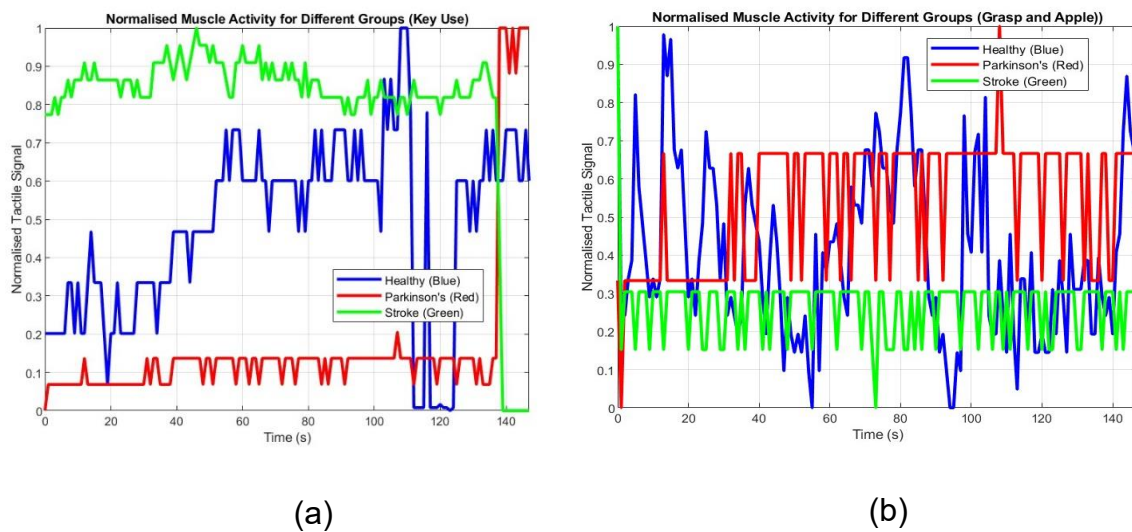


Figure 5.18: (a) Wrist Muscle Activity Across Subjects During Key Use; (b) Forearm Muscle Activity Across Subjects During Grasp of an Apple

The observed differences in muscle activity patterns among individuals with Parkinson's disease, stroke, and healthy controls have significant implications for rehabilitation strategies. For instance, the lower mean muscle activity levels observed in the Parkinson's individual, coupled with higher variability, suggest specific challenges related to motor output and control mechanisms inherent to Parkinson's disease. Tailored rehabilitation interventions could be developed based on these findings to address the unique motor deficits associated with each condition. For Parkinson's patients, interventions may focus on strategies to enhance motor output and mitigate variability in muscle activation. In contrast, stroke survivors may benefit from interventions aimed at capitalising on preserved motor function or compensatory mechanisms. By understanding the distinct patterns of muscle activity and their

underlying mechanisms, clinicians are able to personalise rehabilitation programmes to target specific abnormalities identified in muscle activation.

To further establish confidence in these results and address concerns regarding the “non-human” appearance of the graphs, several validation tests were performed:

- **Sensor Calibration:** Each tactile sensor was calibrated before the experiments to eliminate noise, environmental factors, and variation in sensor sensitivity. This ensured that the recorded resistance changes directly corresponded to muscle activity. This calibration step was essential to eliminate systemic errors that could distort the data.
- **Multiple Trials and Repetition:** To ensure consistency, multiple trials were conducted for each participant under controlled conditions. The repeatability of the muscle activity patterns confirmed the validity of the captured signals.
- **Noise Reduction and Signal Processing:** After the raw data was collected, filtering techniques (The bandpass Butterworth filter detailed in section 5.5.1) were applied to remove non-physiological noise and other artefacts, ensuring the remaining data reflected actual muscle activity.
- **Normalisation and Standardisation:** Normalisation techniques were applied to account for inter-subject variability, such as differences in muscle mass or sensor placement. This allowed for the meaningful comparison of data across subjects.
- **Statistical Significance:** A paired T-test was performed to ensure that differences in muscle activity between (Healthy, Parkinson, and Stroke) were statistically significant, validating the observed patterns.

Additionally, the 'non-human' appearance of the raw signals can be attributed to two main factors: a) The raw data was unprocessed, meaning it contained high levels of detail and small fluctuations in muscle activity, which might appear irregular or non-human at first glance. However, after appropriate filtering and processing, the resulting patterns align with biological muscle contractions. b) The high sensitivity of the tactile sensors could pick up minute changes in muscle activity that may not be immediately visible but are significant in detecting subtle muscle movements, especially in patients with neurodegenerative diseases.

b) Filter the Signal

As previously described in Section 5.2.3, a bandpass Butterworth filter was applied to improve signal quality. The filter settings, with a range of 40-100 Hz and a fourth-order, were carefully chosen to match the sensor characteristics and isolate relevant muscle activity signals (refer to Figures 5.19 through 5.25 for visualisations of the filtered signals).

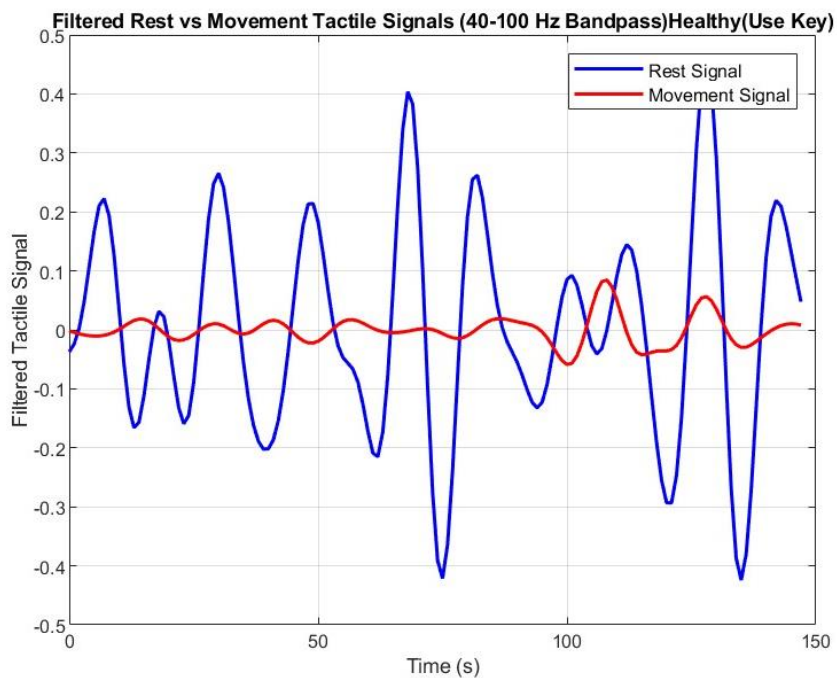


Figure 5.19: Filtered Signals with Wrist Muscle Activity During Key Use for Healthy Subject

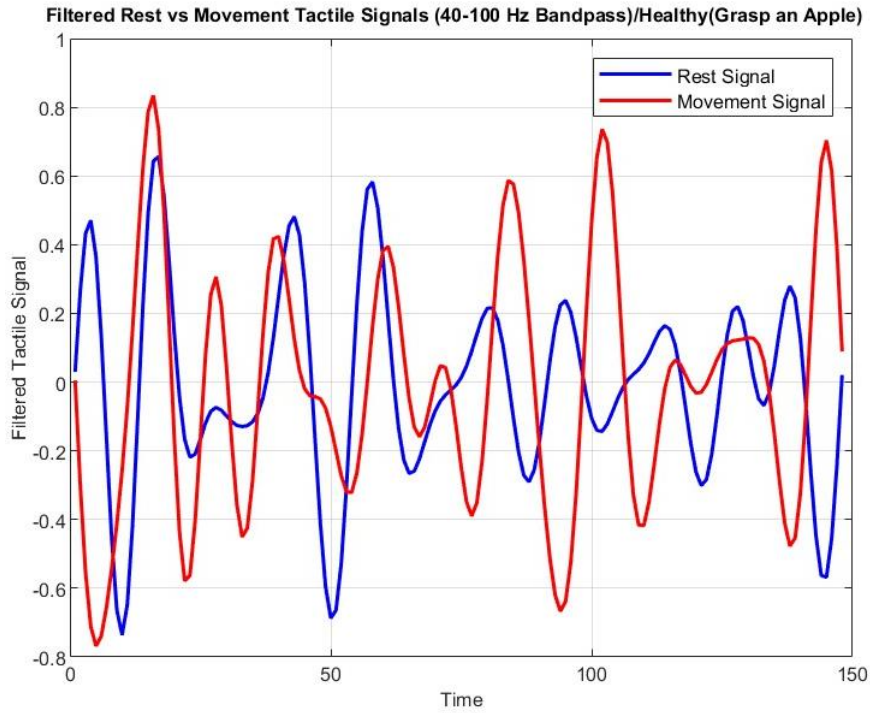


Figure 5.20: Filtered Signals with Forearm Muscle Activity During Grasping an Apple with Healthy Subject

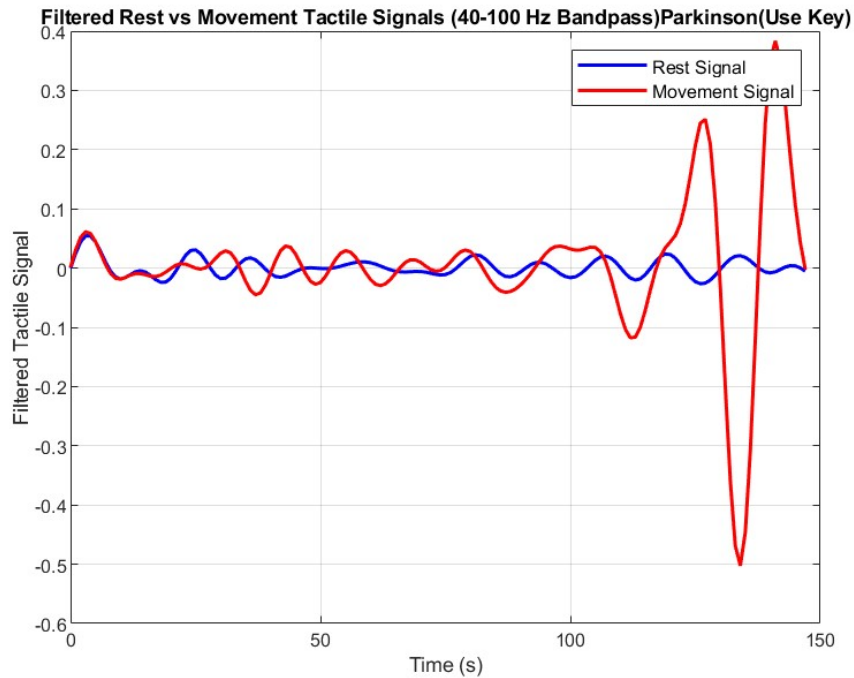


Figure 5.21: Filtered Signals with Wrist Muscle Activity During Key Use for Parkinson's Patient

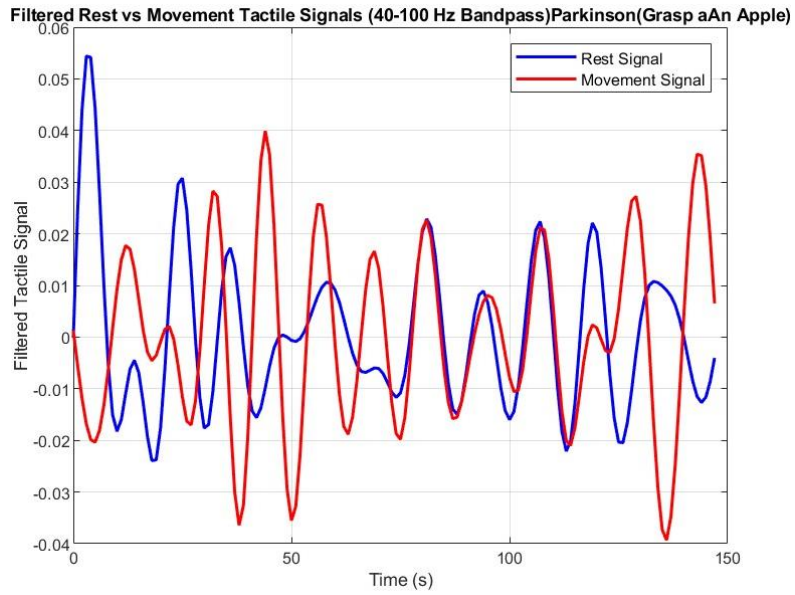


Figure 5.22 Filtered Signals with Forearm Muscle Activity During Grapping an Apple Parkinson’s Patient

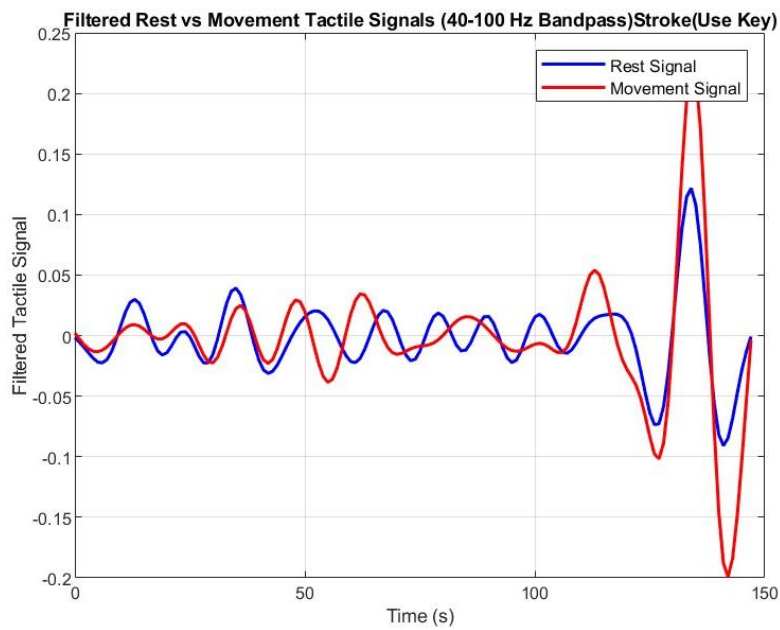


Figure 5.23: Filtered Signals with Wrist Muscle Activity During Key Use for Stroke Patient

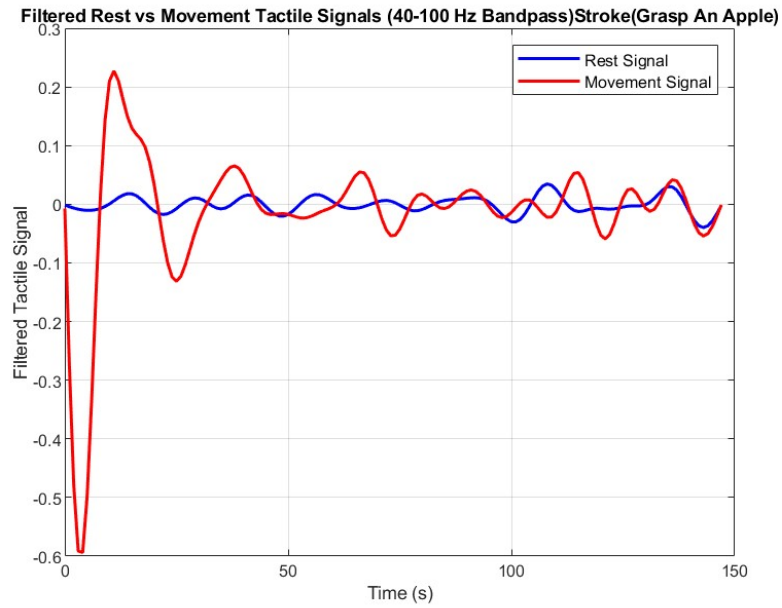


Figure 5.24: Filtered Signals with Forearm Muscle Activity During Grasping an Apple for Stroke Patient

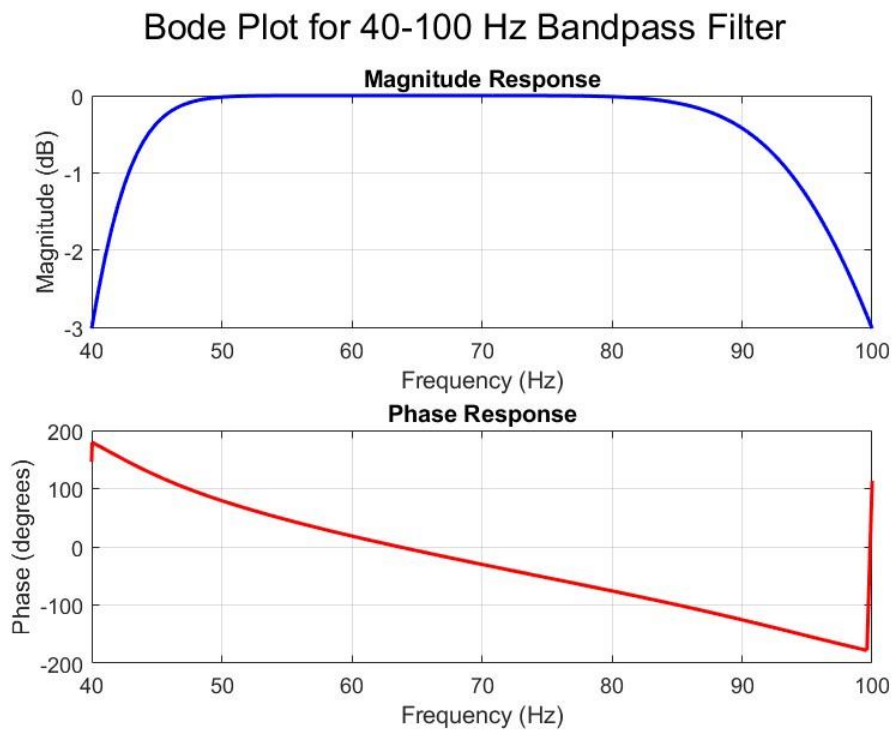


Figure 5.25: Bode plot of the 40-100 Hz bandpass filter used in the analysis

Figure 5.19: Filtered tactile signals during rest and movement phases (40-100 Hz bandpass) for a healthy individual using a key. The rest signal (in blue) shows more distinct oscillations compared to the smoother movement signal (in red), suggesting a higher tactile response during resting. In Figure 5.20 Filtered tactile signals for a healthy individual grasping an apple. The movement signal (red) presents more pronounced peaks and troughs, contrasting with the rest signal (blue), which shows more consistency, indicating varied tactile responses during dynamic tasks.

Figure 5.21 Filtered tactile signals for a Parkinson's patient using a key. The movement signal (red) displays sharper fluctuations toward the end, with the rest signal (blue) maintaining a steady lower amplitude, reflecting challenges in motor control and coordination. While in Figure 5.22 Filtered tactile signals for a Parkinson's patient grasping an apple. Both rest and movement signals exhibit increased variability, though the movement signal (red) has slightly greater oscillations, indicating irregular motor responses during dynamic tasks. Figure 5.23 Filtered tactile signals for a stroke patient using a key. The movement signal (red) spikes significantly around 150 seconds, while the rest signal (blue) remains more stable, highlighting delayed motor activation and recovery challenges in stroke patients.

While Figure 5.24 Filtered tactile signals for a stroke patient grasping an apple. The movement signal (red) exhibits stronger variations compared to the rest signal (blue), with sharp initial deviations, reflecting impaired motor control and recovery during dynamic tasks post-stroke.

Figure 5.25 Bode plot of the 40-100 Hz bandpass filter used in the analysis. The magnitude response shows minimal attenuation across the passband, while the phase response gradually declines, demonstrating stable filter performance suitable for isolating relevant muscle activity frequencies.

To illustrate the disparity in muscle activities among all subjects, Figures 5.26 and 5.27 showcase the differences observed during distinct tasks.

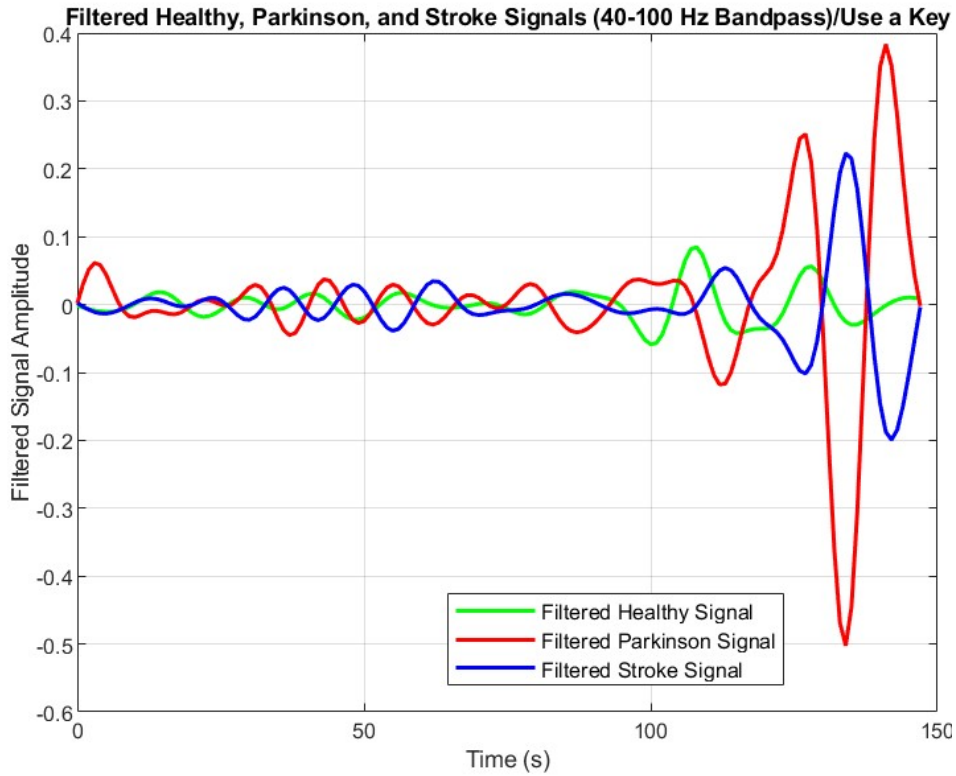


Figure 5.26: Wrist Muscle Activity Across Subjects During Key Use

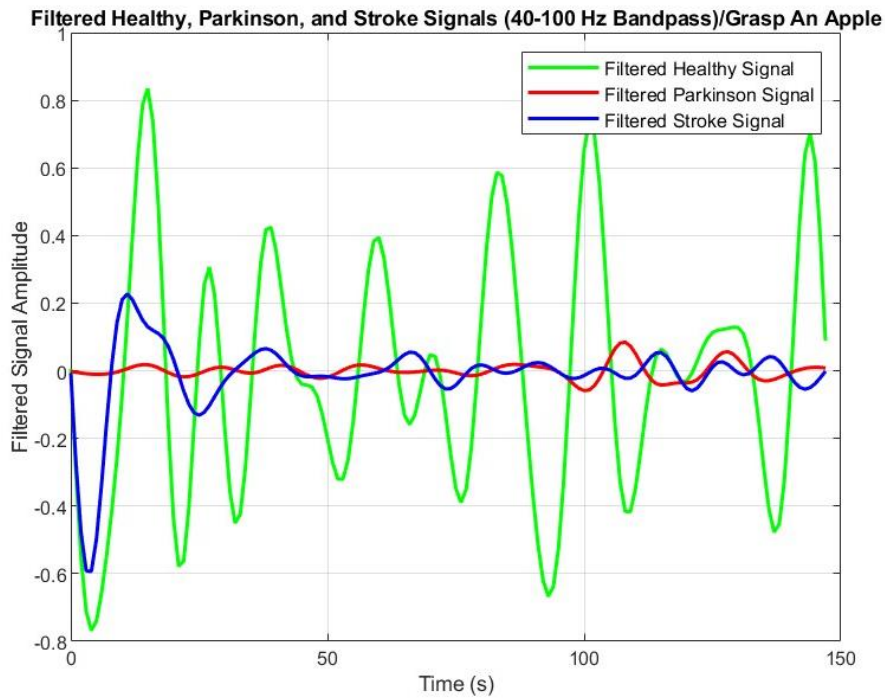


Figure 5.27: Forearm Muscle Activity Across Subjects while Grasping an Apple

Figure 5.26 Filtered tactile signals (40-100 Hz bandpass) during a key use task for healthy, Parkinson's, and stroke subjects. The healthy signal (green) shows relatively consistent low-amplitude oscillations, while the Parkinson's signal (red) displays a large deviation around 150 seconds, indicating difficulty in motor control. The stroke signal (blue) also exhibits irregular patterns but with a lower amplitude, suggesting a more muted response compared to Parkinson's.

In Figure 5.27 Filtered tactile signals during the task of grasping an apple for healthy, Parkinson's, and stroke subjects. The healthy signal (green) has significantly higher peaks and troughs, showing stronger muscle activation during the task. In contrast, the Parkinson's (red) and stroke (blue) signals remain relatively flat with minor oscillations, indicating reduced motor engagement or impaired motor function in comparison to the healthy individual.

The comparison of tactile signals between healthy individuals and patients with Parkinson's and stroke during the key-use and apple-grasping tasks reveals clear differences in motor control and muscle activity. Healthy participants exhibit consistent and robust muscle responses, indicating smooth motor function. In contrast, Parkinson's patients demonstrate larger fluctuations and irregularities in muscle activity, particularly toward the end of tasks, suggesting challenges with motor control. Stroke patients display weaker and more muted signals, reflecting impaired or delayed motor activation. Overall, these findings indicate that both Parkinson's and stroke patients have diminished motor responses compared to healthy individuals, especially during dynamic tasks.

5.7.3 Analysis of Muscle Activity Patterns and Clinical Implications

a. Data Collection and Measurement Techniques

In this section, muscle activity patterns were investigated in individuals with Parkinson's disease, stroke, and healthy controls during specific motor tasks. To quantitatively analyse these patterns, data were collected using a novel tactile sensor designed for this purpose. The sensor allowed the possibility to measure muscle

activity in both forearm and wrist muscles, providing valuable insights into motor control mechanisms underlying these neurological conditions (see Table 5.5 for statistical measurements of muscle activity). In Figures 5.28 and 5.29, which will be presented later in this section, the muscle activity patterns observed for (Healthy, Parkinson's, and Stroke) are illustrated during key motor tasks. These figures provide visual representations of the mean muscle activity levels and variability within each individual, offering further insights into the distinct patterns of muscle activity among the individuals and identifying any significant differences or similarities between them.

Table 5.5: Statistic Measurement with Different Muscle Groups

Statistics Measurement	Forearm Muscle Activity			Wrist Muscle Activity		
	Healthy	Parkinson	Stroke	Healthy	Parkinson	Stroke
Mean	2.1	1.8	1.3	2.1	1.8	1.3
Standard Deviation	0.06	0.1	0.03	0.06	0.6	0.08

The table above (5.5) presents statistical measurements of muscle activity in both forearm and wrist muscles for three individuals: Healthy individuals, those with Parkinson's disease, and individuals who have experienced a stroke. Specifically, the mean muscle activity levels and standard deviations are compared across these individuals for both muscle groups.

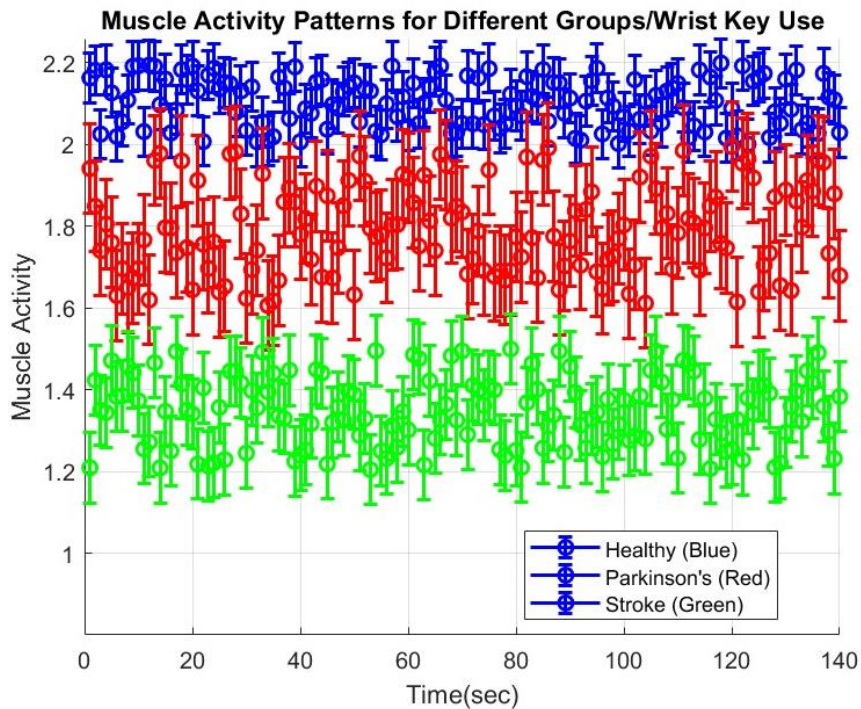


Figure 5.28: Wrist Muscle Activity

Figure 5.28 shows the muscle activity patterns in the wrist for healthy individuals, Parkinson’s patients, and stroke patients during a key-use task. Healthy individuals (blue markers) exhibit the highest average muscle activity, while stroke patients (green markers) show the lowest. Parkinson’s patients (red markers) have muscle activity between the two individuals. Error bars, representing standard deviation, indicate the variability of muscle activation within an individual. Parkinson’s patients demonstrate the greatest variability, suggesting less consistent muscle control during the task. In contrast, healthy individuals have moderate variability, while stroke patients exhibit the lowest variability, reflecting more stable but lower muscle activity.

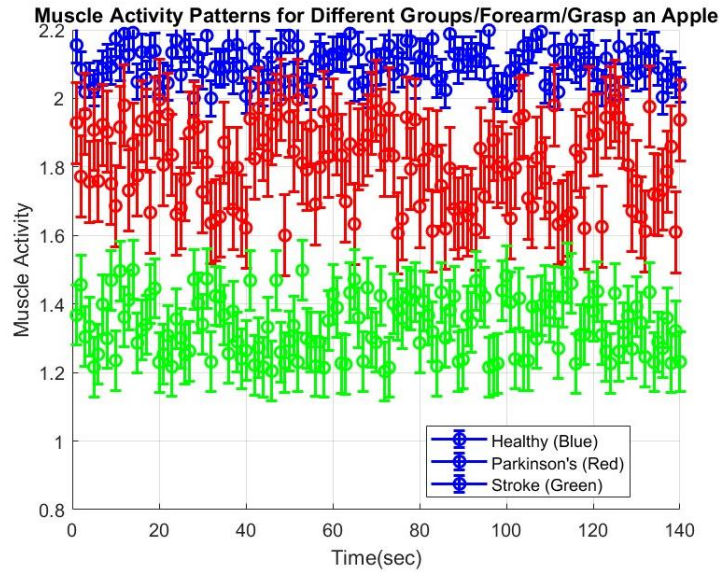


Figure 5.29: Forearm Muscle Activity

Figure 5.29 illustrates the forearm muscle activity of healthy, Parkinson’s, and stroke patients during a task involving grasping an apple. As with wrist activity, healthy individuals show the highest average muscle activity (blue), Parkinson’s patients show intermediate levels (red), and stroke patients display the lowest (green). The error bars indicate the standard deviation, with Parkinson’s patients again showing the largest fluctuations in muscle activation, highlighting inconsistency in motor control. The healthy individual shows more stable but slightly varying muscle activity, while the stroke individual maintains lower muscle activity with minimal variability.

By examining both figures, it is clear that healthy individuals exhibit the highest muscle activity, both in the wrist and forearm, with moderate variability. Parkinson’s patients, while displaying intermediate muscle activity, show the highest variability, indicating fluctuating muscle control. Stroke patients, with the lowest muscle activity and minimal variability, reflect reduced and consistent motor control deficits.

b. Analysis of Forearm and Wrist Muscle Activity

Significant differences in muscle activity were noted between the individuals during the analysis of forearm muscles. Specifically, the Parkinson’s individual displayed lower mean muscle activity levels compared to the healthy individual, accompanied by greater variability in activity. This suggests a reduction in motor output and impaired

motor control mechanisms, characteristic of Parkinson's disease. Conversely, the Stroke individual's mean muscle activity level was closer to that of the healthy individual, suggesting relatively preserved motor function or the use of compensatory mechanisms. However, variability in the Stroke individual's muscle activity remained low, potentially reflecting a more stable, but restricted, motor output due to localized injury.

When analysing wrist muscle activity, both the Parkinson's and Stroke individuals exhibited lower mean muscle activity compared to the healthy individual. As observed in the forearm analysis, the Parkinson's individual demonstrated the highest variability in wrist muscle activity, reflecting the characteristic motor fluctuations of Parkinson's disease. On the other hand, the Stroke individual showed more stable wrist muscle activation patterns, likely due to localised stroke injury and motor adaptations, but with less overall activation compared to the healthy individual.

c. Limitations of the Study

It is important to acknowledge several limitations that may have influenced the findings and their broader applicability.

- **Small Sample Size:** The study only included three individuals representing the Healthy, Parkinson's, and Stroke conditions. This small sample size significantly limits the generalisability of the results, as it is difficult to draw broad conclusions or make statistically powerful comparisons across populations. The lack of a larger and more diverse sample means the results could be influenced by individual-specific factors rather than representing typical patterns of muscle activity in these conditions. This limitation also reduced the statistical power of t-tests, making it harder to detect smaller yet potentially significant differences between the groups.
- **Variability in Participant Characteristics:** Age differences, physical fitness, disease stage, and medication among the participants could have skewed the results. For instance, a Parkinson's patient at a different stage of the disease or under a different medication regimen may exhibit different muscle activity patterns. Similarly, the stroke patient's recovery stage or functional abilities may not be fully representative of all stroke survivors. These variations made it

difficult to attribute observed differences solely to the condition under study, as confounding factors could have influenced muscle activity patterns.

- **Technical Limitations of the Tactile Sensor:** The novel tactile sensor used in this study presented challenges in terms of placement accuracy and reliability of measurements. Factors such as variations in skin impedance, sensor misalignment, and environmental noise may have introduced errors, contributing to the variability in the results. For instance, slight differences in sensor placement could have led to inconsistent readings across individuals, particularly when comparing muscle activity between tasks or groups. These technical issues limited the precision of the data and could explain some of the higher variability observed in the Parkinson’s group.

d. Comparative Analysis of Muscle Activity Patterns

In this section, a comparative analysis is presented of muscle activity patterns observed during key motor tasks among healthy individual, Parkinson’s disease, and Stroke patients. Utilising t-tests [183], an assessment was made of the differences in muscle activation between healthy individuals and those with neurological conditions across two tasks: key use and apple grasping. Through this analysis, the aim is to clarify clear patterns of muscle activity and their clinical implications for individuals with Parkinson’s disease and Stroke. Overall, the t-tests conducted to compare healthy individuals with Parkinson’s disease or Stroke patients for both key use and apple grasping tasks revealed significant differences in muscle activity patterns, as shown in Table 5.6 below.

Table 5.6: T-test Results: Key Use and Apple Grasping Tasks

Test Type (T-test)	Key Use	Apple Grasping
Healthy vs. Parkinson	0.4208	1.4318
Healthy vs. Stroke	0.7382	1.2916

- **Key Use Task:**

For the key use task, the t-statistics were found to be 0.4208 for the Healthy vs. Parkinson's comparison; and 0.7382 for the Healthy vs. Stroke comparison. These results suggest that healthy individuals exhibit higher muscle activity levels compared to both Parkinson's disease and Stroke patients during key use tasks.

- **Apple Grasping Task:**

Similarly, for the apple grasping task, the t-statistics were calculated as 1.4318 for the Healthy vs. Parkinson's comparison, and 1.2916 for the Healthy vs. Stroke comparison. These findings imply that healthy individuals demonstrate higher muscle activity levels than both Parkinson's disease and Stroke patients during apple grasping tasks (see Figure 5.30).

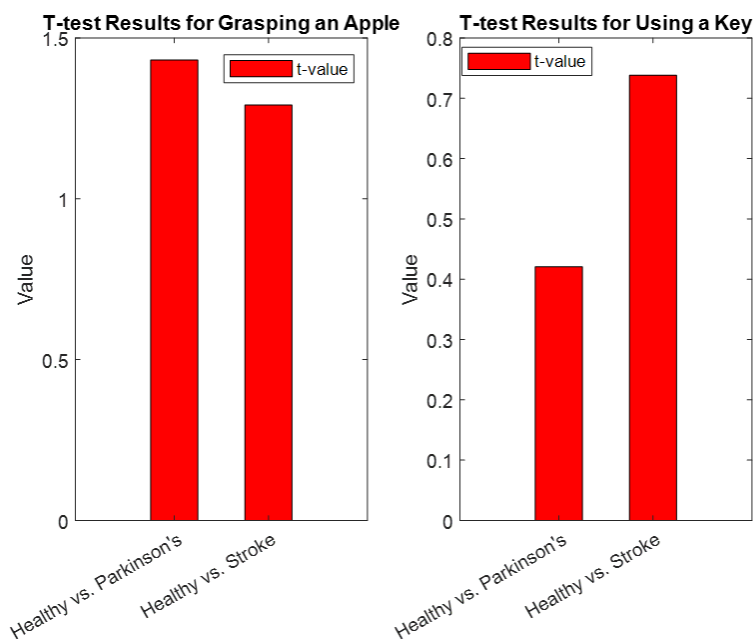


Figure 5.30: T-test Results: Key Use and Apple Grasping Tasks

The accompanying plot shows the t-test results for key use and apple-grasping tasks. Figure 5.30 compares muscle activity levels in healthy individuals with those in Parkinson's and Stroke patients across both tasks. The results highlight significant differences in muscle activity patterns, with Parkinson's and Stroke patients showing lower muscle activity than healthy individuals. Understanding these differences is

crucial for developing tailored rehabilitation strategies for people with neurological conditions. The lower muscle activity in Parkinson's and Stroke patients during key use and apple-grasping tasks can be explained by several factors:

- **Motor Neuron Degeneration in Parkinson's Disease:** Parkinson's affects dopaminergic neurons, which disrupts motor control, leading to reduced and variable muscle activation [1,2]. Bradykinesia and rigidity further reduce muscle activity in fine motor tasks.
- **Impaired Motor Control in Stroke:** Stroke damages brain areas responsible for motor control, weakening neural signals to muscles. This results in lower muscle activity and poor coordination in controlled tasks [28].
- **Muscle Weakness and Atrophy:** Both conditions can lead to muscle disuse, causing atrophy and weakness, which lowers muscle strength and activity in tasks like grasping and key use [14].
- **Altered Neuromuscular Function:** Tremors and rigidity in Parkinson's, along with stroke-related spasticity, disrupt normal muscle activation patterns, making fine motor tasks less efficient [165,114].
- **Compensatory Mechanisms:** Motor deficits often lead patients to rely on compensatory strategies, which can further alter muscle activity during tasks [164,4].

5.7.4 Clinical Implications and Future Research Directions

- **Mechanisms Underlying Muscle Activity Differences**

The differences in muscle activity observed between individuals with Parkinson's disease, Stroke, and healthy controls stem from distinct neurophysiological mechanisms. In Parkinson's disease, motor deficits such as bradykinesia and rigidity are due to degeneration of dopaminergic neurons in the substantia nigra, disrupting motor control circuits in the basal ganglia. This neural degeneration leads to abnormal motor output and variability in muscle activation patterns, reflecting motor fluctuations characteristic of the disease [6,56,176,68].

For Stroke patients, damage to motor pathways, such as the motor cortex and corticospinal tract, results in diminished neural input to muscles. This leads to lower, more stable muscle activation, likely reflecting compensatory mechanisms or use of

spared circuits, rather than true recovery of motor function [99]. In contrast, healthy individuals demonstrate higher muscle activity with moderate variability, indicative of efficient motor unit recruitment and smooth motor control during tasks [100,19].

- Clinical Implications and Rehabilitation Strategies

These distinct muscle activation patterns have important implications for rehabilitation.

For Parkinson's disease, therapy should aim to enhance motor control consistency and reduce variability. Approaches such as motor learning-based therapies, structured exercise programmes, and interventions that support dopamine levels may help mitigate motor fluctuations. Additionally, deep brain stimulation (DBS) can modulate abnormal neural activity, potentially improving motor output [7,114].

In Stroke patients, rehabilitation may focus on strengthening weak muscles and utilising preserved motor pathways. Techniques like task-specific training and neuroplasticity-driven therapies, including constraint-induced movement therapy (CIMT) and functional electrical stimulation (FES), may help promote the reorganisation of motor circuits and more normal muscle activation [167,176].

- Future Research Directions and Technological Advancements

Further research is essential to understand the neurophysiological mechanisms underlying these muscle activity patterns. Techniques such as electromyography (EMG) and functional MRI (fMRI) can provide insights into motor unit recruitment and brain activity changes, deepening understanding of motor control deficits [46,184]. Longitudinal studies tracking muscle activity changes over time and in response to rehabilitation will help assess the effectiveness of different interventions, offering insights into the progression of muscle activation patterns and optimal timing for interventions [185,44].

Advancements in sensor technology and AI-driven data processing present new opportunities for precise monitoring. Wearable devices with real-time biofeedback could enable continuous monitoring during rehabilitation, providing personalised feedback and supporting adaptive rehabilitation programmes for individuals with Parkinson's disease, Stroke, and other neurological conditions.

5.8 Conclusion

In conclusion, the current study has demonstrated a robust correlation between electromyography (EMG) signals obtained from surface EMG (sEMG) sensors and soft tactile sensors across various muscle movements. Notably, hand close and arm flexion movements exhibited particularly strong correlation values, highlighting the efficacy of both sensor types in accurately assessing muscle activity. This compatibility extends to wrist flexion and extension movements, further emphasising their utility in this regard. Even though maximum energy values were relatively low across all movements, it is imperative to acknowledge the influence of factors, such as muscle contraction intensity and sensor-to-muscle distance on these values. Additionally, the extent of agreement between the sensors, as indicated by cross-correlation values, varied across different movements, indicating movement-specific compatibility. The implications of the current findings are substantial, particularly in the domain of affordable soft tactile sensors for understanding muscle activity.

In summary, the positive correlations observed between EMG signals from sEMG and soft tactile sensors underscore the potential utility of tactile sensors in assessing muscle activity. This integration of sensor technologies presents exciting prospects for future advancements in healthcare, sports performance monitoring, and human-machine interfaces. Additionally, the insights gleaned from the series of experiments using the currently designed tactile sensor to measure muscle activity during specific tasks have provided valuable insights into motor control and coordination differences among individuals with varying health conditions. In the second section of the chapter, the participation of volunteers representing healthy individuals was enlisted, as well as those diagnosed with Parkinson's disease and Stroke.

The findings regarding distinct patterns of muscle activation during tasks such as grasping an apple and using a key, as evidenced by changes in resistance in the wrist and forearm muscles, underscore the sensitivity and specificity of the tactile sensor in capturing subtle changes in muscle activity. Moreover, the potential for tailored exercises targeting specific muscle groups to improve motor function and coordination in individuals facing motor challenges due to Parkinson's disease or stroke is significant. In conclusion, the current study contributes valuable insights into the assessment and improvement of motor control and coordination in individuals with

neurological conditions. These findings have implications for the development of personalised rehabilitation strategies tailored to specific muscle activation patterns, ultimately enhancing the quality of life for affected individuals.

Chapter Six: Conclusion and Future Work

6.1 Conclusions

In this PhD study, various aspects of tactile sensors and their applications were explored, focusing on upper limb motion and muscle activity measurement. The design and implementation of a stretchable tactile sensor specifically tailored for the upper limb align with earlier research into wearable and flexible sensors for biomechanics and rehabilitation. Previous studies have explored the integration of soft sensors for tracking muscle activity and movement in upper limbs, such as in sports science and assistive technologies. However, the use of common materials such as Eeon-Tex conductive fibre in this study offers a novel contribution, addressing the demand for affordable, flexible, and user-friendly sensors that can be seamlessly incorporated into textiles and wearable devices—a key consideration highlighted in earlier sensor research.

The challenge of hysteresis nonlinearity in conductive fibre-based tactile sensors was addressed in this study using a backpropagation neural network (BPNN), which aligns with previous work aimed at improving the accuracy and performance of tactile sensors. Existing research has recognised the limitations posed by hysteresis in soft sensors, with several methods, such as hardware compensation and material improvements, being explored. This study, however, builds upon those foundations by offering an advanced method to effectively reduce hysteresis error using BPNNs. This approach enhances the accuracy of soft tactile sensors and supports ongoing efforts to integrate artificial intelligence and machine learning in sensor technology for more precise applications, an area gaining increased attention in the field.

Comparative studies with superficial electromyography (sEMG) sensors have been a common theme in evaluating novel muscle activity sensors. While previous studies demonstrated the superiority of sEMG in certain applications due to its well-established accuracy, this research demonstrates that fabric-based tactile sensors can provide comparable performance in capturing muscle activity for specific movements, such as hand closing and arm flexion. This expands on prior work by offering a reliable,

affordable alternative for scenarios where high-end sEMG equipment may not be accessible or practical.

6.2 Contribution to Existing Research

The findings of this research contribute to the broader body of work on soft robotics, wearable sensors, and neuromuscular activity monitoring. While past research has highlighted the potential of soft sensors in rehabilitation and human-computer interaction, this study's focus on addressing hysteresis nonlinearity and validating a solution for muscle activity sensing extends our understanding of how such sensors can be applied in real-world settings. The correlations observed between tactile sensor outputs and EMG signals align with previous findings but add value by demonstrating the viability of fabric-based sensors, which have not been explored as extensively in dynamic and complex tasks.

Furthermore, the successful application of neural networks for improving sensor accuracy positions this work at the intersection of artificial intelligence and sensor technology, a growing area of interest in both academic and commercial fields. The implementation of BPNNs to mitigate sensor nonlinearity is a significant addition to the field, given that earlier research primarily focused on hardware solutions or algorithmic compensations.

6.3 Addressing Research Objectives in the Context of Existing Literature

This research successfully met its objectives by building upon and expanding previous studies related to tactile sensors and their applications, by:

- **Sensor Development:** The development of the stretchable tactile sensor using Eeon-Text conductive stretchable elastic fibre aligns with ongoing research on flexible, wearable sensors. However, the focus on upper limb applications and the integration of neural networks for improving sensor performance adds a new dimension to existing work.

- **Hysteresis Nonlinearity:** While hysteresis has been previously identified as a limitation in piezoresistive and fibre-based sensors, this study implemented a neural network-based solution that improves sensor accuracy under dynamic conditions, advancing previous methodologies.
- **Comparison to sEMG:** Although sEMG remains the standard for muscle activity measurement, this research confirms that affordable fabric-based tactile sensors offer comparable performance for specific movements, providing a cost-effective solution that complements existing technologies.
- **Data Collection and Categorisation:** The experimental setup was designed to collect and categorise muscle movements, with each movement recorded directly from participants and saved in Excel files for analysis.

6.4 Conclusion and Future Directions in Relation to Prior Work

The outcomes of this research significantly contribute to the future of tactile sensing and soft robotics in healthcare, rehabilitation, and beyond. The findings build on earlier research, highlighting the potential of wearable sensors to improve patient outcomes through flexible, affordable, and accurate monitoring of muscle activity. This PhD further advances the field by addressing technical limitations, such as hysteresis, and provides insights that are poised to inform the next generation of soft sensors for applications ranging from rehabilitation to sports monitoring.

Key Points:

The stretchable tactile sensor, incorporating EeonTex conductive fibres and a Nylon-Spandex fabric blend, effectively detects muscular contractions, especially in the upper limb.

- It discerns between slow and fast hand movements, providing distinct signals corresponding to different speeds.
- Its simplicity, affordability, and non-invasive operation make it suitable for various industries, including healthcare and machine control.
- BPNN-driven methods reduce maximum hysteresis errors, improving the reliability of soft tactile sensors based on piezoresistive materials.

- The study underscores the importance of BPNNs in mitigating sensor nonlinearity and advancing tactile sensing capabilities for robotics, prosthetics, and human-computer interfaces.
- Consistent positive correlations exist between EMG signals from sEMG sensors and soft tactile sensors during various muscle movements.
- Hand close and arm flexion movements show strong agreement between sensor types, accurately capturing muscle activity.
- Affordable soft tactile sensors hold promise for assessing muscle activity in healthcare, sports monitoring, and human-machine interfaces, suggesting.

6.5. Significance of the Findings

This research underscores the importance of soft robotics and soft sensors in healthcare and rehabilitation, offering innovative solutions for individuals with mobility challenges. The insights gained from the study inform the development of future soft robotics technologies and contribute to advancements in healthcare and assistive devices.

References

1. **Burke, J., McNeill, M., Charles, D., Morrow, P., Crosbie, J. & McDonough, S.** (2009) 'Serious games for upper limb rehabilitation following stroke', *Medicine*, 2009 Conference in Games and Virtual Worlds for Serious Applications, 23 March 2009.
2. **Khan, M.A., Al-Jumaily, A.A., Al-Jumaily, M. & Al-Jumaily, H.A.** (2021) 'Converging robotic technologies in targeted neural rehabilitation: A review of emerging solutions and challenges', *Sensors*, 21(6), p. 2084.
3. **Khan, Y., Ostfeld, A.E., Lochner, C.M., Pierre, A. & Arias, A.C.** (2016) 'Monitoring of vital signs with flexible and wearable medical devices', *Advanced Materials*, 28, pp. 4373–4395.
4. **Rao, L., Zhou, L., Chen, Z., Pang, L., Li, X., Liang, K., Li, M., Xu, J., Yang, Y., Liang, J., Cai, Z., Yang, S. & Liu, H.** (2021) 'Smart textiles for electricity generation', *Nano-Micro Letters*, 13(1), pp. 1-20.
5. **Lambeta, M., Chou, P.W., et al.** (2020) 'DIGIT: A novel design for a low-cost compact high-resolution tactile sensor with application to in-hand manipulation', *IEEE Robotics and Automation Letters*, 28 February 2020.
6. **Stroke Association** (2023) *State of the nation: Stroke statistics*. Available at: [Stroke Association website](#).
7. **National Institute for Health and Care Excellence (NICE)** (2023) *Stroke rehabilitation in adults: Recommendations*. Available at: [NICE Guidelines website](#).
8. **ACNR Journal** (2023) 'An expert opinion: Upper limb rehabilitation after stroke'. Available at: [ACNR Journal website](#).
9. **Lawhern, V.J., Solon, A.J., Waytowich, N.R., Gordon, S., Hung, C. & Lance, B.** (2016) 'EEGNet: A compact convolutional neural network for EEG-based brain–computer interfaces', *Journal of Neural Engineering*, 23 November 2016.

10. **Castellanos-Ramos, J., Navas-Gonzalez, R., Macicior, H., Sikora, T., Ochoteco, E. & Vidal-Verdu, F.** (2010) 'Tactile sensors based on conductive polymers', *Microsystem Technologies*, 16, pp. 765-776.
11. **Lebosse, C., Renaud, P., Bayle, B. & de Mathelin, M.** (2011) 'Modelling and evaluation of low-cost force sensors', *IEEE Transactions on Robotics*, 27, pp. 815–822.
12. **Wang, Y., Lu, Y., Mei, D. & Zhu, L.** (2021) 'Liquid metal-based wearable tactile sensor for both temperature and contact force sensing', *IEEE Sensors Journal*, 15(1), pp. 614–621.
13. **Lee, G., Nho, K., Kang, B., Sohn, K. & Kim, D.** (2019) 'Predicting Alzheimer's disease progression using a multi-modal deep learning approach', *Scientific Reports*, 13 February 2019.
14. **Hermens, H.J., Freriks, B., Disselhorst-Klug, C. & Rau, G.** (2000) 'Development of recommendations for SEMG sensors and sensor placement procedures', *Journal of Electromyography and Kinesiology*, 10(5), pp. 361-374.
15. **Guo, J. & Li, Z.** (2023) 'A continuous hand movement recognition method for sEMG signals based on BiLSTM network and attention mechanism', *International Conference on Robotics, Intelligent Control and Artificial Intelligence (RICAI)*, 1 December 2023.
16. **Lepora, N., Lin, Y., Money-Coomes, B. & Lloyd, J.** (2022) 'DigiTac: A DIGITacTip hybrid tactile sensor for comparing low-cost high-resolution robot touch', *IEEE Robotics and Automation Letters*, 27 June 2022.
17. **Bonato, P.** (2010) 'Wearable sensors and systems', *IEEE Engineering in Medicine and Biology Magazine*, 29, pp. 25–36.
18. **Brown, R.G. & Hwang, P.Y.C.** (1997) *Introduction to random signals and applied Kalman filtering*. John Wiley & Sons.
19. **Sánchez-Durán, J.A., Hidalgo-López, J.A., Castellanos-Ramos, J., Oballe-Peinado, Ó. & Vidal-Verdu, F.** (2015) 'Influence of errors in tactile sensors on

some high-level parameters used for manipulation with robotic hands', *Sensors*, 15, pp. 20409–20435. doi: 10.3390/s150820409.

20. **Oballe-Peinado, Ó., Castellanos-Ramos, J., Hidalgo-López, J.A. & Vidal-Verdu, F.** (2009) 'Direct interfaces for smart skins based on FPGAs', *Proceedings of the SPIE Europe Microtechnologies for the New Millennium*, Dresden, Germany.
21. **Bakkouri, I., Afdel, K., Benois-Pineau, J. & Catheline, G.** (2022) 'BG-3DM2F: Bidirectional gated 3D multiscale feature fusion for Alzheimer's disease diagnosis', *Multimedia Tools and Applications*, 16 February 2022.
22. **Baldi, T.L., Spagnoletti, G., Dragusanu, M. & Prattichizzo, D.** (2017) 'Design of a wearable interface for lightweight robotic arm for people with mobility impairments', *International Conference on Rehabilitation Robotics*, 1 July 2017.
23. **Kim, D.H., Lu, N., Ghaffari, R., Kim, Y.S., Lee, S.P., Xu, L. & Wu, J.** (2011) 'Wireless epidermal electronic system for sensing motion and colour on skin', *Science*, 333(6044), pp. 838–843. doi: 10.1126/science.1206157.
24. **Li, W., Yuan, J., Zhang, L., Cui, J., Wang, X. & Li, H.** (2023) 'sEMG-based technology for silent voice recognition', *Computers in Biology and Medicine*, 152, p. 106336.
25. **Kim, W.S., Lee, H.D., Lim, D.H., Han, J.S., Shin, K.S. & Han, C.S.** (2014) 'Development of a muscle circumference sensor to estimate torque of the human elbow joint', *Sensors and Actuators A: Physical*, 208, pp. 95–103.
26. **Lee, H.K., Chang, S.I. & Yoon, E.** (2006) 'A flexible polymer tactile sensor: Fabrication and modular expandability for large area deployment', *Journal of Microelectromechanical Systems*, 15(6), pp. 1681-1686.
27. **Rocha, J.G., Santos, C., Cabral, J.M. & Lanceros-Mendez, S.** (2006) '3 axis capacitive tactile sensor and readout electronics', *Proceedings of the IEEE International Symposium on Industrial Electronics*, Montreal, Que., pp. 2767-2772.

28. **Weber, L.M. & Stein, J.** (2020) 'The use of robots in stroke rehabilitation: A narrative review', *Neurorehabilitation*, 46(1), pp. 25-33.
29. **Hossain, M.A., Rahman, M.A., Hasan, M.R., Islam, M.R., Ahmed, S.M. & Al Mamun, M.A.** (2021) 'Robotic home-based rehabilitation systems design: From a literature review to a conceptual framework for community-based remote therapy during COVID-19 pandemic', *Frontiers in Robotics and AI*, 8, p. 612331.
30. **Kang, M.G., Yun, S.J., Lee, S.Y., Oh, B.M., Lee, H.H., Lee, S.U. & Seo, H.G.** (2020) 'Effects of upper-extremity rehabilitation using smart glove in patients with subacute stroke: Results of a prematurely terminated multicenter randomized controlled trial', *Frontiers in Neurology*, 11, p. 580393. doi: 10.3389/fneur.2020.580393.
31. **Reinkensmeyer, D.J. & Dietz, V.** (2016) *Neurorehabilitation technology*. Springer International Publishing.
32. **Chia, Y. & Rita, M.** (2018) 'Soft robotic devices for hand rehabilitation and assistance: A narrative review', *Journal of NeuroEngineering and Rehabilitation*, 15.
33. **Gavin, H.P.** (2020) 'The Levenberg-Marquardt algorithm for nonlinear least squares curve-fitting problems', Department of Civil and Environmental Engineering, Duke University, Durham, NC, USA.
34. **Guo, X., Hong, W., Liu, L., Wang, D., Xiang, L., Tang, M.Z., Shao, S., Jin, C., Hong, Q., Zhao, Y., Xia, Y., Yang, L. & Xing, G.** (2022) 'Highly sensitive and wide-range flexible bionic tactile sensors inspired by octopus sucker structure', *ACS Applied Nano Materials*, 5, pp. 11028–11036. doi: 10.1021/acsanm.2c02242.
35. **Ponraj, G., Kirthinka, S.K., Lim, C.M. & Ren, H.** (2018) 'Soft tactile sensors with inkjet-printing conductivity and hydrogel biocompatibility for retractors in cadaveric surgical trials', *IEEE Sensors Journal*, 18(23).

36. **Han, H. & Kim, J.** (2013) 'Active muscle stiffness sensor based on piezoelectric resonance for muscle contraction estimation', *Sensors and Actuators A: Physical*, 194, pp. 212–219.
37. **Guo, J.Y., Zheng, Y.P., Xie, H.B. & Chen, X.** (2010) 'Continuous monitoring of electromyography (EMG), mechanomyography (MMG), sonomyography (SMG) and torque output during ramp and step isometric contractions', *Medical Engineering and Physics*, 32, pp. 1032–1042.
38. **Kenney, L.P., Lisitsa, I., Bowker, P., Heath, G.H. & Howard, D.** (1999) 'Dimensional change in muscle as a control signal for powered upper limb prostheses: A pilot study', *Medical Engineering and Physics*, 21, pp. 589–597.
39. **Jung, P.G., Lim, G., Kim, S. & Kong, K.** (2015) 'A wearable gesture recognition device for detecting muscular activities based on air-pressure sensors', *IEEE Transactions on Industrial Informatics*, 11, pp. 485–494.
40. **Gargiulo, G.D., Bifulco, P., Cesarelli, M., Jin, C., McEwan, A. & van Schaik, A.** (2010) 'Wearable dry sensors with Bluetooth connection for use in remote patient monitoring systems', *Studies in Health Technology and Informatics*, 161, pp. 57–65.
41. **Camarillo, D.B., Carlson, C.R. & Salisbury, J.K.** (2018) 'Configuration tracking for continuum manipulators with coupled tendon drive', *IEEE Transactions on Robotics*, 25, pp. 798–808.
42. **Kadowaki, Y., Noritsugu, T., Takaiwa, M., Sasaki, D. & Kato, M.** (2011) 'Development of soft power-assist glove and control based on human intent', *Journal of Robotics and Mechatronics*, 23(2), pp. 281.
43. **Sasaki, D., Noritsugu, T., Takaiwa, M. & Konishi, H.** (2014) 'Control method based on EMG for power assist glove using self-organizing maps', *International Journal of Automation Technology*, 8(2), pp. 177-185.
44. **Galloway, K.C., Clark, J.E. & Koditschek, D.E.** (2013) 'Variable stiffness leg for robust, efficient, and stable dynamic running', *Journal of Mechanisms and Robotics*, 5(1), p. 011009.

45. **Agcayazi, T., McKnight, M., Kausche, H., Ghosh, T. & Bozkurt, A.** (2016) 'A finger touch force detection method for textile-based capacitive tactile sensor arrays', *Proceedings of IEEE Sensors 2016*, Orlando, FL, pp. 1-3.
46. **Allain, P., Hamon, M., Saoût, V., Verny, C., Dinomais, M. & Besnard, J.** (2020) 'Theory of mind impairments highlighted with an ecological performance-based test indicate behavioral executive deficits in traumatic brain injury', *Frontiers in Neurology*, 22 January 2020.
47. **Erukainure, F.E., Parque, V., Hassan, M. & Fathelbab, A.M.R.** (2022) 'Towards estimating the stiffness of soft fruits using a piezoresistive tactile sensor and neural network schemes', *Proceedings of the 2022 IEEE/ASME International Conference on Advanced Intelligent Mechatronics (AIM)*, 11 July 2022.
48. **Tseghai, G.B., Mengistie, D.A., Malengier, B., Fante, K.A. & Van Langenhove, L.** (2020) 'PEDOT a conductive textiles and their applications', *Sensors*, 20, p. 1881.
49. **Fayazi, M., Daneshmand, H. & Dehzangi, O.** (2020) 'Recent advancements in flexible and stretchable electrochemical biosensors: A review', *Chemical Communications*, 56, pp. 9891–9903.
50. **Lee, J.H., Kim, Y.S., Ru, H.J., Lee, S.Y. & Park, S.J.** (2022) 'Highly flexible fabrics/epoxy composites with hybrid carbon nanofillers for absorption-dominated electromagnetic interference shielding', *Nano-Micro Letters*, 14, p. 188.
51. **Fouly, A., Nasr, M., Fath El Bab, A.M.R. & Abouelsoud, A.** (2015) 'Design and modelling of micro tactile sensor with three contact tips for self-compensation of contact error in soft tissue elasticity measurement', *Proceedings of the Annual Conference of the Society of Instrument and Control Engineers*, 1 October 2015.

52. **Bullock, I.M., Ma, R.R. & Dollar, A.** (2013) 'A hand-centric classification of human and robot dexterous manipulation', *IEEE Transactions on Haptics*, 1 April 2013.
53. **Do, W.K. & Kennedy, M.** (2022) 'DenseTact: Optical tactile sensor for dense shape reconstruction', *Proceedings of the IEEE International Conference on Robotics and Automation*, 4 January 2022.
54. **Elgeneidy, K., Lohse, N. & Jackson, M.** (2018) 'Bending angle prediction and control of soft pneumatic actuators with embedded flex sensors—a data-driven approach', *Mechatronics*, 50, pp. 234–247.
55. **Elsahy, A.M., Parque, V., Esmael, A., Hassan, M.A. & El-Bab, A.F.** (2023) 'Evaluating the viscoelastic behavior of elastomers using a piezoelectric tactile sensor and an optimization approach', *Proceedings of the Annual Conference of the Society of Instrument and Control Engineering*, 6 September 2023.
56. **Nguyen, T.T., Tran, V.T., Pham, T.H.N., Nguyen, V.T., Thanh, N.C., Thi, H.M.N., Duy, N.V.A., Thanh, D.N. & Nguyen, V.T.T.** (2023) 'Influences of material selection, infill ratio, and layer height in the 3D printing cavity process on the surface roughness of printed patterns and casted products', *Micromachines*, 14(2), pp. 1–11. doi: 10.3390/mi14020395.
57. **Zhao, Z., Tang, J., et al.** (2022) 'Large-scale integrated flexible tactile sensor array for sensitive smart robotic touch', *ACS Nano*, 23 August 2022.
58. **Zhu, J., Zhou, C. & Zhang, M.** (2021) 'Recent progress in flexible tactile sensor systems: From design to application', *Soft Science*, 9 July 2021.
59. **Chia, Y. & Rita, M.** (2018) 'Soft robotic devices for hand rehabilitation and assistance: A narrative review', *Journal of NeuroEngineering and Rehabilitation*, 15.
60. **Dai, H., Zhang, C., Pan, C., Hu, H., Ji, K., Sun, H., Lyu, C., Tang, D., Li, T., Fu, J. & Zhao, P.** (2023) 'Split-type magnetic soft tactile sensor with 3D force decoupling', *Advanced Materials*, 28 November 2023. doi: 10.1002/adma.202310145.

61. **Kadowaki, Y., Noritsugu, T., Takaiwa, M., Sasaki, D. & Kato, M.** (2011) 'Development of soft power-assist glove and control based on human intent', *Journal of Robotics and Mechatronics*, 23(2), pp. 281.
62. **Kai, K., Tsuji, T., Hiramoto, K., Fukuda, K., Tanioka, A. & Miki, N.** (2019) 'Flexible wearable sensor network for multi-point measurement of human joint flexibility', *IEEE Sensors Journal*, 19, pp. 6948–6955.
63. **Kasahara, T., Mizushima, M., Shinohara, H., Obata, T., Futakuchi, T., Shoji, S. & Mizuno, J.** (2011) 'Simple and low-cost fabrication of flexible capacitive tactile sensors', *Japan Journal of Applied Physics*, 50, pp. 0165026016502–5.
64. **Fontana, F., D'Angelo, G. & Centonze, D.** (2016) 'Wearable low-power devices for continuous monitoring of environment and health for human wellness', *IEEE Sensors Journal*, 16, pp. 5058–5067.
65. **Hou, Z., Chen, Z., Wang, H., Zhou, Y., Zhang, Z. & Chen, J.** (2020) 'Tactile sensing technologies for robotic grasping and manipulation: A review', *Frontiers in Neurorobotics*, 14, p. 10.
66. **Hu, Y. & Lu, Z.** (2020) 'Wearable and flexible sensors: Essential materials and emerging designs', *Matter*, 3, pp. 1253–1279.
67. **Hua, Q., Sun, J., Liu, H., Bao, R., Yu, R., Zhai, J., Pan, C. & Wang, Z.L.** (2018) 'Skin-inspired multifunctional autonomic-intrinsic conductive self-healing hydrogels with pressure sensitivity, stretchability, and 3D printability', *Advanced Materials*, 30, p. 1705918.
68. **Hughes, A., Freeman, C., Burridge, J., Chappell, P., Lewin, P. & Rogers, E.** (2009) 'Feasibility of iterative learning control mediated by functional electrical stimulation for reaching after stroke', *Neurorehabilitation and Neural Repair*, 3 February 2009.
69. **In, V., Kho, A., Longhinit, P., et al.** (2005) 'Effect of delays in softness display using contact area control: Rendering of surface viscoelasticity', *Proceedings of the Italian National Conference on Sensors*, 31 October 2005.

70. **Tarnowski, J., Hollender, L., Jentsch, E., Haldemann, A., Janabi-Sharifi, S. & Mazzeo, A.D.** (2019) 'Soft robotic manipulation and locomotion with a 3D printed electrorheological soft actuator', *Scientific Reports*, 9(1).
71. **Li, Y., Yang, Y., Zhang, C. & Li, Z.** (2019) 'Recent developments in sensors for wearable devices', *Sensors*, 19, p. 2173.
72. **Visintin, A.** (1994) *Differential Models of Hysteresis*. Berlin: Springer Berlin Heidelberg.
73. **Zareinejad, M., Rezaei, S.M., Ghidary, S.S., Abdullah, A. & Motamedi, M.** (2009) 'Robust impedance control of a piezoelectric stage under thermal and external load disturbances', *Control and Cybernetics*, 38, pp. 635–648.
74. **Dwivedi, A., Kwon, Y., McDaid, A. & Liarokapis, M.** (2018) 'EMG based decoding of object motion in dexterous, in-hand manipulation tasks', *Proceedings of the International Conference on Biomedical Robotics and Biomechatronics*, 1 August 2018.
75. **Al-Fahaam, A.A., Xie, S.Q., Dwivedi, A.K. & Nair, N.K.C.** (2021) 'Review of control strategies for lower-limb exoskeletons to assist gait', *Journal of NeuroEngineering and Rehabilitation*, 18(1), p. 126.
76. **Amft, O.** (2005) 'Analysis of wearable computing for health and well-being applications', *Proceedings of the 9th International Symposium on Wearable Computers (ISWC'05)*, Osaka, Japan, 18–21 October 2005.
77. **Brokate, M. & Sprekels, J.** (1996) *Hysteresis and Phase Transitions*. New York: Springer.
78. **Kuhnen, K. & Janocha, H.** (2001) 'Inverse feedforward controller for complex hysteretic nonlinearities in smart-material systems', *Control Intelligent Systems*, 29, pp. 74–83.
79. **Gu, G.Y., Zhu, L.M. & Su, C.Y.** (2014) 'Modeling and compensation of asymmetric hysteresis nonlinearity for piezoceramic actuators with a modified

- Prandtl-Ishlinskii model', *IEEE Transactions on Industrial Electronics*, 61, pp. 1583–1595. doi: 10.1109/TIE.2013.2257153.
80. **Janaideh, M.A., Rakheja, S. & Su, C.Y.** (2011) 'An analytical generalized Prandtl-Ishlinskii model inversion for hysteresis compensation in micropositioning control', *IEEE/ASME Transactions on Mechatronics*, 16, pp. 734–744. doi: 10.1109/TMECH.2010.2052366.
81. **Castellanos-Ramos, J., Navas-González, R., Macicior, H., Sikora, T., Ochoteco, E. & Vidal-Verdú, F.** (2010) 'Tactile sensors based on conductive polymers', *Microsystem Technologies*, 16, pp. 765-776.
82. **Sánchez-Durán, J.A., Hidalgo-López, J.A., Castellanos-Ramos, J., Oballe-Peinado, Ó. & Vidal-Verdú, F.** (2015) 'Influence of errors in tactile sensors on some high-level parameters used for manipulation with robotic hands', *Sensors*, 15, pp. 20409–20435. doi: 10.3390/s150820409.
83. **Oballe-Peinado, Ó., Castellanos-Ramos, J., Hidalgo-López, J.A. & Vidal-Verdú, F.** (2009) 'Direct interfaces for smart skins based on FPGAs', *Proceedings of SPIE Europe Microtechnologies for the New Millennium*, Dresden, Germany.
84. **Zhu, W., Wang, D. & Rui, X.T.** (2016) 'Hysteresis modeling and displacement control of piezoelectric actuators with frequency-dependent behavior using a generalized Bouc-Wen model', *Precision Engineering*, 43, pp. 299–307. doi: 10.1016/j.precisioneng.2015.10.011.
85. **Jiang, H., Ji, H., Qiu, J. & Chen, Y.** (2010) 'A modified Prandtl-Ishlinskii model for modeling asymmetric hysteresis of piezoelectric actuators', *IEEE Transactions on Ultrasonics, Ferroelectrics, and Frequency Control*, 57, pp. 1200–1210. doi: 10.1109/TUFFC.2010.1533.
86. **Li, Z., Shan, J. & Gabbert, U.** (2018) 'Inverse compensation of hysteresis using the Krasnoselskii-Pokrovskii model', *IEEE/ASME Transactions on Mechatronics*, 23(2), pp. 966–971. doi: 10.1109/TMECH.2018.2799185.

87. **Zareinejad, M., Rezaei, S.M., Ghidary, S.S., Abdullah, A. & Motamedi, M.** (2009) 'Robust impedance control of a piezoelectric stage under thermal and external load disturbances', *Control and Cybernetics*, 38, pp. 635–648.
88. **Fazekas, G. & Tavaszi, I.** (2019) 'The future role of robots in neuro-rehabilitation', *Expert Review of Neurotherapeutics*, 19(5), pp. 471-473.
89. **Brokate, M. & Sprekels, J.** (1996) *Hysteresis and Phase Transitions*. New York: Springer.
90. **Kuhnen, K. & Janocha, H.** (2001) 'Inverse feedforward controller for complex hysteretic nonlinearities in smart-material systems', *Control Intelligent Systems*, 29, pp. 74–83.
91. **Janaideh, M.A., Rakheja, S. & Su, C.Y.** (2011) 'An analytical generalized Prandtl-Ishlinskii model inversion for hysteresis compensation in micropositioning control', *IEEE/ASME Transactions on Mechatronics*, 16, pp. 734–744. doi: 10.1109/TMECH.2010.2052366.
92. **O'Kane, J. & Sherrington, D.** (1990) 'Hysteresis-like behaviour in the swelling/deswelling of polystyrene crosslinked resins using binary solvent mixtures', *Materials Science Chemistry*, 1 December 1990.
93. **Carlson, P. & The, A.** (1991) 'A cognitively-based neural network for determining paragraph coherence', *Proceedings of the 1991 IEEE International Joint Conference on Neural Networks*, 18 November 1991.
94. **Buan, T.A.** (2019) 'In-depth analysis of Long-Short-Term-Memory neural networks with the purpose of detecting cyberbullying', *Computer Science*, 2019.
95. **Christo, V.R.E., Nehemiah, H.K., Minu, B. & Kannan, A.** (2019) 'Correlation-based ensemble feature selection using bioinspired algorithms and classification using backpropagation neural network', *Computational and Mathematical Methods in Medicine*, 23 September 2019.
96. **Çukurtepe, H., Yayimli, A. & Mukherjee, B.** (2012) 'Inverse multiplexing gain considering physical layer impairments in mixed line rate networks',

Proceedings of the International Symposium on Computers and Communication, 1 July 2012.

97. **Deng, P., Li, X., Wang, Y., He, Z., Zhu, W., Zhang, Y., Schalm, G.M. & Tian, J.** (2023) 'Highly stretchable ionic and electronic conductive fabric', *Advanced Fiber Materials*, 5, pp. 198–208. doi: 10.1007/s42765-022-00208-w.
98. **Xiang, Y., Donley, J., Seletskiaia, E., Shingare, S., Kamerud, J. & Gorovits, B.** (2018) 'A simple approach to determine a curve fitting model with a correct weighting function for calibration curves in quantitative ligand binding assays', *The AAPS Journal*, 20, p. 45. doi: 10.1208/s12248-018-0208-7.
99. **Guo, H., Tang, R., Ye, Y., Li, Z. & He, X.** (2017) 'DeepFM: A factorization-machine based neural network for CTR prediction', *Proceedings of the International Joint Conference on Artificial Intelligence*, 13 March 2017.
100. **Hecht-Nielsen, R.** (1989) 'Theory of the backpropagation neural network', *Proceedings of the 1989 International Joint Conference on Neural Networks*, 1989.
101. **Khachnaoui, H., Mabrouk, R. & Khelifa, N.** (2020) 'Machine learning and deep learning for clinical data and PET/SPECT imaging in Parkinson's disease: A review', *IET Image Processing*, 1 December 2020.
102. **Khushi, M., Amjad, M. & Anpalagan, A.** (2020) 'Performance analysis of autonomous mobile robot cooperative transport with machine learning technique', *IEEE Access*, 8, pp. 129221-129231.
103. **Kornblith, S., Norouzi, M., Lee, H. & Hinton, G.E.** (2019) 'Similarity of neural network representations revisited', *Proceedings of the International Conference on Machine Learning*, 1 May 2019.
104. **Li, Y., Dong, W.H., Yang, Q., Zhao, J., Liu, L. & Feng, S.** (2019) 'An automatic impedance matching method based on the feedforward-backpropagation neural network for a WPT system', *IEEE Transactions on Industrial Electronics*, 1 May 2019.

105. **Cort, J.A. & Potvin, J.R.** (2011) 'Maximum isometric finger pull forces', *International Journal of Industrial Ergonomics*, 41(2), pp. 91-95.
106. **Zhou, T., Hou, Y. & Zhou, Z.** (2019) 'A review of Backpropagation Neural Network on image classification', Proceedings of the International Conference on Artificial Intelligence and Machine Learning, 13 July 2019, pp. 1-7. doi: 10.1109/ICMLA.2019.889657.
107. **Kim, H., Kim, J. & Park, H.** (2018) 'An improved BPNN-based approach for the prediction of industrial equipment failure', *Journal of Computational Intelligence and Neuroscience*, pp. 1-9. doi: 10.1155/2018/3895617.
108. **Sánchez-Durán, J.A., Oballe-Peinado, O., Castellanos-Ramos, J. & Vidal-Verdu, F.** (2012) 'Hysteresis correction of tactile sensor response with a generalized Prandtl-Ishlinskii model', *Microsystem Technologies*, 18(8), pp. 1127–1138. doi: 10.1007/s00542-012-1455-7.
109. **Zhou, C., Yuan, M., Feng, C. & Ang, W.T.** (2021) 'A modified Prandtl–Ishlinskii hysteresis model for modeling and compensating asymmetric hysteresis of piezo-actuated flexure-based systems', *Sensors*, 21(4), p. 1223. doi: 10.3390/s21041223.
110. **Ozioko, O., Karipoth, P. et al.** (2021) 'SensAct: The soft and squishy tactile sensor with integrated flexible actuator', *Advanced Intelligent Systems*, 21 January 2021.
111. **Zhang, J., Torres, D. & Sepulveda, N.** (2016) 'A compressive sensing-based approach for Preisach hysteresis model identification', *Smart Materials and Structures*, 25(7), pp. 12–20. doi: 10.1088/0964-1726/25/7/075001.
112. **Zhang, S., Chen, Z. et al.** (2022) 'Hardware technology of vision-based tactile sensor: A review', *IEEE Sensors Journal*, 15 November 2022.
113. **Galloway, K.C., Clark, J.E. & Koditschek, D.E.** (2013) 'Variable stiffness leg for robust, efficient, and stable dynamic running', *Journal of Mechanisms and Robotics*, 5(1), 011009.

114. **Merletti, R. & Parker, P.J.** (2004) *Electromyography: Physiology, engineering, and non-invasive applications*. Hoboken: Wiley-IEEE Press.
115. **Farina, D., Merletti, R. & Enoka, R.M.** (2014) 'The extraction of neural strategies from the surface EMG: An update', *Journal of Applied Physiology*, 117(11), pp. 1215-1230.
116. **Lucarotti, C., Oddo, C.M., Vitiello, N. & Carrozza, M.C.** (2013) 'Synthetic and bio-artificial tactile sensing: A review', *Sensors*, 13(2), pp. 1435-1466.
117. **De Luca, C.J.** (2002) 'Surface electromyography: Detection and recording'. DeSys Incorporated.
118. **Basmajian, J.V. & De Luca, C.J.** (1985) *Muscles alive: Their functions revealed by electromyography*. Williams & Wilkins.
119. **Kubota, S., Nakata, Y., Eguchi, K. et al.** (2013) 'Feasibility of rehabilitation training with a newly developed wearable robot for patients with limited mobility', *Archives of Physical Medicine and Rehabilitation*, 94(6), pp. 1080-1087.
120. **Morales, R., Badesa, F.J., Garcia-Aracil, N., Sabater, J.M. & Perez-Vidal, C.** (2011) 'Pneumatic robotic systems for upper limb rehabilitation', *Medical & Biological Engineering & Computing*, 49(10), pp. 1145-1156.
121. **Truong, T.T.N., Kim, J.S. & Kim, J.** (2021) 'Design and optimization of embroidered antennas on textile using silver conductive thread for wearable applications', *Fibers and Polymers*, 22(10), pp. 2900–2909. doi: 10.1007/s12221-021-0030-1.
122. **Vélez-Guerrero, M.A., Callejas-Cuervo, M. & Mazzoleni, S.** (2021) 'Artificial intelligence-based wearable robotic exoskeletons for upper limb rehabilitation: A review', *Sensors*, 21(6), p. 2084.
123. **Liu, Y., Pharr, M. & Salvatore, G.A.** (2017) 'Lab-on-skin: A review of flexible and stretchable electronics for wearable health monitoring', *ACS Nano*, 11, pp. 9614–9635.

124. **Ma, X., Wang, C. et al.** (2022) 'Bimodal sensor without signal fusion for user-interactive applications', *ACS Nano*, 21 January 2022.
125. **Manda, M.** (2018) 'Hand gestures controlled wheelchair', *Proceedings of the 2018 IEEE International Conference on Robotics and Automation*, 1 September 2018.
126. **Moll, M. & Erdmann, M.** (2002) 'Shape reconstruction using active tactile sensors', *Proceedings of the 2002 IEEE International Conference on Robotics and Automation*, 2002.
127. **Al-Fahaam, H.S.** (2019) 'Wearable exoskeleton systems based on pneumatic soft actuators and controlled by parallel processing', University of Salford Dissertation, UK. Available via ProQuest Dissertations & Theses.
128. **Bansal, A.K., Hou, S., Kulyk, O., Bowman, E.M. & Samuel, I.D.W.** (2015) 'Wearable organic optoelectronic sensors for medicine', *Advanced Materials*, 27, pp. 1521–4095.
129. **Nelson, A., Schmandt, J. & Varadan, V.** (2013) 'Wearable multi-sensor gesture recognition for paralysis patients', *Proceedings of the Italian National Conference on Sensors*, 19 December 2013.
130. **Norman, G.R. & Streiner, D.L.** (2008) *Biostatistics: The bare essentials*. PMPH-USA.
131. **Owens, J. & Simonds, C.** (2008) 'Beyond the wheelchair: Development of motorised transport for people with severe mobility impairments in developing countries', *Disability and Rehabilitation: Assistive Technology*, 13 May 2008.
132. **Paudel, D., Démonceaux, C., Habed, A., Vasseur, P. & Kweon, I.S.** (2014) '2D-3D camera fusion for visual odometry in outdoor environments', *Proceedings of the 2014 IEEE/RSJ International Conference on Intelligent Robots and Systems*, 6 November 2014.
133. **Peng, X., Liu, Y. et al.** (2023) 'A novel transformer-based approach for simultaneous recognition of hand movements and force levels in amputees

using flexible ultrasound transducers', IEEE Transactions on Neural Systems and Rehabilitation Engineering, 15 November 2023.

134. **Pohtongkam, S. & Srinonchat, J.** (2021) 'Tactile object recognition for humanoid robots using newly designed piezoresistive tactile sensor and DCNN', Proceedings of the Italian National Conference on Sensors, 1 September 2021.
135. **Ponraj, G., Kirthika, S.K., Lim, C.M. & Ren, H.** (2018) 'Soft tactile sensors with inkjet-printing conductivity and hydrogel biocompatibility for retractors in cadaveric surgical trials', IEEE Sensors Journal, 18(23).
136. **Shepherd, R.F., Ilievski, F., Choi, W., Morin, S.A., Stokes, A.A., Mazzeo, A.D., Chen, X., Wang, M. & Whitesides, G.M.** (2011) 'Multigait soft robot', Proceedings of the National Academy of Sciences, 118, pp. 20400-20403.
137. **Qu, X., Xue, J., Liu, Y., Rao, W., Liu, Z. & Li, Z.** (2022) 'Fingerprint-shaped triboelectric tactile sensor', Social Science Research Network, 1 April 2022.
138. **R.F. Shepherd, F. Ilievski, W. Choi, S.A. Morin, A.A. Stokes, A.D. Mazzeo, X. Chen, M. Wang & G.M. Whitesides** (2011) 'Multigait soft robot', Proceedings of the National Academy of Sciences, 118, pp. 20400-20403.
139. **Rafferty, J., Nugent, C.D., Liu, J. & Chen, L.** (2017) 'From activity recognition to intention recognition for assisted living within smart homes', IEEE Transactions on Human-Machine Systems, 47(3), pp. 124–124.
140. **Rocha, J.G., Santos, C., Cabral, J.M. & Lanceros-Mendez, S.** (2006) '3 axis capacitive tactile sensor and readout electronics', Proceedings of the 2006 IEEE International Symposium on Industrial Electronics, Montreal, Que., pp. 2767-2772.
141. **Salvo, P., Dini, G. & Militano, L.** (2020) 'Performance assessment of a new generation of wearable sensors for health monitoring', Sensors, 20, p. 354.

142. **Schall, M.C., Fethke, N.B. & Chen, H.** (2018) 'Evaluation of three commercial activity monitors for sleep and activity tracking in a healthy population', *European Journal of Sport Science*, 18, pp. 1–9.
143. **Song, Y., Yao, Z., Yuan, W., Zhu, H. & Hu, Y.** (2019) 'Recent advances in tactile sensing technology: Materials, devices, and applications', *Advanced Materials Technologies*, 4(6), p. 1800545. doi: 10.1002/admt.201800545.
144. **Stefanou, T., Chance, G., Assaf, T. & Dogramadzi, S.** (2019) 'Tactile signatures and hand motion intent recognition for wearable assistive robotics and AI', *Proceedings of AI Robotics Conference*, 2019, pp. 124–124.
145. **Sun, Y., Choi, W.M., Jiang, H., Huang, Y.Y. & Rogers, J.A.** (2006) 'Controlled buckling of semiconductor nanoribbons for stretchable electronics', *Nature Nanotechnology*, 1, pp. 201–207.
146. **Sundara Siva Kumar, V., Nagesh, P. & Gandhi Memorial.** (2015) 'MEMS-based hand gesture wheelchair movement control for disabled persons', *Proceedings of the 2015 IEEE International Conference on MEMS Technology*, 2015.
147. **Agcayazi, T., McKnight, M., Kausche, H., Ghosh, T. & Bozkurt, A.** (2016) 'A finger touch force detection method for textile-based capacitive tactile sensor arrays', *Proceedings of the 2016 IEEE SENSORS Conference*, Orlando, FL, pp. 1-3.
148. **Kasahara, T., Mizushima, M., Shinohara, H., Obata, T., Futakuchi, T., Shoji, S. & Mizuno, J.** (2011) 'Simple and low-cost fabrication of flexible capacitive tactile sensors', *Japan Journal of Applied Physics*, 50, pp. 016502-6016502-5.
149. **Lee, T., Lee, D., Jang, J., Lee, J., Lee, S.H. & Koo, J.** (2019) 'A wearable piezoelectric touch sensor array for environmental monitoring', *Nano Energy*, 61, pp. 614-621.

150. **Tao, K., Chen, Z. et al.** (2022) 'Ultra-sensitive, deformable, and transparent triboelectric tactile sensor based on micro-pyramid patterned ionic hydrogel for interactive human–machine interfaces', *Advanced Science*, 31 January 2022.
151. **Tiwana, M., Redmond, S. & Lovell, N.** (2012) 'A review of tactile sensing technologies with applications in biomedical engineering', *Sensors and Actuators A: Physical*, 179, pp. 17–31.
152. **Tran, T., Hettinga, B.A. & Buchowski, M.** (2016) 'A wearable system for physical activity assessment during active video gaming', *Journal of Sports Engineering and Technology*, 230, pp. 271–278.
153. **Lazarov, V.K. & Laschi, T.** (2019) 'Soft robotics: Emerging trends and applications', *Advanced Engineering Materials*, 21(11).
154. **Wang, H., Cen, Y. & Zeng, X.** (2021) 'Highly sensitive flexible tactile sensor mimicking the microstructure perception behaviour of human skin', *ACS Applied Materials and Interfaces*, 13 June 2021.
155. **Wang, M., Tu, J. et al.** (2022) 'Tactile near-sensor analogue computing for ultrafast responsive artificial skin', *Advanced Materials*, 11 July 2022.
156. **Wang, Y., Jin, J., Lu, Y. & Mei, D.** (2021) '3D printing of liquid metal-based tactile sensor for simultaneously sensing temperature and forces', *International Journal of Engineering*, 2021.
157. **Wang, Y., Lu, Y., Mei, D. & Zhu, L.** (2021) 'Liquid metal-based wearable tactile sensor for both temperature and contact force sensing', *IEEE Sensors Journal*, 15 January 2021.
158. **Chia, Y. & Rita, M.** (2018) 'Soft robotic devices for hand rehabilitation and assistance: A narrative review', *Journal of NeuroEngineering and Rehabilitation*, 2018.
159. **Yang, M., Cheng, Y. et al.** (2022) 'High-performance flexible pressure sensor with a self-healing function for tactile feedback', *Advanced Science*, 15 April 2022.

160. **Yang, W., Xie, M. et al.** (2021) 'Multifunctional soft robotic finger based on a nanoscale flexible temperature-pressure tactile sensor for material recognition', *ACS Applied Materials and Interfaces*, 15 November 2021.
161. **Zhang, J., Yao, H. et al.** (2021) 'Finger-inspired rigid-soft hybrid tactile sensor with superior sensitivity at a high frequency', *Nature Communications*.
162. **Avants, B., Epstein, C., Grossman, M. & Gee, J.** (2008) 'Symmetric diffeomorphic image registration with cross-correlation: Evaluating automated labelling of the elderly and neurodegenerative brain', *Medical Image Analysis*, 1 February 2008.
163. **Babu, G.R., Sudarsanam, T.D. & Mohanta, G.P.** (2004) 'Kendall's coefficient of concordance and Spearman's rank correlation coefficient: An overview', *Journal of the Indian Academy of Applied Psychology*, 30(1), pp. 43-46.
164. **De Luca, C.J.** (1997) 'The use of surface electromyography in biomechanics', *Journal of Applied Biomechanics*, 13(2), pp. 135-163. doi: 10.1123/jab.13.2.135.
165. **Merletti, R. & Parker, P.A.** (2004) *Electromyography: Physiology, engineering, and non-invasive applications*. Hoboken: John Wiley & Sons.
166. **Yang, J., Mathiassen, S.E. & Hallman, D.M.** (2018) 'Variation of forearm muscle activity during grip force exertions and functional precision gripping', *Journal of Electromyography and Kinesiology*, 38, pp. 215-221. doi: 10.1016/j.jelekin.2018.02.009.
167. **Dasari, K. & Devarakonda, N.** (2022) 'TCP/UDP-based exploitation DDoS attacks detection using AI classification algorithms with common uncorrelated feature subset selected by Pearson, Spearman and Kendall correlation methods', *International Information and Engineering Technology Association*, 36(1), pp. 61-71.
168. **Lian, R., Zhou, C. & Goertzel, B.** (2020) 'The probabilistic supports Kendall correlation and its transitivity properties', *Communications in Statistics - Theory and Methods*, 17 January 2020.

169. **Shaikh, M.A.H. & Barbé, K.** (2019) 'Wiener–Hammerstein system identification: A fast approach through Spearman correlation', *IEEE Transactions on Instrumentation and Measurement*, 5 March 2019.
170. **Samirbhai, M.D., Chen, S. & Low, K.** (2019) 'A Hamming distance and Spearman correlation-based star identification algorithm', *IEEE Transactions on Aerospace and Electronic Systems*, 1 February 2019.
171. **Yu, H. & Hutson, A.** (2020) 'A robust Spearman correlation coefficient permutation test', *Communications in Statistics - Theory and Methods*, 3 August 2020.
172. **Sheng, Z., Zhang, X., Wang, Y., Hou, W. & Yang, D.** (2018) 'An energy ratio feature extraction method for optical fiber vibration signal', *Photonic Sensors*, 8(1), pp. 48–55.
173. **Dahlhaus, R.** (2000) 'Cross-correlation and autocorrelation of linear processes', *Annals of Statistics*, 28(2), pp. 633-685.
174. **Liu, S., Yang, B., Wang, Y., Tian, J., Yin, L. & Zheng, W.** (2022) '2D/3D multimode medical image registration based on normalized cross-correlation', *Applied Sciences*, 9 March 2022.
175. **Mukaka, M.** (2012) 'Statistics corner: A guide to the appropriate use of correlation coefficient in medical research', *Malawi Medical Journal*, 24(3), pp. 69–71.
176. **Redfield, R.U. & Freeman, A.G.** (2020) 'Cross-correlation', *Definitions*, 7 February 2020.
177. **Sinha, A., Dey, S., Basu, A. & Chatterjee, A.** (2018) 'A novel cross-correlation-based feature extraction technique for speaker recognition system', *Signal, Image and Video Processing*, 12(5), pp. 947-954.
178. **Burgund, D., Nikolovski, S., Galić, D. & Maravić, N.** (2023) 'Pearson correlation in determination of quality of current transformers', *Proceedings of the Italian National Conference on Sensors*, 1 March 2023.

179. **Gnambs, T.** (2023) 'A brief note on the standard error of the Pearson correlation', *Collabra: Psychology*, 2023.
180. **Zou, Q., Zhang, L., Xu, R. & Wang, Z.** (2006) 'Comparison study of Pearson correlation coefficient and mutual information', *Proceedings of the 2006 International Conference on Machine Learning and Cybernetics*, 3, pp. 1890–1894.
181. **Saglia, J.A., Rocon, E., Moreno, J.C., Brunetti, F., Pons, J.L. & Frisoli, A.** (2019) 'Design, development and clinical results of a novel total-body rehabilitation robot: Hunova®', *Proceedings of the 2019 IEEE 16th International Conference on Rehabilitation Robotics (ICORR)*, pp. 417-422.
182. **Valmadre, J., Bertinetto, L., Henriques, J.F., Vedaldi, A. & Torr, P.H.S.** (2017) 'End-to-end representation learning for correlation filter-based tracking', *Computer Vision and Pattern Recognition*, 20 April 2017.
183. **Ugoni, A. & Walker, B.F.** (1995) 'The t-test: An introduction', *COMSIG Review*, 4(2).
184. **Logothetis, N.K., Pauls, J., Augath, M., Trinath, T. & Oeltermann, A.** (2001) 'Neurophysiological investigation of the basis of the fMRI signal', *Nature*, 412, pp. 150–157.
185. **Yang, J., Liu, S. et al.** (2022) 'Self-powered tactile sensor for gesture recognition using deep learning algorithms', *ACS Applied Materials and Interfaces*, 25 May 2022.

Appendix A

Focus group: Recruitment Email

Recruitment Email/Letter

Dear [Name]:

I am conducting a research study by using wearable soft sensors to recognise the gesture of the upper limb. The sensor is made up totally of fabric, you can wear it as a sleeve on the different parts of the upper limb: arm, forearm, and wrist to measure your muscle's activities, it is easy to set up and fully safe to use. Participation will take [15-20 minutes only]. The data will be collected anonymously and confidentially and will be kept securely and protected from unauthorised, accidental, or malicious access. There are no known risks involved in this research.

If you are interested in measuring your muscle strength, please contact the investigator. Further instructions will be followed in a separate email/Letter.

If you have any queries, please do not hesitate to contact me.

Gasak Abdul-Hussain

PhD student/ Robotics

SEE Building

University of Salford

g.c.abdul-hussain@edu.salford.ac.uk

Mobile no. :07490671441

